Role of integrin α11 in oral carcinogenesis

In vitro and in vivo studies

Himalaya Parajuli

Dissertation for the degree of philosophiae doctor (PhD)
at the University of Bergen

2016

Dissertation date: 29.04.2016

Year: 2016
Title: Role of integrin α11 in oral carcinogenesis
In vitro and in vivo studies
Author: Himalaya Parajuli
Print: AiT Bjerch AS / University of Bergen

Dedication

This thesis is dedicated to my parents.

ACKNOWLEDGEMENT

First and foremost, I would like to express my sincere gratitude to my main supervisor Professor Daniela Elena Costea for the continuous support during this period. Thank you for your patience and motivation in this study. I would like to express my sincere appreciativeness to my co supervisors, Professor Anne Christine Johannessen and Professor Donald Gullberg for constant supervision, guidance encouragement and support. Huge thanks to Gunnvor Øijordsbakken and Edith Fick for all the technical support and guidance.

I would like to express my gratitude to University of Bergen, the Quota program, the Norwegian Educational Loan Fund, Department of Global Public Health & Primary Care and Department of Clinical Medicine for the opportunity.

Thank you all Professor Kathrine Skarstein, Dipak Sapkota, Tarig Osman, Salwa Suliman, Saroj Rajthala, Amani Osman, Nada Suliman, Xiao Liang, Eivind Salmorin Birkeland, Victoria Konstantinova and Elisabeth Sivy Nginamau for the great discussions, guidance, support and creating a great working environment.

I would like to thank, Mona Grønning, Malgorzata Barczyk, Ning Lu, Pugazendhi Murugan Erusappan, Joanna Godawa Stormark, Professor Emmet Mc Cormack and Mihaela Popa from the collaborating departments: Department of Biomedicine, Laboratory Animal Facility and Department of Clinical Science for their support and successful collaboration. I also would like to thank to all my co-authors for their valuable contribution for this study.

I am glad to have you, Rajib Chaulagain, Sushma Bartaula-Brevik, Ridaya Paudel, Chirag Nepal and all Nepali friends and families in Bergen, thank you for making our stay easier and for the great moments we shared together.

I would like to thank my strength, my parents Madan Kumari Parajuli and Mukti Raman Parajuli for their love, care, and tireless efforts for my education. Thank you, Dr. Krishna Chandra Paudel, Basu Dev Bhattarai, Dr. Bishnu Pahari, Keshab Raj Baral and Shashi Kala Baral for constant motivation and support.

Thanks to my supporters Dibyashwori Parajuli Paudel, Kamala Parajuli Bhattarai, Ranjana, Niranjan and Pratikshya for taking care of every detail. Thank you, Anish, Bidhan, Kristina, Aavash, Bhabya, Ashraya, Karun and Kalyan.

To my special ones, Kapila, Aadishree and Aakar, thank you for being there for me.

IIimal
Bergen 2016

SCIENTIFIC ENVIRONMENT

Study performed at:

- Gade Laboratory for Pathology,
  Department of Clinical Medicine,
  Faculty of Medicine and Dentistry, UiB
- Matrix Biology,
  Department of Biomedicine, UiB

Project involved collaborators from:

- Haematology Section, Department of Clinical Science, UiB
- Centre for Clinical Dental Research, Department of Clinical Dentistry UiB
- The Laboratory Animal Facility, Department of Clinical Medicine

Tissue samples obtained from:

- Archived patient material from the tissue archive at Department of Pathology, Haukeland University Hospital, Bergen.
- Fresh patient tissue samples for primary cell cultures received from:
  - Department of Maxillofacial Surgery, Haukeland University Hospital, Bergen, Norway
  - Department of Ear-Nose-and-Throat Surgery, Head and Neck Clinic, Haukeland University Hospital, Bergen, Norway

This study done under the supervision of

The principle supervisor:

Professor Daniela Elena Costea

Co supervisors:

Professor Anne Christine Johannessen and

Professor Donald Gullberg

SUMMARY

Cancer research has provided evidence for several advanced and better ways of treatment, helping the community for a better living. Nevertheless, for head and neck cancer there is still a long way to go for achieving an earlier and a more precise diagnosis and a better, more targeted and less toxic treatment plan, which would ensure a longer survival with a better quality of life for the patients. Research has shown, in the recent years that the tumour microenvironment is an important cluster of players for tumour progression and response to therapy, which can be used for patient stratification and for a better, more efficient therapy.

Head and neck cancer is the eighth most common type of human cancer, squamous cell carcinoma being the most common variant. The number of head and neck cancer cases is increasing worldwide, but particularly in the low-income countries, and mainly for the cases limited to the oral cavity. As an oral cancer lesion progresses, directly or indirectly the environment around is affected, which either promote or try to resist the growth of the tumour. Nevertheless, the specific role of the various components of microenvironment and their importance for tumour prognosis and treatment are still not fully understood. The aim of this study was to determine the expression pattern and the role of integrin α11, a collagen receptor recently associated with the carcinoma associated fibroblast (CAF) phenotype, in oral cancer progression, in order to determine its potential as a biomarker and as a key player for oral carcinogenesis.

The expression pattern of integrin α11 was characterized in patient tumour tissue samples both at protein and mRNA level, and compared with α-SMA, one of a previously established CAF marker of poor prognosis in oral and tongue carcinoma. Our results showed that integrin α11 was overexpressed in the stroma of head and neck cancer compared with normal mucosa and correlated positively with the expression of α-SMA. The differences obtained by analysing the expression of α-SMA at the invasive tumour front (ITF) versus tumour centre (TC) pinpointed the

importance of selection of relevant tumour region, when evaluating a potential biomarker.

Furthermore, the putative biological role of integrin α11 for the development of oral carcinoma was studied in integrin α11 knockout (KO) SCID mice versus wild type (WT) SCID mice, by exposing them to a chemical carcinogen (4NQO) in drinking water. An important role for α11 in the transition from a hyper proliferative stage till a malignant, invasive stage was indicated by the fact that the tumours formed in the KO mice took longer to develop from the oral papillomas and were smaller when compared to the tumours formed in the WT mice.

To study the role of α11 in human oral carcinogenesis, integrin α11 expression was also knocked-down in human oral CAFs by using shRNA constructs. CAFs with knocked-down integrin α11 showed lesser migration, were less efficient in remodelling the collagen matrix and supported a more shallow cancer cell invasion in 3D organotypic cultures when compared to control cells.

For *in vivo* studies, a microenviromentally-induced oral cancer mice model was developed. The use of a luciferase transfected oral dysplastic cell line assisted in the establishment of a non-invasive, yet consistent and more sensitive method of assessment of intraoral tumour progression. Co-injection of integrin α11 knocked-down CAFs the luciferase expressing dysplastic cell line induced smaller and less vascularized tumours than the control CAFs.

Taken together, the results of this work showed that expression of integrin α11 in oral cancer is increased at various levels in the stroma of oral cancer and plays a biological role for tumour progression both by directly affecting the invasive properties of oral cancer cells and by providing a pro-angiogenesis microenvironment.

LIST OF PAPERS

The thesis is based on the following papers

Paper 1.

Himalaya Parajuli, Muy-Teck Teh, Siren Abrahamsen, Ingrid Christoffersen, Evelyn Neppelberg, Stein Lybak, Tarig Osman, Anne Chr. Johannessen, Donald Gullberg, Kathrine Skarstein, Daniela Elena Costea. Integrin α11 is overexpressed by tumour stroma of head and neck squamous cell carcinoma and correlates positively with α-SMA expression.

Submited manuscript

Paper 2.

Salwa Suliman, Himalaya Parajuli, Yang Sun, Anne Christine Johannessen, Anna Finne–Wistrand, Emmet McCormack, Kamal Mustafa, Daniela Elena Costea. Establishment of a bioluminescence model for microenvironmentally induced oral carcinogenesis with implications for screening bioengineered scaffolds.

Head and Neck. DOI 10.1002/HED

Paper 3.

Himalaya Parajuli, Dipak Sapkota, Saroj Rajthala, Ning Lu, Tarig Osman, Salwa Suliman, Emmet Mc Cormack, Evelyn Neppelberg, Stein Lybak, Per Gunnar Liavaag, Anne Christine Johannessen, Donald Gullberg, Daniela Elena Costea. Stromal integrin α11 regulates growth and invasion of oral squamous cell carcinoma.

Manuscript

Other publications during the study period

- Daniela Elena Costea, Allison Hills, Amani H Osman, Johanna Thurlow, Gabriela Kalna, Xiaohong IIuang, Claudina Pena Murillo, IIimalaya Parajuli, Salwa Suliman, Keerthy K. Kulasekara, Anne Chr. Johannessen, Max Partridge.
  Identification of two distinct carcinoma-associated fibroblast subtypes with differential tumour-promoting abilities in oral squamous cell carcinoma.
  Cancer Res. 2013. doi: 10.1158/0008-5472

- Dipak Sapkota, Ove Bruland, Himalaya Parajuli, Tarig Osman, Muy-Teck Teh, Anne Christine Johannessen, Daniela Elena Costea.
  S100A16 promotes differentiation and contributes to a less aggressive tumour phenotype in oral squamous cell carcinoma.
  BMC Cancer. 2015. doi: 10.1186/s12885-015-1622-1.

- Tarig Osman, Himalaya Parajuli, Dipak Sapkota, Israaa Ahmed, Anne Christine Johannessen, Daniela Elena Costea.
  The low-affinity nerve growth factor receptor p75NTR identifies a transient stem cell-like state in oral squamous cell carcinoma cells.
  J Oral Pathol Med 2015, doi: 10.1111/jop.1225

- Salwa Suliman, Kamal Mustafa, Anke Krueger, Doris Steinmüller-Nethl, Anna Finne-Wistrand, Tereza Osdal, Amani O. Hamza, Yang Sun, Himalaya Parajuli, Thilo Waag, Joachim Nickel, Anne Christine Johannessen, Emmet McCormack, Daniela Elena Costea.
  Nanodiamond modified copolymer scaffolds impair tumour progression of early neoplastic oral keratinocytes.
  Submitted Manuscript

ABBREVIATIONS

2D	Two dimensional
3,4 BP	3,4-benzpyrene / benzo(a)pyrene
3D	Three dimensional
4NQO	4-Nitroquinoline-1-oxide
20MC	20-methyl cholanthrene
α11β1 / ITGA11	Integrin alpha11 beta 1 complex (alpha 11)
α-SMA / ACTA2	Alpha smooth muscle actin
BLI	Bioluminescence imaging
BM	Basement membrane
BMA	N-Benzylmethylamine
BOCG	Bergen Oral Cancer Group
BSA	Bovine serum albumin
CIN	Chromosome instability numbers
CAFs	Cancer associated fibroblasts
CD	Cluster of differentiation
DAB	3, 3`-diaminobenzidine tetra hydrochloride
DAF	Dysplasia associated fibroblasts
DIPS	Distribuert Informasjons og Pasientdatasystem i Sykehus
DMBA	9,10-dimethyyl-1,2-benzanthracene
DMEM	Dulbecco's Modified Eagle's Medium
DNA	Deoxyribonucleic acid
cDNA	complementary deoxyribonucleic acid
DOF	Dysplastic oral fibroblast
DOK^{WT}	Dysplastic oral keratinocyte (wild type)
DOK^{Luc}	Dysplastic oral keratinocyte (luciferase transduced)
E-coli	Escherichia coli
ECM	Extracellular matrix
EGF	Epidermal growth factor
EMT	Epithelial to mesenchymal transition
ESA	Epithelial specific antigen
FACS	Fluorescence activated cell sorting
FBS	Fetal bovine serum
FF	Fresh frozen
FFPE	Formalin fixed paraffin embedded
FGF	Fibroblast growth factor
GAPDH	Glyceraldehyde 3-phosphate dehydrogenase
HGF	Hepatocyte growth factor
HIF	Hypoxia-Induced Factor
HNSCC	Head and neck squamous cell carcinoma
HPV	Human papilloma virus
HZ	Heterozygous
ICAM	intracellular cell adhesion molecules

IGF-2	Insulin-like growth factor 2
IHC	Immunohistochemistry
IL	Interleukin
KGF	Keratinocyte growth factor
Ki67	MKI67, proliferation marker
KO	Knockout
LP	Lichen planus
MF	Mitotically active fibroblasts
MIDAS	Metal-ion-dependent adhesion site
MMP	Matrix metalloproteinase
MPF	Irreversible post mitotic fibrocytes
NBMA	N-nitroso-N-methylbenzylamine
NHOM	Normal human oral mucosa
NOFs	Normal oral fibroblasts
NOD/SCID	Non-obese diabetic / severe combined immune deficient
NSG	NOD/SCID IL2γ^{null} mice
OD	Oral dysplasia
OSCC	Oral squamous cell carcinoma
OT	Organotypic tissue culture
PBS	Phosphate-buffered saline
PCR	Polymerase chain reaction
PDGF	Platelet-derived growth factor
PVDF	Polyvinylidene fluoride
RNA	Ribonucleic acid
mRNA	Messenger ribonucleic acid
shRNA	small hairpin ribonucleic acid
RIPA	Radio immunoprecipitation assay RIPA buffer
RGD	Arginine-Glycine-Aspartic acid
RT	Room temperature
SCC	Squamous cell carcinoma
SDS-PAGE	Sodium dodecyl sulfate polyacrylamide gel electrophoresis
SF	Serum free
SM22	Transgellin
SV40	Simian vacuolating virus 40 (Simian virus 40)
TAMs	Tumour associated macrophages
TBST	Tris-buffered saline with tween 20
TE	Tris EDTA (buffer solution)
TGF-β	Transforming growth factor-beta
TNF-α	Tumour necrosis factor α
TP53	Tumour protein p53
VEGF	Vascular endothelial growth factor
WHO	World Health Organization
WT	Wild type

TABLE OF CONTENTS

LIST OF TABLES

LIST OF FIGURES

1 Introduction

1.1 Oral mucosa

Oral mucosa is composed of a stratified squamous epithelium and an underlying connective tissue comprised of lamina propria and submucosa. It is continuous with the skin (vermilion/border of lip), and mucosa of oropharynx. Oral mucosa is classified into 3 main categories based on its functions and histology: lining mucosa (covering the mobile structures of the oral cavity), masticatory mucosa (attached gingiva and hard palate, covering the structures exposed to mechanical forces) and specialized mucosa (tongue mucosa with the taste buds) (Figure 1 & Table 1) [1, 2].

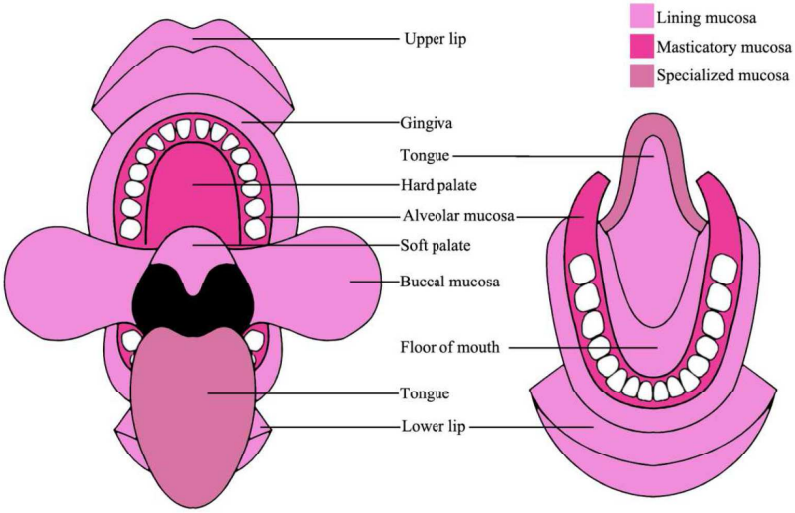

Figure 1: Sketch depicting the distribution of various types of oral mucosa, picture modified from [3]

Lining	***Masticatory***	***Specialized***
Lips, floor of mouth, buccal mucosa, alveolar mucosa		
Soft palate	Hard palate	
Tongue (ventral)	Tongue (dorsal)	
Gingiva		

Table 1: Classification of oral mucosa

1.1.1 Oral epithelium

Oral epithelium is a stratified squamous epithelium. A stratified squamous epithelium consists of, in general, stratum basale, stratum spinosum, stratum granulosum and stratum superficiale (Figure 2). Oral mucosa displays different degrees of epithelial keratinization depending on its function and location, thus the composition of the epithelial layer will vary accordingly and not comply with the general structure of a stratified squamous epithelium. The lining mucosa has to be able to distend and thus is not keratinized, while the masticatory mucosa has to resist to the tearing mechanical forces during mastication and for this it presents various degrees of keratinization. The stratum granulosum is present only in orthokeratinized mucosa (Table 2) [1, 2].

<table>
<tr><th colspan="3">Stratified squamous epithelium</th></tr>
<tr><th rowspan="2">Non Keratinized</th><th colspan="2">Keratinized</th></tr>
<tr><th>Parakeratinized</th><th>Orthokeratinized</th></tr>
<tr><td rowspan="3">Stratum spinosum (2)</td><td>Stratum corneum (retained nucleus) (4)</td><td>Stratum corneum (4)</td></tr>
<tr><td rowspan="2">Stratum spinosum (2)</td><td>stratum granulosum (3)</td></tr>
<tr><td>Stratum spinosum (2)</td></tr>
<tr><td colspan="3">Stratum basale (1)</td></tr>
</table>

Table 2: Layers of stratified squamous epithelium. Number adjacent denotes the layers in Figure 2.

The stratified squamous epithelium is maintained as a result of a balance between the continuous cell proliferation in the basal compartment with consecutive differentiation while the cells move towards the upper layer, and the continuous shedding off of cells from the superficial cell layer. The proliferative property is attributed to the stem cells and the transit amplifying cells in the basal and parabasal cell layers. The newly divided cells generate pressure to push the older and more differentiating cells towards the surface as they also mature. In the keratinized epithelium, when the keratinocytes are approaching the surface, they gradually lose their nuclei and cytoplasmic organelles. After losing the cell contents, they get tightly packed together forming the cornified layer of the masticatory mucosa [1, 2].

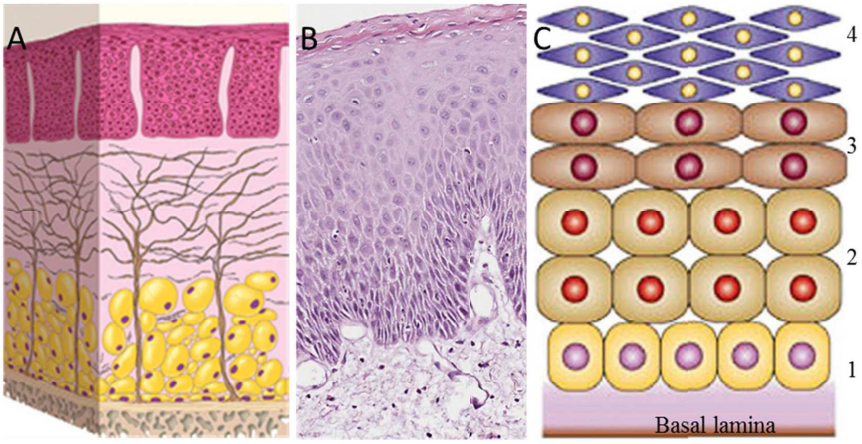

Figure 2: Graphic representation and histological section of stratified squamous oral mucosa. Pictures modified from [2, 4].

1.1.2 Epithelial-mesenchymal interface (basement membrane)

The basal pole of the oral epithelial cell rests on a sheet of amorphous extracellular material known as the basement membrane (BM). It comprises of two layers, the basal lamina and the reticular lamina, and it is composed of type IV collagen (which is unique to basement membranes), tissue-specific laminin isoforms, fibronectin, and heparan sulphate proteoglycans. BM acts not only as a structural support to organize cells, but it also provides a functional input to modulate cellular function. BM acts also as a growth factor reservoir, provides multiple binding sites for cell adhesion molecules and serves as ligands for cell surface receptors. This complex structure initiates intracellular signalling pathways influencing cell behaviour, cellular differentiation and inhibiting or promoting cell proliferation and migration [1]. The important function of the BM in tissue homeostasis is illustrated by rare genetic disorders in which the BM is disturbed, as well as by animal models using gene knockout technology. Some of the diseases related to BM destruction are, for example, Alport Syndrome and Goodpasture Syndrome [5].

1.1.3 Oral lamina propria and submucosa

The oral lamina propria underlying the oral epithelium can be described as having two layers: a superficial, papillary layer between the epithelial ridges, in which the collagen fibres are thin and loosely arranged; and beneath this, a deep, reticular layer dominated by thick, parallel bundles of collagen fibres. Nevertheless, the difference between those two layers is not that obvious as in skin. The superficial lamina propria has the architecture in a form of projections and indentations that contains the terminals and loops of neurovascular bundles aiding the supplies to adjacent avascular structure [1]. The connective tissue of oral mucosa consists, as any other connective tissue, of individual cells (predominantly fibroblasts, adipocytes, microvascular endothelial cells, pericytes, bone marrow derived mesenchymal cells, nerve cells, mast cells, macrophages and some immigrant inflammatory cells like lymphocytes, monocytes and neutrophils) scattered within a three dimensional mesh of macromolecules known as the extracellular matrix (ECM). The macromolecules (collagens, glycoproteins, elastin and proteoglycans) that constitute the extracellular matrix are mainly produced locally by the cells, primarily by fibroblasts. The composition of ECM and the relative amounts of its components determines the properties of tissues, as exemplified by the gingiva covering the hard tissue like bone and teeth. This organization/reorganization has an obvious role in the tissue development as well as active participation in the pathological conditions such as inflammation, tissue repair/wound healing, and tumour invasion and metastasis [6, 7].

Characteristic	***Lining mucosa***	***Masticatory mucosa***	***Specialized mucosa***
Surface	Non cornified	Cornified / parakeratinized	Cornified and non cornified
Submucosa	Loose connective tissue	Dense connective tissue	Loose connective tissue
Fibers	Collagen fibers (low) Elastic fibers (high)	Collagen fibers (high) Elastic fibers (low)	Collagen fibers (medium) Elastic fibers (medium)

Table 3: Differences between the content of fibers of submucosa of different types of oral mucosa Table modified from [1]

1.1.4 Fibroblasts

Fibroblasts are cells of mesenchymal origin. They are elongated, spindle shaped cells present in almost all types of tissues. Fibroblasts express vimentin as a characteristic feature when present in the normal tissue. The fibroblasts secrete and synthesize most of the ECM components such as collagens, proteoglycans and fibronectin. Their cytoskeletal proteins, in association with cell surface integrins and their coordination with the ECM, facilitate fibroblasts' motility as well as the homeostasis of the tissue. Studies using three dimensional co-cultures of fibroblasts with keratinocytes have demonstrated that the fibroblasts are responsible for the formation of basal lamina-anchoring zone [8]. However, fibroblasts are a heterogeneous population of cells, mainly due to their different origin, but also due to their different localization and functions of the organ/area they reside in. The microscopically observed differences were recently backed up by differences between the transcriptome of the fibroblasts residing in different organs/parts of the body [9-11].

There are several studies performed on normal tissues in order to identify putative differences between different fibroblasts types. For example, papillary fibroblasts from the superficial dermis were found to produce less versican but more decorin, in contrast to reticular fibroblasts from deep dermis [12]. Papillary fibroblasts have longer life span in cultures than the cortical fibroblasts from kidney of the rabbit [13]. Oral human fibroblasts from different areas in the mouth differ with respect to their motility pattern. Fibroblasts from periodontal membrane were found to have a low motility when compared to those isolated from the buccal tissue and skin, which had a high motility [14].

Several studies on fibroblast populations from different organs and species have listed the fibroblasts into two different populations as mitotically active fibroblasts (MF) and irreversible postmitotic fibrocytes (PMF). The MF-progenitor fibroblasts have been further classified into MF I, MF II and MF III, subsequently differentiating into PMF. The differences between these types of fibroblasts are described in Table 4.

Fibroblasts express a wide range of genes [9] and several soluble growth factors like interleukin 6 (IL-6), interleukin 8 (IL-8), hepatocyte growth factor (HGF), keratinocyte growth factor (KGF), transforming growth factor-beta (TGF-β), *etc.* These different growth factors act in both autocrine and paracrine manner to maintain tissue homeostasis [15, 16]. Differences in the production level of growth factors have been also described between different fibroblast subtypes. For example, HGF and KGF are produced at higher levels by oral fibroblasts when compared to skin fibroblasts [17]. One study reported increased capacity of oral fibroblasts over skin fibroblasts to organize collagen lattices, suggested to occur due to an increased matrix metalloproteinase-2 (MMP-2) production [18]. Oral mucosal fibroblasts have received considerable attention as they exhibit a preferential scarless wound healing response [19]. There have been published several studies on the hyaluronan involvement in the regulation of a distinct fibroblastic phenotype of oral fibroblasts, indicating that the oral fibroblasts, in contrast to skin fibroblasts, are resistant to TGF-β1 driven myofibroblast differentiation [20]. Our own studies have shown that at least a subset of normal oral buccal fibroblasts is able to respond by increased motility to TGF-β1 treatment [21].

Parameter	***MF I***	***MF II***	***MF III***	***PMF***	***Reference***
Cell division potential	High	Moderate	Low	Negative	[22]
Sa-β-Gal expression	Negative	Very low	Low	High	[23]
Total collagen synthesis	Very low	Low	Low	High	[22]
KGF production	Very low	Low	Moderate	High	[22]
TGFβ1-production	Low	Low	High	High	

Table 4: Fibroblast cell types analysed on the basis of cell biological and biochemical parameters table adapted from [24]

The study of fibroblast function has benefited enormously from their isolation and experimentation on cultures. In this context it is worth mentioning the differences observed between the populations of fibroblasts that are cultured using conventional two dimensional (2D) methods versus those maintained in three dimensional (3D) constructs on a prepared collagen matrix. Among the 3D study models, nested

collagen matrices have been described as a new, better model for the migration of fibroblasts [25]. The 3D matrix-cell culture models have been used to analyse functional and biomechanical features of cell-matrix interactions in normal as well as pathologic conditions. The superiority of the 3D models is now well acknowledged and proved to have the advantages of a well-defined, more *in vivo*-like geometry, the possibility of cell-to-cell interactions by inclusion of different phenotypes of cells, over the limitations of 2D cultures lacking the structural 3D architecture and cellular interactions [26, 27].

1.2 Head and neck squamous cell carcinoma

Head and neck squamous cell carcinoma (HNSCC) is the 8th most common type of human cancer [28]. Squamous cell carcinoma (SCC) is the most common variant of oral squamous cell carcinoma (OSCC) arising from the squamous epithelial cells lining of the oral cavity [28, 29]. There is increasing number of OSCC cases worldwide, but particularly in the low-income countries [30]. When geographical distribution is taken into consideration, there is a greater incidence in the south-Asian countries, especially India, whereas Hungary from Europe, and Brazil from South America are the ones in the front line for the incidence in other parts of the world [28, 31]. Reports from the World Health Organization (WHO) lists tobacco (both smoked and smokeless) and alcohol consumption as the main risk factors, and the condition is worse when these are combined, resulting in approximately 80% of the total OSCC/HNSCC to be attributed to these risk factors in the western world [32]. Other risk factors include areca nut, betel quid chewing, poor oral health, human papilloma virus (HPV) infection [33] and genetic predisposition. The risks factors for OSCC have been categorized as 'established', 'strongly suggestive', 'possible' and 'speculative' factors [29, 34] (Table 5). Most of the risk factors are or can be controlled / restricted, holding the hope that the number of cases can be reduced in the future, but cultural habits are difficult to change and would take a long time before the preventive measures taken today will be reflected in the incidence. Early detection of

OSCC holds the most promising aspect not only to improve the survival of the patients but also to limit the level of disfigurement and improve the quality of life [35]. Despite some progress during the past 20 years, the 5-year survival of OSCC patients has remained poor (50%) [28, 36]. This unsatisfactory result could be ascribed to a high frequency (more than 50%) of locoregional recurrences, presentation of the cases at late stages and to an increasing incidence of distant metastases, usually arising during the initial 2 years after surgery [37]. In addition, the recognized toxic effects of second line treatments indicates a strong need for the development of more efficient cancer therapies, and for this more basic knowledge on the biology of this poorly understood disease is needed.

A multistep model of OSCC development has been proposed and it is supported by the molecular evidence, at least in the cases associated with dysplastic or pre-malignant lesions. Nevertheless, there are oral cancer lesions occurring without the existence of a premalignant lesion and most of pre-malignant lesions do not actually evolve to become malignant. Various malignant transformation risk levels have been published for leukoplakia and erythoplakia, the highest being 36% and 50% respectively. This has been reported to correlate with the severity of the dysplastic changes [38]. Nevertheless, some recent studies have shown that early neoplastic lesions exhibit similar genetic abnormalities as invasive OSCC, leading to early loss of cellular control and phenotype transformation promoting invasion and metastasis [39].

Established	***Strongly suggestive***	***Possible***	***Speculative***
Smoking	Radiation	Viruses	Periodontal diseases
Snuff	Sunlight	Immune deficiency	Mate Drinking
Tobacco chewing		Dentition	Mouth-washes
Alcohol consumption		Ethnicity	
Use of Betel quid			

Table 5: Different categories of risk factors for OSCC. Table adapted from [34]

This substantiates the concept that OSCC development is a complex process, unfortunately not specifically related to a certain pathway or a set of 'drivers' as

identified in salivary gland malignancies, such as, for example, the *MYB-NFIB* fusion that characterizes a subset of Adenoid Cystic Carcinoma and contributes to MYB overexpression [40, 41]. Recent studies have revealed the genetic landscape of HNSCC, identifying a large number of mutated genes [42, 43] as seen in other solid tumours. Genetic alterations are described to occur in oncogenes, tumour suppressor genes and genome stability genes, as classically described [44], but in addition to those, many more other genes also seem to be affected in head and neck and oral cancer, making difficult a stratification of oral cancers based on their molecular profile. So far, the only factor enabling a robust and sensitive stratification of head and neck cancers according to their prognosis is the HPV status, the HPV positive cancers (approximately 20%) having a much better prognosis than the HPV negative ones (approximately 80%). Starting with this separation, a further segregation of HPV negative cases was proposed [45], the HPV^- group being subdivided according to the level of chromosome instability number (CIN) into high CIN (65%) and low CIN (15%) [45] (Figure 3), but this needs further confirmation on other cohorts of patients.

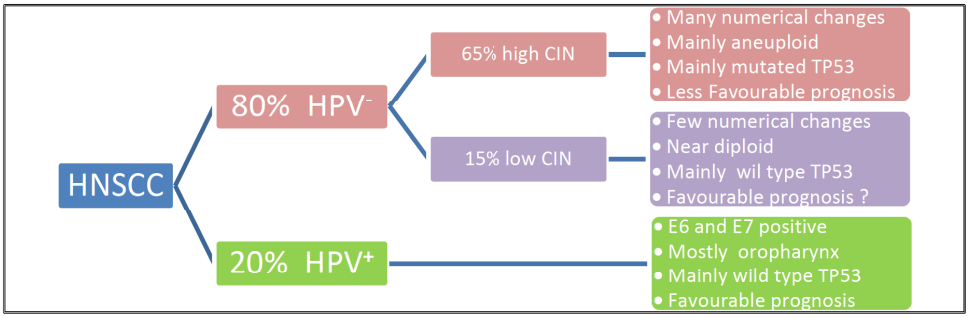

Figure 3: Illustration of the proposed subtypes of HNSCC, Picture modified from [45]

The mutated genes that are associated with cancer development are known as cancer genes. The mutations involved are generally those that confer a selective advantage on the growth and proliferation of cells, as illustrated in Figure 4. Nevertheless, there are also various genes altered in the cancer cells which are not accountable for the cancer development or progression [46, 47].

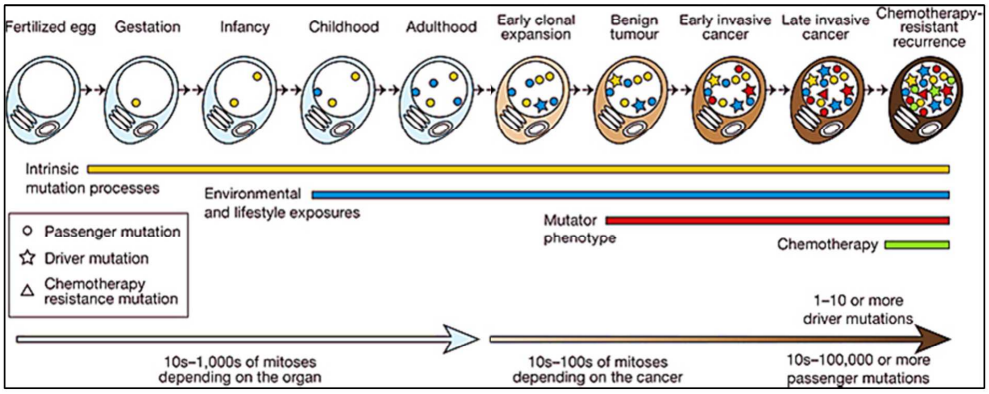

Figure 4: The lineage of mitotic cell divisions from the fertilized egg to a single cell within a cancer, showing the timeline of the somatic mutations acquired by the cancer cell and their contributing processes. Picture taken from [47]

As mentioned, the stepwise model for the development of HNSCC has also been showed at the molecular level, at least in part, molecular analysis showing the development from a patch of tumour protein p53 (TP53) mutated cells to a field of cells with several cancer-related genetic alterations and further to an invasive lesion. Progression of the lesion from the field to carcinoma was shown to involve a number of additional genetic alterations and loss of heterozygosity for chromosome locations 3p, 9p, 8p, 18q. Amplification of 11q13 is also listed as an important step in the progression from a field to invasive HNSCC [48]. This phenomenon has been reported in 70-80% of the oral dysplastic lesions analysed, along with inactivation of the remaining alleles by promoter hypermethylation, representing one of the most frequent and earliest events involved in oral carcinogenesis. In the carcinogenesis process, the loss of heterozygosity of *TP53* has been reported to occur as early as in dysplastic lesions [48-50].

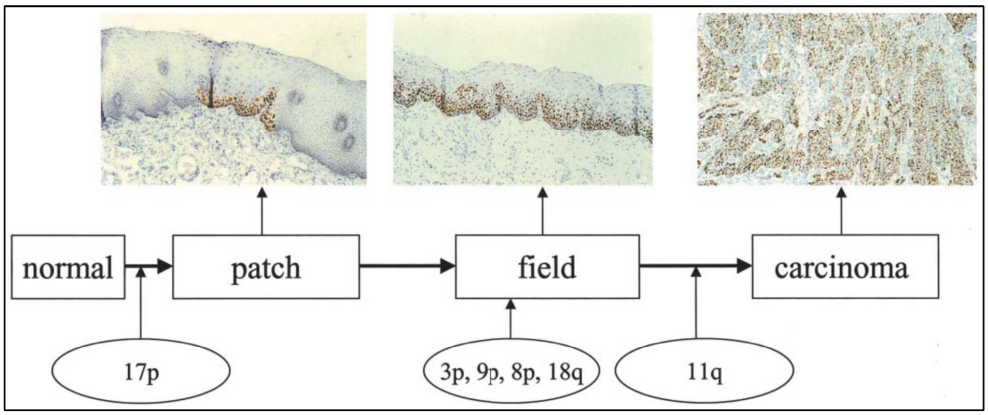

Figure 5: Progression of OSCC, Picture from [48] used with permission

1.2.1 Chemical induction of oral carcinoma

Exposure to high levels of carcinogenic substances in different forms such as alcohol and tobacco (such as benzo-(a)-pyrene and nitrosamines) [51], as well as the ability of *Candida albicans* to transform N-methylbenzylamine (BMA) to N-nitroso-N-methylbenzylamine (NBMA) [52] may lead to development of dysplastic lesions and progress to invasive OSCC under further genetic alternations.

The development of the chemical-induced carcinoma progresses in 3 different stages: initiation, promotion and progression [53, 54]. Chemical carcinogen initiation of the tumour involves the permanent damage of the DNA, which alone is not sufficient for tumour development. After the initiation phase, the promoters or other agents can increase the proliferation as well as development of additional mutations of initiated cells. This promotion phase is reversible at early stages, if the promoter agents (agents that can induce tumours in initiated cells) are eliminated. Promotor agents are not tumorigenic by themselves but have the capacity to add more mutations to the cells [5]. When the initiated group of cells are forced to proliferate and accumulate more mutations, they eventually develop into a malignant tumour [5].

Various chemical carcinogens such as, 3,4-benzpyrene (3,4BP), 9,10-dimethyyl-1,2-benzanthracene (7,12-dimethylbenz[*a*]anthracene) (DMBA) [55], 20-methyl

cholanthrene (20MC) and 4NQO (4-Nitroquinoline-1-oxide)[56, 57] have been used and compared [54, 55, 58] for induction of oral tumours in experimental animals.

Several animal studies have described the multistage development of cancer from dysplasia to OSCC after exposure to carcinogens such as 4NQO and DMBA [55, 59, 60]. As described, many chemicals have been identified to have a carcinogenic potential at different sites and stages [61]. OSCC developed from local or systemic administration of 4NQO has been one of the most representative, robust and well characterized study models of the chemically-induced carcinogenesis [62-64].

The 4NQO animal cancer model has been frequently used in oral cancer studies because of similarity of the pathognomonic features to the cancers caused by carcinogens present in the tobacco, as well as the similar sequential pattern of development when compared to humans [57, 65].

1.2.2 Cancer biomarkers

Early diagnosis and precise treatment of cancer is a key step for a prolonged survival and increased quality of life as well has a great epidemiological impact. A recent report from the U.S. Preventive Services Task Force (an independent volunteer panel of US national experts in prevention and evidence-based medicine) found inadequate evidence that the current methods of oral screening examination accurately detects oral cancer [66]. Also, to date, there are no reliable methods for patient stratification for individualized treatment of OSCC, although several histopathological parameters have been indicated to predict loco-regional spread and overall survival, like tumour thickness, tumour budding and the worst pattern of invasion [67-69]. Since this disease is growing at an alarming rate with new cases annually exceeding a total of 640 000 worldwide, there is an immediate urge for developing reliable and affordable diagnostic tools.

Molecular biomarkers are increasingly recognised as key knowledge to better understand cancer biology, but also to provide earlier and more precise diagnosis, and to assign patients to the best targeted treatment available for avoiding ineffective

overtreatment. A panel of molecular biomarkers for early detection and/or prognostic evaluation of oral cancer have been suggested by several studies [70-76], but apart of HPV screening [77, 78] that is now tested in several clinical trials across Europe and US, none of those markers have entered into clinics [79]. A better selection of biomarkers is required for precise diagnostic and prognostic evaluation leading to better treatment option of OSCCs, but the ever emerging range of biomarkers should demonstrate its efficiency despite the heterogeneity of the tumours.

1.2.3 Biology of cancer

The origin of cancer is considered to be a mutated cell that accumulates several genetic alterations over time. This has been shown by several studies for OSCC [48, 80, 81], as well as for gastric, pancreatic and colorectal carcinomas [82-84]. There have been described several essential traits or hallmarks required for cancer development. These hallmarks of cancer have been originally described as a set of six biological capabilities, organizing and rationalizing the complexities of neoplastic disease. They include: sustaining proliferative signalling, evading growth suppressors, resisting cell death, enabling replicative immortality, inducing angiogenesis, and activating invasion and metastasis [85]. Supporting these hallmarks, later on, genome instability & mutation and tumour promoting inflammation where included. Further, two more 'emerging' hallmarks of cancer were added: deregulated cellular energetics and avoidance of immune destruction [86]. Tumour microenvironment, forgotten for long time, gained again the deserved attention, being included as another dimension adding to neoplastic complexity due to a series of planned concepts/programs through which the normal cells aid in the acquisition of hallmark traits. The identification of these broad planned programs is recognized today and they may bring advancement in the development of new cancer treatment modalities [85, 86].

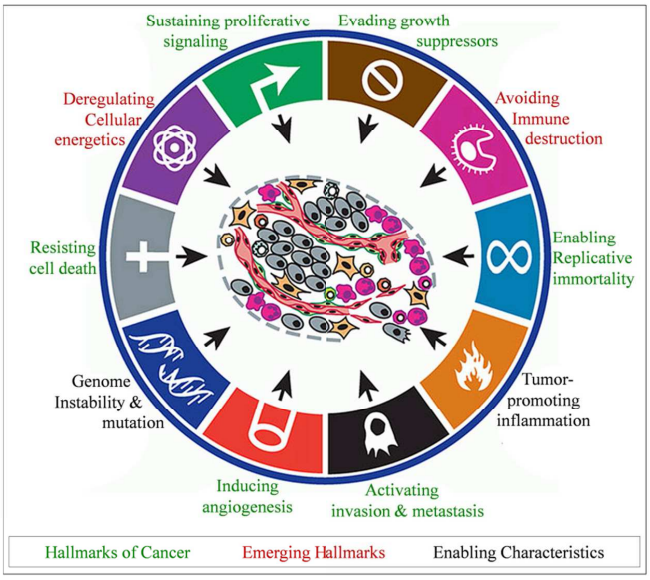

Figure 6: Hallmarks of Cancer Picture from [86]

1.2.4 Tumour microenvironment

The components neighbouring the neoplastic tissue comprise the tumour microenvironment. Several lines of evidence show that the tumour microenvironment is in an activated form, different from the normal homeostasis. The cellular components of the tumour microenvironment were attributed names suggestive of the fact that although not mutated, they are activated and thus different from their normal counterparts, such as for example 'cancer associated fibroblasts (CAFs)' [87], and 'tumour associated macrophages (TAM)', *etc.* [88, 89]. Paget suggested that interaction between seed (cancer cell) and soil (adjoining stromal compartment) is important for metastasis already back in 1889 [90]. Now there are numerous studies supporting Paget's concept that tumour stroma is a key regulator of cancer progression and metastasis, as well as for the response in radiotherapy and patient prognosis [91, 92].

Today there is a large amount of data suggesting that the stromal cells in the tumour microenvironment regulate tumour growth, progression, invasion as well as metastasis.

There is also available evidence for these functions in HNSCC and OSCC [87, 93-95]. The mesenchymal-epithelial cross talk, essential for the maintenance of epithelial tissue homeostasis, is increasingly disturbed during neoplastic progression [93, 96].

1.2.4.1 Cancer associated fibroblasts

Under particular situations such as wound healing, fibrosis or neoplasia, normal fibroblasts tend to change their phenotype to myofibroblasts, which are more contractile in nature [97]. Myofibroblasts display smooth muscle-like features and are a central cell type for wound contraction in the granulation tissue during wound healing [98]. Major factors known to drive myofibroblast differentiation are mechanical tension and TGF-β [99]. In the presence of mechanical stress and TGF-β1 proto-myofibroblasts differentiate into myofibroblasts. Myofibroblasts have been described to possess high migratory ability and to be beneficial to the tissue in the repair process. The origin of myofibroblasts is still a debated issue, but evidence shows that not only fibroblasts but also other precursor cells present in the ECM such as endothelial cells, hematopoietic cells, and pericytes can transdifferentiate and assume a myofibroblast phenotype [100, 101]. *De novo* expression of alpha smooth muscle actin (α-SMA) is the main and most used molecule to characterize the myofibroblasts [98, 102]. Nevertheless, CAFs are a very heterogeneous population, and there are several different markers used for their identification. The fact that CAFs might have a different origin might explain their heterogeneity. The wide spread heterogeneity of the CAFs as compared to the dysplastic oral fibroblasts (DOFs) and normal oral fibroblasts (NOFs) has also been described by microarray studies [21]. Transdifferentiation of NOFs towards a myofibroblastic phenotype has been described to be the key step in the activation of the stroma, and it was shown to be driven by IL-1, TNF-α, PDGF, FGF, TGF-β [103] as well as integrin α11β1 [104]. Among these, TGF-β has been listed as the most important factor involved in the development of myofibroblasts [105, 106].

It has been shown that one way the fibroblasts could aid to the OSCC invasion is by the formation of tracks in the extracellular matrix, within which the oral carcinoma cells invade, merely following the fibroblasts [94]. Higher number of myofibroblasts at the invasive front of tumour stroma has been also shown to be associated with poor prognosis in colorectal cancer [107], breast cancer [108] as well as in OSCC [109, 110]. Nevertheless, some studies have shown contrasting results, namely that depletion of α-SMA from the myofibroblasts in an *in vivo* model would increase the aggressiveness of the tumour in pancreatic cancer [111, 112], indicating that other fibroblast sub-populations might be also of importance for cancer progression, especially in absence of myofibroblasts. In addition to a TGF-β response signature of CAFs in OSCCs, we have also recently demonstrated an up-regulation of integrin α11 expression in CAFs as compared to the fibroblasts derived from normal mucosa [21].

Multiple studies have addressed the role of integrin family in myofibroblast differentiation [113-115]. Integrin α11-mediated stimulation of myofibroblast differentiation has been studied and shown in cultured fibroblasts, diabetic cardiomyopathy and during excisional wound healing [116-118].

Expression of integrin α11 has been reported in the tumour stroma of non-small cell lung cancer, where it has been suggested to play a role in progression and metastasis of non-small cell lung cancer [119, 120], but its role on development and progression of OSCC is not known, although we have shown that it is overexpressed in the CAFs derived from OSCCs as well [21].

1.2.4.2 Inflammatory components of tumour microenvironment

Presence of lymphocytes, macrophages, leucocytes, dendritic cells and neutrophils in the stromal component is regarded as the inflammatory microenvironment. Already back in 1863 Rudolf Virchow observed and described the presence of leucocytes as "lymphoreticular infiltrate" in relation to the origin of cancer at sites of chronic inflammation [88, 121]. On average, 15 to 20% of the cancer incidences are linked to infectious diseases such as gastric cancer from *Helicobacter pylori* induced gastritis

[122], cervical cancer with history of cervical infection with human papillomavirus (HPV) [123], hepatocellular carcinoma developed from hepatitis virus B and C infection, *etc.* indicating the importance of inflammation for development of malignancies.

Tumour-associated macrophages (TAMs) are one of the major inflammatory components found in tumours [89]. Circulating monocytes are the precursors of TAMs and are directed by chemoattractant cytokines (chemokines) into or towards the tumour tissue. There have been studies that reported the TAMs infiltration association with the vascularity and prognosis. A reduced amount of TAM infiltration has been associated with better prognosis in OSCC [124] and breast cancer [125, 126], whereas improved survival has been related with the TAMs infiltration along the tumour front in colon [127], prostate [128], and lung cancer [129]. The contrasting results might be related to the fact that TAMs can assume two different phenotypes, a pro-inflammatory phenotype (M1) and an anti-inflammatory phenotype (M2), and a simple analysis of TAMs based on CD68 expression only, as the majority of the mentioned studies did, does not provide information on whether the infiltrate is of M1 or M2 type.

Macrophages of the M1 or M2 type have the unique ability to metabolize arginine to nitric oxide (killer molecule) or ornithine (repair molecule), respectively [130]. The *in-vivo* studies have shown that M1 and M2 macrophages stimulate a TH1 or TH2 response [130]. T helper cells will assume a TH1 or a TH2 phenotype depending on their cytokine environment [131]. T lymphocytes mainly infiltrate into the invasive tumour front and draining lymphoid organs, whereas B lymphocytes although present on both the locations, are more common in draining lymph organs adjacent to tumour microenvironment. The $CD8^+$ memory T cells seem to be associated with good prognosis and are supported by $CD4^+$ T helper cells (TH1). Other $CD4^+$ cell populations, TH2 and TH17 cells, support a B cell response and have a tumour promoting action [132]. Although the $CD4^+$ cells have been associated with poor

prognosis, studies have shown that they are associated with favourable results in breast cancer with TH2 cells and in oesophageal cancer with TH17 cells [133].

1.2.4.3 Vascular components

In contrast to the physiological condition, except for the process of embryogenesis and wound healing, the angiogenic switch is always activated in case of tumour development. The activation of the angiogenic switch leads to sprouting of new vessel from the existing vessels, in order to support the growth of the tumour mass [134]. Vascular endothelial growth factor (VEGF) is an inducer of angiogenesis, and its expression is triggered by the hypoxic condition in the tumour mass (*HIF-1α*), as well as by oncogene signalling [134-136]. The process of neo-vascularization has been associated with the early adaptation and reorganization of the pericytes that are the supporting structure for the endothelium [137]. VEGF has been shown not only to initiate angiogenesis and tumour progression, but also to be involved in immune tolerance and immune suppression [138]. Angiogenesis is directly related to the poor clinical outcome in different studies of breast [139, 140], prostrate [141] and oral cancer [142].

In addition to the VEGF family, the fibroblast growth factor (FGF) and insulin growth factor (IGF) families are also important factors for tumour angiogenesis. Both FGFs and IGFs play a significant role in the physiology of endothelial cells by promoting migration and tube formation. These actions are mediated by the IGF1 and IGF2/mannose 6-phosphate receptors in the case of IGFs, and by FGF2 in the case of FGFs. IGFs were also shown to increase the number and function of endothelial progenitor cells. IGFs were found to promote angiogenesis, and dysregulation of the IGF system may contribute to this process in cancer [143]. Deregulation of FGFR signalling through genetic modification or overexpression of the receptors (or their ligands) has been also observed in numerous tumour settings, the FGF/FGFR axis playing a key role in driving tumour angiogenesis [144].

1.3 Tissue matrix and cell communication

Three dimensional mesh-works of macromolecules with all the connective tissue content and cells are known as the extracellular matrix (ECM). The interaction between the cells and the matrix takes place by different aspects of communication. The cell adhesion between cells and the extracellular matrix contribute to maintain normal cell functions [6]. In addition to cell adhesion, autocrine, paracrine and endocrine signalling through soluble mediators bring also a flow of information to the cells through different cell receptors such as ion-channel linked, G-protein linked, enzyme linked receptors and integrins [6].

1.3.1 Integrins

Integrins are heterodimeric transmembrane receptors which are formed by combination of two different polypeptide chains. There are 24 heterodimers of integrin known till date and these are formed by different combination of 18 α and 8 β subunits [145, 146]. These combinations are non-covalently associated [147]. Each of these heterodimers has specific ligands to bind with, such as collagens, fibronectin, laminins, fibrinogen. In addition, some integrins bind to the cell surface proteins [6, 145].

Integrins are transmembrane receptors which contain an extracellular domain, a short transmembrane domain and an intracellular cytoplasmic tail. The arrangement/structure of the integrin physically links the cytoskeleton between the cells as well as cell cytoskeleton to the ligands on a cell surface (like vascular cell adhesion molecule) and ECM glycoproteins (like collagen, laminins, and fibronectin). A subset of integrins binds to cell surface proteins present on other cells, including the intracellular cell adhesion molecules (ICAM) family [6, 145, 148].

The integrin extracellular domain is a large and organized structure of several subdomains forming a globular ligand binding N-terminal continuous with C-terminal legs, connecting the transmembrane domain. The transmembrane domain is a single span α-helical coil. The cytoplasmic domains are generally short and unstructured.

Integrins are involved in various cellular signalling pathways as well as extracellular matrix reorganization, manipulating/affecting different cellular and tissue functions such as cell proliferation, cell adhesion, cell migration, cell differentiation as well as apoptosis. Integrins have the potential to signal bi-directionally both 'inside-out' and 'outside-in' signalling across the membrane [6].

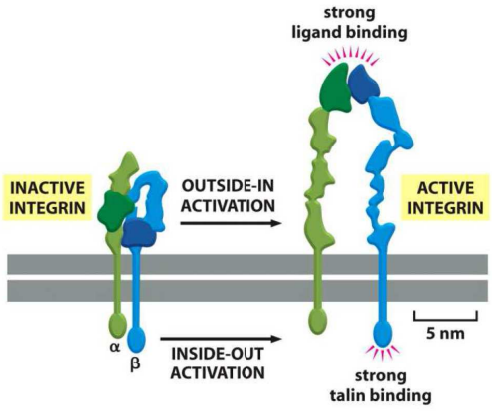

Figure 7: Inactive and active stages of integrin, and demonstration of inside out and outside in signalling. Picture used from [6]

It is the α subunit of the integrin heterodimers that determines the ligand-specificity. Out of 18, 9 α chains contain αI domain, which includes the α chains of collagen receptors (α1, α2, α10 and α11) and α chains of leucocyte receptors, which pair with β7 and β2 (αE, αD, αL, αM and αX). This αI domain is essential for ligand binding and it contains the metal-ion-dependent adhesion site or MIDAS motif [149]. If the α chain does not contain an αI domain, the β chains that will pairs with the α chain would have to contain an αI domain like region which will then take part in ligand binding[150].

Integrin subunits in pairs across the membrane are folded and close to each other in the inactivated state. In response to ligand binding, or in response to an activation signal from inside/outside of cells, the integrin is activated, leading to unfolding of the extracellular domains and separation of cytoplasmic tails as illustrated in Figure 7 [6].

1.3.2 Classification of integrins

Integrins are classified according to their receptors' specificity and are dependent on the extracellular domains of their subunits, mainly collagen receptors, leucocyte receptors, RGD receptors, and laminin receptors. The various combination of α and β chains are shown in Table 6.

Receptors	α and β chain combinations			
Collagen	*α1β1	*α2β1	*α10β1	*α11β1
Leucocyte	α4β1	α9β1	α4β7	*αEβ7
	*αDβ2	*αLβ2	*αMβ2	*αXβ2
Laminin	α3β1	α7β1	α6β1	α6β4
RGD	α5β1	α8β1	αVβ1	αIIbβ3
	αVβ8	αVβ6	αVβ5	αVβ3

Table 6: 24 Different combinations of α and β chains of integrin family with respective receptors (α subunit with I-domain).*

1.3.3 Integrin α11β1

Human *ITGA11* is localized on chromosome 15q23 (Figure 8) and contains 30 exons and 29 introns. Integrin α11β1 belongs to the collagen type I binding receptor group of integrins, although it also binds to collagen IV with lower affinity [151, 152]. In *in vitro* studies α11 have been localized at focal contact of the cells in culture [151], mediating events such as adhesion and cell migration on collagen, as well as collagen gel contraction. Initially it was named $\alpha_{mt,}$ as it was identified in human fetal myotubes in culture [153]. Later, in 1999, its asscciation with β1 was described [154]. Its involvement in collagen reorganization and cell migration as a collagen receptor was described in 2001 by transfecting α11β1 in a C2C12 cell line [151]. This integrin migrates as a band at 155kDa in Sodium dodecyl sulphate polyacrylamide gel electrophoresis (SDS-PAGE) under non-reducing condition and encodes the mature protein of 1166 amino acids [154].

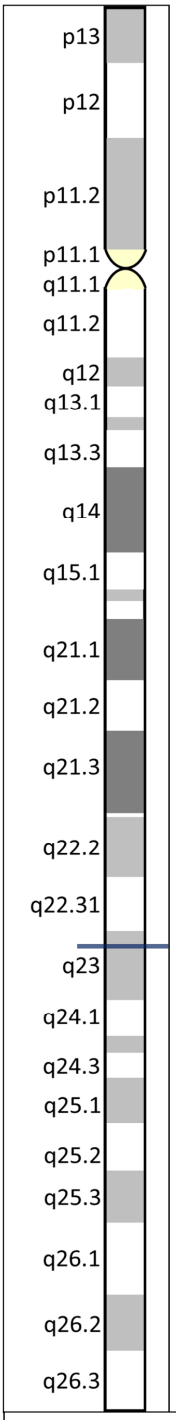

Figure 8: Position marked for ITGA11 in human Chromosome no 15

After the development of the genetically modified α11 knockout mice, dwarfism was observed as an important feature over the wild type phenotype. Studies over these phenotypes demonstrated the role of α11β1 in reorganization of extracellular matrix, leading to incisor eruption defect as well as thickening of periodontal ligament in $\alpha11^{-/-}$ mice [151, 155]. This defect in the development of the incisors is suggested to contribute to the malnutrition and increased mortality observed in the $\alpha11^{-/-}$ mice[155].

In addition to the various soluble components/factors affecting myofibroblast differentiation, the role of some integrins for myofibroblast differentiation have been clarified [113-115]. Recently the ability of certain RGD-binding integrins to activate TGF-β to affect myofibroblast differentiation has received considerable attention [156, 157]. Although indicated by several *in vitro* studies, the role of integrin α11 in myofibroblast differentiation is unclear. Stimulation of myofibroblast differentiation by integrin α11 has been studied in cultured mouse and human fibroblasts [117] and in diabetic cardiomyopathy in a rat model [116]. Recently, integrin α11β1 was shown be mediating the contraction of granulation tissue in excisional wounds [158].

It is possible that a major function of α11β1 in the stromal compartment is to reorganize the collagen matrix and change mechanical properties to allow for myofibroblast differentiation. A recent study in breast cancer has listed α11β1 as one of the highly expressed gene in trailblazer cells and showed that α11β1 was required to initiate collective invasion [159].

1.4 Rationale for the present study

Recent microarray based studies at Bergen Oral Cancer Group (BOCG) identified integrin α11 as one of the significantly over expressed molecules by oral CAFs [21]. Studies on other types of carcinomas showed a relationship between expression of α11 by carcinoma-associated fibroblasts and cancer progression [119, 120, 159]. To date, the biological role of integrin α11 in oral carcinogenesis and whether it can be used as a marker of CAFs in OSCC and as a predictor factor for clinical outcome of oral cancer and pre-malignant lesions have not been studied so far.

2 Aim

The general aim of this study was to identify the role of integrin α11 in oral carcinogenesis.

2.1 Specific Aims

1. To detect the presence of α11 in tumour stroma of head and neck squamous cells carcinoma and examine its correlation with tumour growth clinicopathological parameters and patient outcome.
2. To establish a method for bioluminescence imaging of microenvironmentally-induced oral cancer for detection and evaluation of oral carcinogenesis.
3. To examine the role of integrin α11 in oral cancer development by employing integrin α11 knock-down CAFs and KO mice models.

3 Methodological considerations

3.1 Choice of methods

We identified integrin α11 as one of the top upregulated genes in the microarray data from cultured CAFs isolated from OSCC patients, when compared with dysplasia associated fibroblasts (DAFs) or NOFs [21]. Many studies have described the activation of CAFs and their transdifferentiation towards a myofibroblastic phenotype. As a result, α-SMA emerged as a marker to be used for the detection of CAF, but its universal use for identification of all CAF subpopulations is still debated, and there is a need for a better marker for CAFs. With its specific upregulated expression in CAFs isolated from OSCC, integrin α11 seemed to be a very good candidate for a novel, more specific CAF marker. For this purpose we first examined the patient material to check if our microarray data obtained from cultured CAFs were representative for the changes in the stroma of the OSCC patients (Table 7: Study Outline). We have examined both protein and mRNA levels of integrin α11 on the tissue samples available at our department. The limitation of the integrin α11 antibody [154] was that it could not be used on the formalin fixed paraffin embedded (FFPE) samples. Fresh frozen (FF) samples, containing only tumour centre (TC) were used for immunohistochemistry for both α11 and α-SMA antibodies, but FFPE samples, which contained both the TC and the invasive tumour front (ITF) could be used only for α-SMA staining. In parallel, the FF samples were used to determine the level of respective gene expression on those tumour tissue samples by qPCR. (Paper I)

Having validated the over-expression of integrin α11 on HNSCC patient samples at both mRNA and protein levels, we wanted to examine the potential functional role of integrin α11 in oral carcinogenesis, for this we have used both *in vitro* and *in vivo* models in which the level of α11 expression was knocked-down (KD).

Animal models have been extensively used in different studies in order to identify the complex biological aspects of the cancer disease, despite of their difference in tissue

response and reactions when compared to humans. For our studies on stromal-tumour cell interactions, we had thus to establish a robust microenvironmentally-induced oral cancer model. In addition, we wanted to develop a model that avoids the difficulty and errors of the manual measurement of the tumour lesions in the tongues of mice. Thus, we have first developed a non-invasive, yet sensitive microenvironmentally-induced oral cancer model that uses the method of bioluminescence in order to quantify tumours in the animal model (Paper II).

Specific shRNAs targeting ITGA11 were designed and the endogenous level of integrin α11 was knocked-down in order to study the effect of α11 on different aspects of oral tumorigenesis (Paper III).

In addition, we did also used a syngeneic model of chemically induced tumour development in $\alpha11^{+/+}$ (wild type) (WT), $\alpha11^{-/-}$ (knockout) (KO) and $\alpha11^{+/-}$ (heterozygous) (HZ) mice (Paper III).

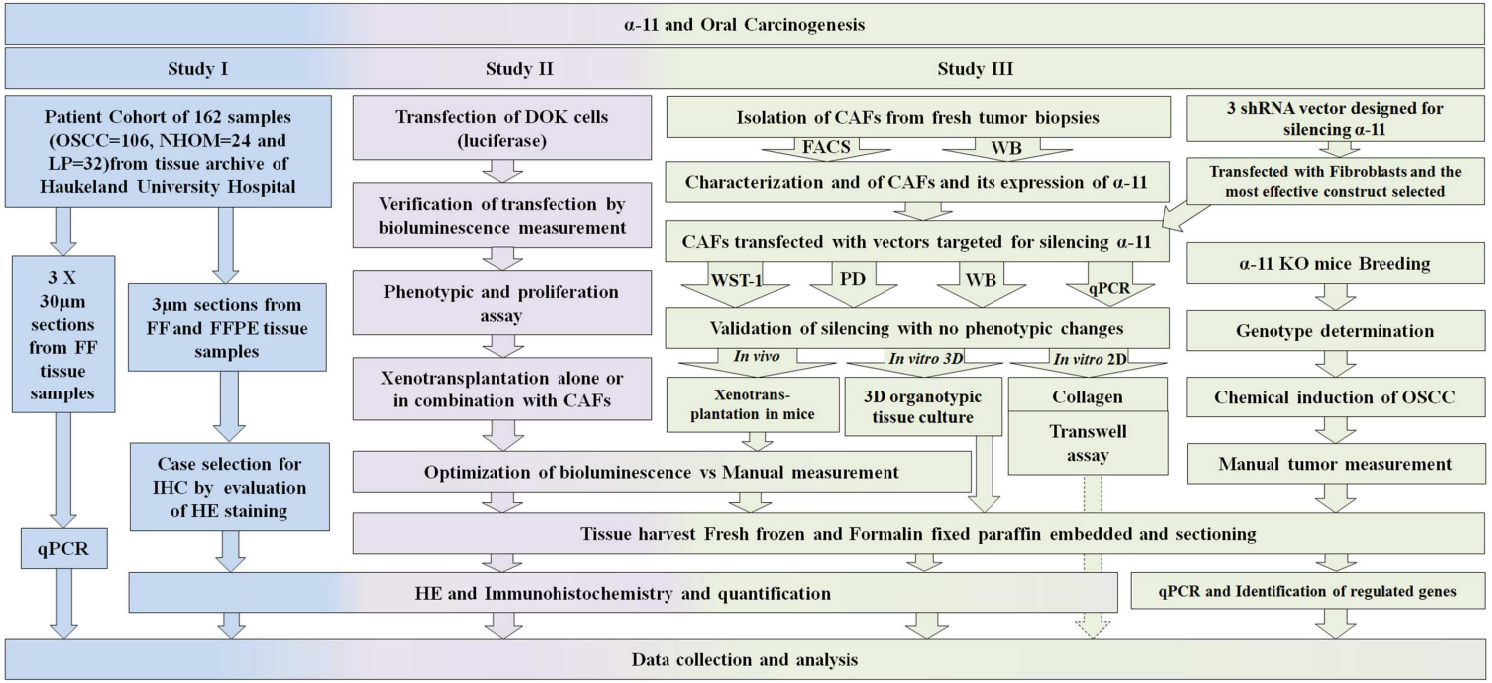

Table 7: Study Outline

3.2 Clinical cohort

FFPE and FF samples of normal human oral mucosa (NHOM) from healthy volunteers (n=10), patients with oral lichen planus (LP) (n=32), oral dysplasia (OD) (n=5), and OSCC (n=106), with clinicopathological data (age, sex, date of birth, date of diagnosis, cancer status, tumour size, node involvement, date of recurrence, date of metastasis, date of death, relation of death to cancer etc.) were obtained from the diagnostic bio-bank at Department of Pathology, Haukeland University Hospital, and from the patient journal system (DIPS), Haukeland University Hospital with informed consent after approval from Regional Medical Ethical Committee (2010/481/REK vest).

FFPE samples were sectioned at 3 microns thickness; sections were collected on super frost glass slides and incubated for 24 hours at 60˚C and stored at 4˚C for further use.

FF samples were sectioned at 4 microns thickness. Electrostatical retrieval of the cut section was done on glass slide at room temperature (RT). Slides were left at room temperature for 5 minutes and transferred to -20˚C for immediate use, the remaining slides were packed in small boxes and stored at -80˚C for future use. Likewise, 3 cryo sections of 30 microns thick, sectioned from each frozen samples were preserved in RNA Later (Ambion, Applied Biosystems, Warrington, UK) prior to mRNA extraction. These preserved samples were used for respective methods as explained further.

3.2.1 Immunohistochemistry (IHC)

Three microns thick FFPE samples were deparaffinised in xylene for 30 minutes and rehydrated in decreasing alcohol gradient. Epitope retrieval for FFPE was performed either by microwave heating or by incubating with Proteinase K at RT. FF sections were fixed in ice cold acetone 50% for 30 seconds, followed by 100% ice cold acetone for 5 minutes.

Tissue preservation	*FF Samples*	*Both FFPE and FF Samples*	*FFPE Samples*				
Species	**Human tissue samples**		**Mice tissue samples**				**3D OT tissue samples**
Primary antibodies	α11 [154]	Monoclonal, α-Smooth Muscle (α-SMA) (Sigma A2547)	Cytokeratin DAKO	EGFR (DAKO M3563)	Ki67 (DAKO M7240)	Factor VIII (DAKO A0082)	Cytokeratin DAKO (M0821)
Antigen retrieval		Proteinase K, DAKO REAL™		Tris EDTA pH 9		Proteinase K, DAKO REAL™	
		5 minutes at RT		Microwave till boiling and continue cooking for 15 minutes		15 minutes at RT	5 minutes at RT
Primary antibody concentration	1/2000, 60 minutes at RT	1:2000, 60 minutes at RT	1:50, 60 minutes at RT	1:50 Overnight at 4˚C	1:25, 60 minutes at RT	1:1200, 60 minutes at RT	1:400, 60 minutes at RT
Secondary antibody	DAKO Envision '+' 30 minutes at RT						
Chromogen DAB DAKO	2 minutes	2-3 Minutes	3 minutes	10 Minutes		5 Minutes	2 Minutes

Table 8: Immunohistochemistry

After that, all the procedures were similar for both FF and FFPE samples as explained. Details for different antibodies and conditions are listed in Table 8. Blocking of unspecific binding was done for 30 minutes in the humidity chamber at room temperature with 10% Goat Serum (DAKO, Golstrup, Denmark) in 3% bovine serum albumin in phosphate buffered saline (PBS) (Sigma, US). The slides were then treated with primary antibody. Endogenous enzyme activity was blocked using peroxidase block (DAKO) for 5 minutes. The slides were treated with Secondary Antibody EnVision+ kit (DAKO) for 30 minutes at room temperature. All the steps as required were performed in the humidity chamber. The bound reaction was visualized using 3, 3`-diaminobenzidine tetra hydrochloride (DAB, DAKO). Finally, the slides were mounted using Eukit (O. Kindler GmbH & Co, Freiburg, Germany) after counterstaining them with haematoxylin and dehydrating over increasing alcohol gradient.

Antibody diluent was used for negative controls. Positive staining of blood vessels for α-SMA was used as internal positive control. A competitive blocking IHC using human integrin α11 peptide (NH2-) CRREPGLDPTPKVLE (-COOH) (INNOVAGEN AB, Lund, Sweden) was performed for validation of the specificity of the integrin α11 antibody.

Double immunostaining for α11 and αSMA was performed using a double stain kit (Envision G|2 double stain system, DAKO) following the manufacturer's instructions on FF sections only.

Evaluation of the staining for the patient samples for study was done blinded with clinical information. After series of discussion for the calibration under Leica DMLB microscope (Leica Microsystems) at 200X magnification between 5 independent observers protocol for quantification was established, as listed below:

- The percentage of the cells stained as:
    - Score 0 = 0-5%
    - Score 1 = 5-25%
    - Score 2 = 25-75%
    - Score 3 = more than 75%

- Position pattern of the stained fibroblasts on the stromal compartment as:
    - Spindle or Network Pattern
- Heterogeneity of the fibroblast staining
    - Homogenous or Heterogeneous

After the calibration, all the readings/observations were done individually by two independent observers and discussed over for the appropriate final scores for the ones in conflict.

3.2.2 RNA extraction and qPCR

Thirty microns thick sections from the archival frozen human tissue were pseudo-anonymized and tested blindly to ensure that the assays were performed objectively. These samples preserved in RNA Later (Ambion, Applied Biosystems, Warrington, UK) were digested with nuclease-free proteinase K at 60ºC prior to mRNA extraction. RNA was extracted using the RNeasy kit (Qiagen, Valencia, CA, USA) and total RNA was quantified and its quality determined spectrophotometrically with the Nano drop 1000 Spectrophotometer (Wilmington, DE, USA). Only samples with 260/230 ratio: >1.8, 260/280 ratio: >1.8 were used for the single-gene assays. Following manufacturers' instructions, 200-300 nanograms of total RNA was converted to cDNA (Transcriptor cDNA kit, Roche). qRT-PCR amplifications for *ITGA11* and *ACTA2* were performed on the LightCycler 480 qPCR system (Roche) using LightCycler® 480 Probes Master (#04707494001, Roche). Comparative $2^{-\Delta\Delta Ct}$ method was used to quantify the relative mRNA expression. GAPDH and ACTB were used as endogenous controls.

Similarly following manufacturers' instructions, total RNA from CAF1 cells and 4NQO-induced tongue tumours from mice (n=12) was extracted using RNeasy fibrous tissue mini kit protocol (Qiagen Inc., Valencia, CA, USA). Quantity and purity of the extracted RNA was checked using NanoDrop spectrophotometer (NanoDrop technologies, Inc., Wilmington, DE, USA).

3.2.3 Protein extraction and Western blot

Fibroblasts in culture were washed two times with cold PBS, lysed with RIPA buffer supplemented with protease and phosphatase inhibitors (Sigma Aldrich P8340 and P5726). Cell lysate was centrifuged at 4˚C at 13000rpm and protein concentration was measured using bovine serum albumin (BSA) protein assay (Bio-Rad).

Twenty-five µg of protein in 1X laemmli sample buffer (Bio-Rad) was separated using 6% polyacrylamide gel. The separated protein was transferred to Polyvinylidene fluoride (PVDF) membrane (Hybond-P, GE healthcare, RPN2020F) by wet electroblotting. Blocking of the membrane was done with 5% non-fat dry milk (Bio-Rad (170-6405) in tris buffered saline-tween (TBST), Membrane was immunoblotted with polyclonal rabbit anti human α11 antibody (1:1000). Anti-GAPDH (AB 9484, Abcam, Cambridge, UK, 1:5000) was used as a loading control. Membrane was visualized on KODAK Image Station 2000R (Eastman Kodak Company, Rochester, NY, USA) using enhanced chemiluminescence reagent (Supersignal® West pico or Supersignal® West femto; Pierce Biotechnology, Rockford, IL, USA).

3.3 In vitro studies

3.3.1 Media formulation and the cells used in the study

Constituents	*Volume*	*Firm*	*C. No.*
Fibroblast medium (fibroblasts) and phoenix medium (Phoenix-A cells)			
Dulbecco's Modified Eagle's Medium High Glucose (DMEM)	445 ml	Sigma	D6429
Fetal Bovine Serum (FBS)	50 ml	Invitrogen	10270-106
Antibiotic Antimycotic	5 ml	Invitrogen	15240-062
Total Volume	500 ml		
FAD Medium			
Dulbecco's Modified Eagle's Medium/ Nutrient Mixture F-12 Ham	440 ml	Sigma	D8437
Fetal Bovine Serum	50 ml	Invitrogen	10270-106
Antibiotic Antimycotic	5 ml	Invitrogen	15240-062
Insulin transferrin (100X)	250 µl	Gibco	41400-045
Ascorbic acid (Stock prepared 50mg/ml in DMEM)	500 µl	Sigma	A7631
Hydrocortisone (Stock prepared 500µg/ml in DMEM)	400 µl	Sigma	H0888
EGF (stock prepared 10µg/ml)	500 µl	Sigma	E4269-1mg
Total Volume	500 ml		
FAD-OT Medium			
Dulbecco's Modified Eagle's Medium/ Nutrient Mixture F-12 Ham	484 ml	Sigma	D8437
Bovine Serum Albumin 7.5%	6.66 ml	Invitrogen	10270-106
Antibiotic Antimycotic	5 ml	Invitrogen	15240-062
Insulin transferrin	250 µl	Gibco	41400-045
Ascorbic acid (Stock prepared 50mg/ml in DMEM)	500 µl	Sigma	A7631
Hydrocortisone (Stock prepared 500µg/ml in DMEM)	400 µl	Sigma	H0888
EGF (stock prepared 10µg/ml)	500 µl	Sigma	E4269-1mg
Total Volume	500 ml		
DOK Medium			
Dulbecco's Modified Eagle's Medium Low Glucose (DMEM)	440 ml	Sigma	D6046
Fetal Bovine Serum	50 ml	Invitrogen	10270-106
Antibiotic Antimycotic	5 ml	Invitrogen	15240-062
Hydrocortisone (Stock prepared 500µg/ml in DMEM)	5 ml	Sigma	H0888
Total Volume	500 ml		
ECGM-2 Medium			
EBM-2 Basal Medium with Fetal Calf Serum (5%), Epidermal Growth Factor (5 ng/ml), Basic Fibroblast Growth Factor (10 ng/ml), Insulin like growth factor (20 ng/ml), Vascular Endothelial Growth Factor (0.5ng/ml), Ascorbic Acid (1µg/ml), Hydrocortisone 0.2µg/ml)	500 ml	Lonza	EGM-2 MV BulletKit (CC-3156 & CC-4147

Table 9: Media formulations for cells in culture, Henceforth only the medium nomenclature is used for the combination

Normal fibroblasts	*Cancer associated fibroblasts*	*Dysplastic cell line*	*Cancer cell line*	*Endothelial cell line*
NF208	CAF1	DOK [160]	Ca1	HPEAC (Promocell)
NF231	CAF4		LuC4 [161]	
NOF10	CAF11		CaLH3 [162]	
NOF11	CAF15			
SF4 (Skin Fibs)				

Table 10: List of cells used in the study

3.3.2 Sample collection and primary cell extraction

Following the ethical approval by the Ethical Research Committee of Western Norway, and with informed consent, OSCC patient samples were collected and transported in transport medium (DMEM+10% Antibiotic Antimycotic), minced in pieces and allowed to adhere on the tissue culture dishes, after the attachment of the tissue bits, these were incubated and cultured in FAD medium 37˚C in presence of 5% CO_2.

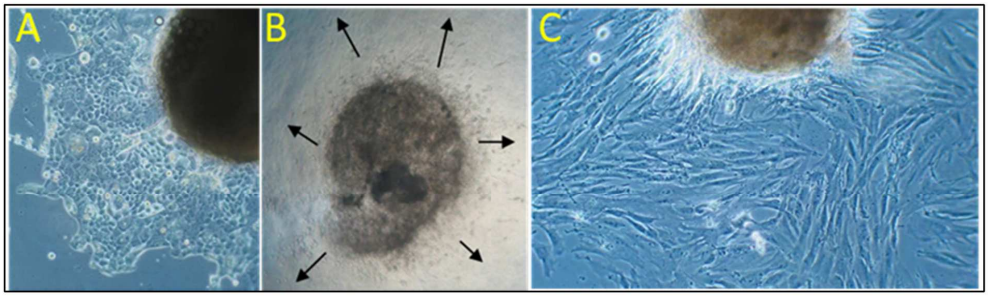

Figure 9: Tissue explants in culture. (A) outgrowth of keratinocyte, (B) Tissue explant and (C) outgrowth of fibroblasts

The culture medium was replenished in regular interval for weeks. Fibroblasts growing out from the explants were harvested separately from the other cells in the culture plate with the help of clonal rings after morphological assessment. Isolated cells were further propagated and were characterized using linage specific markers (absence of epithelial cells (ESA), endothelial cells (CD31) [163], leukocyte common antigen (CD45) [164] and presence of mesenchymal cell markers for pericytes and mesenchymal stem cells (CD146) [165], platelet derived growth factor for mesenchymal cells (CD140b)) (all from BD biosciences NJ USA).

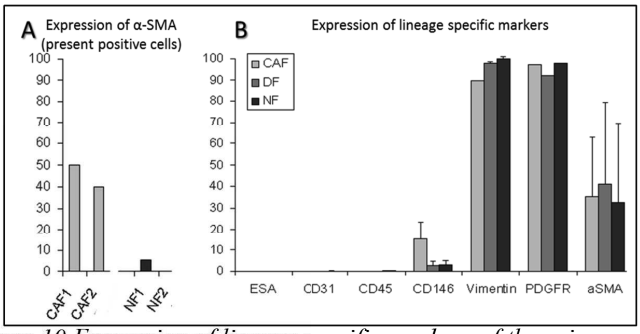

Figure 10 Expression of lineage specific markers of the primary cells

The selected fibroblast strains were immortalized by Simian vacuolating virus 40 (Simian virus 40) (SV40) [166], and used for subsequent *in vitro* and *in vivo* functional assays.

3.3.3 Generation of integrin α11 knock down (CAF $^{\alpha 11KD}$) cell line

shRNA targeting *ITGA11* mRNA was constructed using the following oligonucleotides:

shRNA1

F: 5'-GATCCCC AGGAGCCAAGAAGGTGATGATTCAAGAGATCATCACCTTCTTGGCTCCTTTTTTGGAAA-3';

R: 5'-AATTTTTCCAAAAAAGGAGCCAAGAAGGTGATGATCTCTTGAATCATCACCTTCTTGGCTCCTGGG-3'),

shRNA2

F: 5'-GATCCCC TGCCCGATTTGGGTCCTCCA TTCAAGAGA TGGAGGACCCAAATCGGGCA TTTTTGGAAA -3';

R: 5'- AATTTTTCCAAAAA TGCCCGATTTGGGTCCTCCA TCTCTTGAA TGGAGGACCCAAATCGGGCA GGG -3',

shRNA3

F: 5'- GATCCCC GAGTCAACTCCAACTTCAGG TTCAAGAGA CCTGAAGTTGGAGTTGACTC TTTTTGGAAA-3';

R: 5'- AATTTTTCCAAAAA GAGTCAACTCCAACTTCAGG TCTCTTGAA CCTGAAGTTGGAGTTGACTC GGG -3' and

shRNA4

F: 5'-GATCCCC CCACGCAGGAGCCATCTACATC TTCAAGAGA GATGTAGATGGCTCCTGCGTGG TTTTTGGAAA -3';

R: 5'- AATTTTTCCAAAAA CCACGCAGGAGCCATCTACATC TCTCTTGAA GATGTAGATGGCTCCTGCGTGG GGG -3'

Assuming 100% annealing, 100μM of top and bottom strands of shRNA oligonucleotides were suspended separately in TE buffer. These strands were than mixed in the ratio 1:1 to get double stranded shRNA oligonucleotide of 50 μM. To

remove the secondary structure the prepared mixture was heated at 95°C for 30 seconds and gradually heated down to 72°C, 37°C and 25°C for 2 minutes each.

The annealed shRNA oligonucleotide was diluted to a concentration of 0.5 µM in TE buffer before ligation with the RNAi-Ready pSIREN-RetroQ-ZsGreen1-Express expression vector (cat. no: 632455, AH Diagnostics). The reaction mixtures were incubated for 3 hours at RT and transferred to -20°C until ready for further use. (All the reagents used were purchased from Clontech).

shRNA carrying vector was transformed by heat shock method into competent *Escherichia coli* (Clontech). The transformed E.coli, were then plated on LB-agar medium containing ampicillin (Invitrogen) and incubated at 37˚C overnight. Four isolated colonies from each plate were inoculated into a small-scale liquid culture (5 ml; Invitrogen)) at 37˚C, overnight, shaking at 250 rpm, Isolation of plasmid DNA from bacteria was done using Quagen Miniprep following the manufacturer's instructions.

The oligonucleotides were verified by sequencing using Sanger Sequencing method using Applied Biosystem 3730XL Analyzer The samples with correct sequences were then used for transfection to generate viral packaging of the constructs.

Five hundred thousand Phoenix-A (viral packaging cells) cells per well were plated on 6 well plate and grown in phoenix medium. Next day, 1.5 hour before transfection, medium was replaced with 1.75 mL of antibiotic-antimycotic free medium. About 500 ng of plasmid DNA and 10 µL of LipofectamineR 2000 Transfection Reagent (Invitrogen) were mixed separately with 250 µL of serum free (SF) DMEM in separate tubes and incubated for 5 minutes at RT. Contents in two tubes were mixed and incubated at RT for 20 minutes. This mixture was drop by drop in the wells with Phoenix-A cells in culture. Next day, the medium was changed with DMEM medium supplemented with fetal bovine serum and visualized under fluorescence microscope (Nikon Eclipse TS100) to detect the transfection status. The culture was left for next 2 days for generation of virus particles.

One hundred and fifty thousand fibroblasts per well were plated in six well plates. 2 µL of protamine sulphate (Sigma-Aldrich) was added and swirled gently to the virus containing medium of Phoenix-A cells in culture. The virus containing medium from Phoenix-A cells was then drawn on a syringe and transferred to the wells with fibroblasts in culture through filter unit of pore size 0.22 µM. To increase the virus infection rate the plate was centrifuged rate at 1200 g for 90 minutes at room temperature. Following day the fibroblasts were inspected through fluorescence microscope to examine the infection efficiency by visualizing the presence of green fluorescence protein. The cells were further propagated before fluorescence activated cell sorting (FACS).

3.3.4 Generation of luciferase transfected oral dysplastic keratinocytes

Oral dysplastic keratinocytes (DOK cell line purchased from European Collection of Cell Cultures (Salisbury, Wiltshire, UK)) [160] was transfected with retroviral expression construct with gene encoding for luciferase, selected using puromycin in culture [167]. These cells are here after referred as DOK^{Luc}. DOK^{Luc} cells were routinely maintained in DOK Medium.

3.3.5 Fluorescence activated cell sorting (FACS)

FACS was used to sort out the fibroblasts transduced with shRNA constructs, using green fluorescence protein as a marker. FACS is a type of flow cytometry, which is used to separate heterogeneous mixture of cells based on light scattering and fluorescence of each cell.

Sample preparation for FACS

The virus infected fibroblasts were trypsinized and centrifuged. The cells were then suspended in 10 ml of PBS buffer supplemented with 2% FBS and 1% HEPES (4-(2-hydroxyethyl)-1-piperazineethanesulfonic acid) buffer and filtered through 40 µm strainer (BD FalconTM; BD Biosciences). The cells were again centrifuged and re-suspended in the supplemented PBS buffer to a population of around 5 $x10^6$ cells per

ml. Wild-type non-infected cells were also prepared in the same way, to serve as a control during FACS.

Cells (fibroblasts) were sorted using BD FACS Caliber flow cytometer, and the cells were grown in penicillin-streptomycin supplemented growth (FAD) medium, to keep the cells safe from possible bacterial contaminations during cell sorting. Cells were left to grow for further experiments and future stocks.

RNA and Protein were extracted from the fibroblasts in culture for RT-PCR and western blot for validation of knock down. Only the most effective shRNA construct (ITGA11-shRNA1) was used further for functional assays. Cells infected with control and ITGA11-shRNA are henceforth referred with additional indicators after the cell name $\sim^{\alpha 11CTRL}$ and $\sim^{\alpha 11KD}$ respectively.

3.3.6 Population doubling time

Seeding population and total yield cells were counted at each passage and the population doubling was calculated using a standard formula (number of population doublings $=\text{Log}_{10}(N/N_o)$ x3.33). Where N_o is the seeding number and N is the final number of cells. Total hours in culture were then divided with the number of population doublings.

3.3.7 Proliferation assay

Proliferation of $CAF1^{\alpha 11CTRL}$ and $CAF1^{\alpha 11KD}$ were assessed with WST-1 (05015944001, Roche Diagnostics Mannheim Germany) assay. 2000 and 1000 cells/well in total volume of 100µl were seeded in separate 96-well plates in 5 replicates and incubated at 37°C and 5% CO_2. For following 5 days one set of 96 well plate was treated with WST-1 reagent every day and optical density was measured.

The growth rate of wild type DOK (DOK^{WT}) and transfected DOK (DOK^{Luc}) was analysed using a colorimetric assay based on methylthiazol tetrazolium (MTT) mitochondrial reaction over 7 days on 96-well plates seeded with 1000 cells/well (n−6) [167].

Absorbance of medium for samples was measured against a background as a blank control at 570 nm, using a microplate reader (FLUOstar Omega, BMG Labtech, Germany).

3.3.8 Collagen gel contraction assay

Overnight blocking of 96 well plate with 225µL of 2% bovine serum albumin (BSA) in phosphate buffered saline (PBS) per well was done at 37°C. Plates were washed three times with PBS. Cell in cultures were trypsinized, washed, re-suspended in DMEM to concentration of $1X10^6$ cells/ml and mixed with 1ml collagen solution (48% of 2X DMEM, 40% of collagen I (3mg/ml) (BD Biosciences, 354249), 10% HEPES (0.2M, pH 8.0) (Sigma) 1% of Glutamin (200mM) and antibiotics). 100µL of collagen gel cell suspension was added in each well and allowed to polymerize for 90 minutes. The gels were floated with 100 µL of DMEM with (5 or 10%) or without FBS. At 1.5, 3, 4.5 and 6 hours, the gel dimensions were measured under the microscope. The dimensions were calculated as the percentage of the initial area of gel at each given time point.

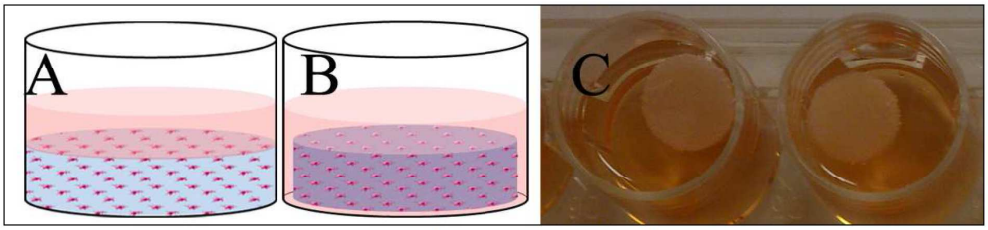

Figure 11: Collagen matrix remodelling.

3.3.9 Transwell invasion assay

The 8 µm transwell membranes were washed with 300µL SF medium and coated with Matrigel® (BDbiosciences). 60µg of Matrigel was used in 40µL volume per well and incubated for 30 minutes at 37°C. 400 µL SF medium was added on both chambers and incubated overnight. Trypsinized cells were re-suspended in SF medium containing 1mg/ml BSA at concentration of $2.5x10^5$. 200µL of prepared cell suspension was used to replace the medium over the Matrigel. Lower chamber was

filled with 400µL of culture media supplemented with 20% FBS to set a chemoattractant gradient. The medium and cells on the upper chamber were discarded after 20 hours of incubation at 37°C. The invaded florescent cells were counted under the florescence microscope (Nikon Eclipse TS100).

3.3.10 Three-Dimensional (3D) organotypic models

Collagen type I matrix containing 0.3 million fibroblasts per ml (700µl) was seeded in 24 well palates. After polymerization of the gel at 37°C it was supplemented with growth medium (for parent fibroblasts) (Figure 12 A).

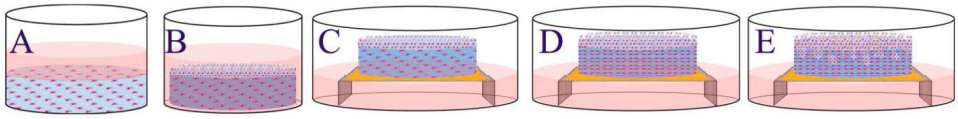

Figure 12: Sketch representing 3D organotypic model for tissue culture.

Next day 0.5 million OSCC cells in their respective growth medium were seeded over the matrix complex and let the tissue grow for next two days, (Figure 12 B).

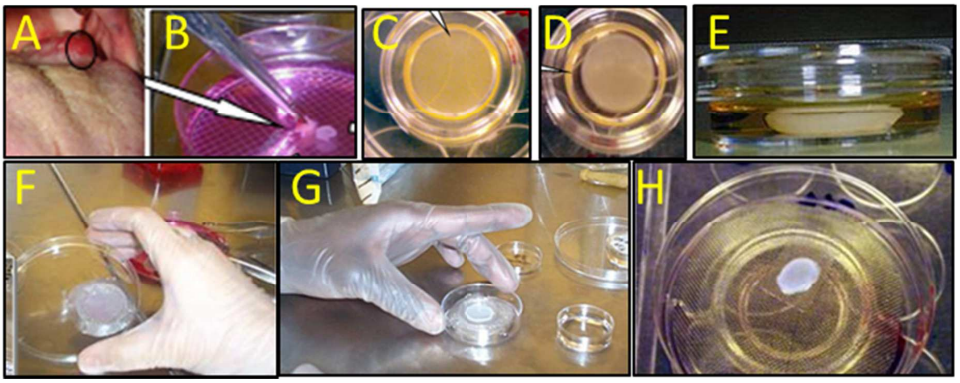

Figure 13: Successive steps in 3D tissue culture from patient sample.

On 4th day, Metal grid was placed in 6 well plate, a piece of cut lens paper was soaked in culture medium was placed over the metal grid. The growing tissue in the 24 well plates was transferred over to the lens paper. FAD OT medium is used to fill the 6 well plates up to the level of lens paper (Figure 12 C). The tissue was cultured (Figure 12_D & E) with regular replenishment of medium and harvested and processed on 11th day.

Half of each organotypic tissue was frozen in tissue TEK and stored at -80˚C and the remaining half was formalin fixed and paraffin embedded. FFPE tissues were sectioned and HE stained, measurement of the invaded OSCC cells was done using Olympus DP.Soft 5.0 software. The central and the terminal parts of the tissue were excluded; remaining two-fifth of the tissue was assessed on every 200µm point along the basement membrane as the vertical distance of invasion XY and also the ratio of invasion in relation to the total matrix thickness (XY/XZ) distance covered (illustrated in Figure 14).

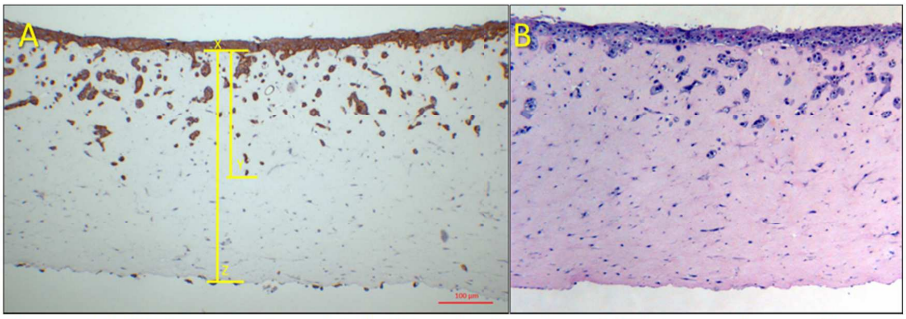

Figure 14: IHC (pancytokeratin) & HE stained section of OT tissue cultures, illustration for the invasion measurement.

3.3.11 Vessel formation assay

Each wells in ibiTreat 4 well µ-Slide (ibidi) was layered uniformly with 200 µl of 9.7mg/ml growth factor reduced Matrigel (Cornings), and polymerized at 37°C for 30 minutes. One hundred and forty thousand endothelial cells at passage 3-5 were then seeded in each of the Matrigel layered wells in the respective growth media (ECGM-2 Medium) as a positive control medium and conditioned medium from $CAF1^{\alpha 11CTRL}$ and $CAF1^{\alpha 11KD}$ cultures). Conditioned media was collected during the log phase of cell growth after 30 hours of culture in in DMEM supplemented with 10% fetal calf serum in T75 flasks. The endothelial cells supplemented with conditioned medium were allowed to grow for 16 hours and images were taken (magnification 40x, Nikon Eclipse TS100) and analysed using Image J Angiogenesis Analyzer plugin for pseudo capillary formation.

3.4 *In vivo* studies

All animal experiments were approved by the Norwegian Animal Research Authority.

Experiment setup for animal studies								
	Code	Cell Combination	Tongue		Skin			Details
Assessment of BLI specificity	BLI-1	DOK^{WT} DOK^{Luc}	1×10^3 -------	------- 1×10^3	1×10^3 ------	------ 1×10^3		Injected in the tongue of NSG mice, (n=6 each), Total volume 50µl
		DOK^{WT} DOK^{Luc}	1×10^5 -------	------- 1×10^5	1×10^5 ------	------ 1×10^5		
	BLI-2	DOK^{Luc} CAF			1×10^3 1×10^5	1×10^5 1×10^5	1×10^6 1×10^5	Scaffolds with growing cells transplanted to NSG mice (n=6 each)
	BLI-3	DOK^{Luc} CAF15_13 CAF15_23	1×10^3 1×10^5 ---------	1×10^3 --------- 1×10^5				Injected in the tongue of NSG mice (n=6 each) Total volume 50µl
Xenograft DOKs + CAF1 (integrin α11 modulated)	BLI-α11	DOK^{Luc} $CAF1^{\alpha11CTRL}$ $CAF1^{\alpha11KD}$	1×10^3 1×10^5 ---------	1×10^3 -------- 1×10^5				Injected in the tongue of NSG mice (n=7 each), Total volume 30µl
		$CAF1^{\alpha11CTRL}$ $CAF1^{\alpha11KD}$	1×10^5 -------	------- 1×10^5				Injected in the tongue of NSG mice (n=3 each), Total volume 30µl
Syngeneic	4NQO							4NQO 50µg/ml in Drinking water C57BL/6J background $\alpha11^{-/-}$ mice

Table 11: Experiment setup for animal studies

3.4.1 Xenotransplantation model

3.4.1.1 Animal Model for assessment of BLI specificity

Study codes BLI-1, BLI-2 and BLI-3 as described in Table 11 are used for to determine the BLI specificity over tumour formation and growth assessment.

3.4.1.2 Xenograft of DOKs with integrin α11 modulated CAF1

Twenty Non-obese diabetic/severe combined immune deficient (NOD/SCID IL2γ ^{null}) (NSG) 6 weeks old male mice (Jackson Laboratory) were randomly divided into four groups (7+7+3+3) DOK^{Luc}, CAF1$^{\alpha 11KD}$, and CAF1$^{\alpha 11CTRL}$ were injected into the tongue of each mouse as explained in Table 11, code BLI-α11.

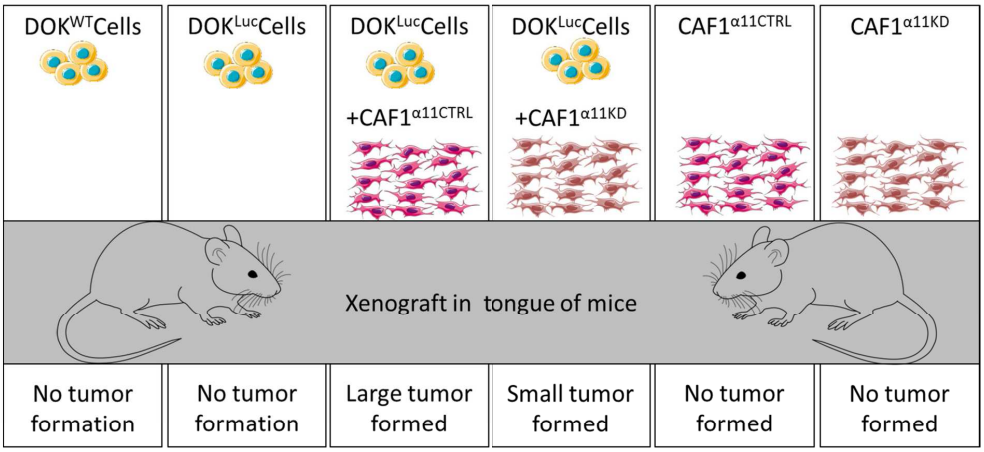

Figure 15: Illustration for the xenograft model for animal experiment. Vector images acquired from [168, 169]

Cultured cells in different densities were either seeded in the scaffolds or were re-suspended to a required total volume using growth factor reduced Matrigel (BD Biosciences, San Jose, CA, USA) and injected in tongue and skin of NOD/SCID IL2γ ^{null} (NSG) mice (6-10 weeks old).

For the studies where the scaffolds are used are transplanted to the back of the mice. The scaffolds were first pre-wet with DOK medium and were seeded with required no

of cells (DOK^{Luc} alone or in combination with CAF) and then allowed to attach overnight.

Each week after xenotransplantation the length and width of the formed tumours were measured using Vernier callipers. For bioluminescence imaging each mouse was scanned for single exposure of 1.5min after 10 minutes of intraperitoneal injection of 150 mg/kg of D-luciferin (Promega, Madison, WI). Images captured by In Vivo MS FX PRO (Carestream Health Inc. Rochester, NY) were analysed using Carestream MI SE version 5.0.6.20.

3.4.1.3 Exposure of 4-Nitroquinoline 1-oxide (4NQO) in drinking water in $\alpha11^{-/-}$ nude mice

Six week old SCID $\alpha11^{-/-}$ (n=6), $\alpha11^{+/-}$ (n=3), and $\alpha11^{+/+}$ (n=6) nude mice were used [120]. Breeding was maintained with crossing the $\alpha11^{+/-}$ (HZ) pairs for reproduction and taking care of the offspring generations. Genotyping was done as described [120, 155], briefly, DNA was isolated from the mouse ear tissue samples using 40µl of digestion buffer (1X-MGB) by heat activation at 95˚C for 5 minutes followed by proteinase K digestion. Extracted DNA was diluted 10 times before setting up the reaction. 2µl of diluted DNA was mixed with 18µl of prepared master mix containing required primers, the PCR reaction was set for:

95˚C	35 cycles			72˚C	4˚C
	95˚C	58˚C	72˚C		
6 minutes	1 minute	45 seconds	45 seconds	5 minutes	Hold

Table 12: PCR reaction cycle

PCR product were mixed with the loading buffer and run for 30 minutes in 1% agarose gel for separation and analysed in GEL DOC. Selected mice were treated with 4NQO (N 8141, Sigma, St. Louis, MO) in their drinking water at a concentration of 50µg/mL for 20 weeks. The carcinogenic solutions were prepared every week and delivered in drinking water bottles protected from light.

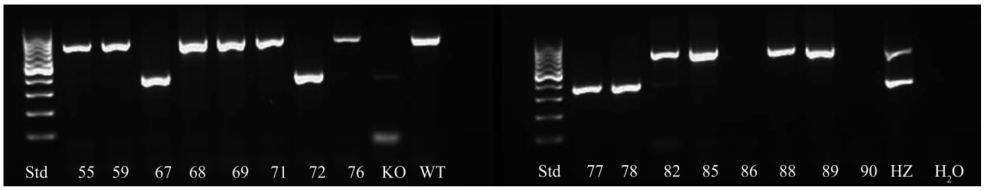

Figure 16: α11 Genotype determination of SCID α11$^{-/-}$ mice

Following the 4NQO exposure period, the mice were given normal drinking water. During the entire period, mice were weighed and examined weekly for visible morphological changes on the tongue and oral cavity under gas anaesthesia. Any accessible and distinct outgrowths were measured using Vernier callipers. Mice with reduced body weight by 20% or more were euthanized.

3.4.2 Sample collection

Tongue samples from the mice of all experimental studies were cut in half longitudinally, taking into consideration the position of cut so as to obtain equal amount of visible tumour tissue in both pieces. One half of the tongue was snap frozen in tissue TEK, while the other half was fixed in 4% buffered formalin and paraffin embedded. FFPE Samples were sectioned at 3 microns thickness and collected on Super frost glass slides, and one slide from each mouse was haematoxylin and eosin stained.

3.5 Expression analysis of genes related to wound healing

To examine the genes involved in stromal re-modelling, possibly modulated by integrin α11, pathway focused wound healing RT^2 Profiler™ PCR arrays PAMM-121Z and PAHS-121Z (SABiosciences, Frederick, MD, USA) were used respectively for 4NQO-induced tongue tumours from mice and for human CAF1 cells as described previously in section 3.3.2. Total RNA (3 μg) from three replicates (n = 3), for both CAF1$^{\alpha 11CTRL}$and CAF$^{\alpha 11KD}$ was converted to first strand cDNA using RT^2 First Strand Kit (C-03, SABiosciences, Frederick, MD, USA). For 4NQO-induced tongue tumours from mice, 500ng of total RNA from α11$^{+/+}$ (*n*=6) and α11$^{-/-}$ mice (*n*=4) were used for

cDNA synthesis. PCR amplification was performed using the following cycling conditions: 95°C for 10 minutes, (95°C for 15 seconds, and 60°C for 1 minute) × 40 cycles in ABI Prism Sequence Detector 7900 HT (Applied Biosystems, Foster City, USA). Threshold cycle (Ct) was used to calculate $2^{-\Delta\Delta Ct}$ value for each gene using PCR Array Data Analysis Web Portal (SABiosciences). $2^{-\Delta\Delta Ct}$ values were then exported to microarray data analysis software (J-Express, 2009).

3.6 cDNA synthesis and quantitative RT-PCR (qRT-PCR) using TaqMan assay

Following manufacturer's instructions, total RNA (500-950 ng) was converted to cDNA using High-Capacity cDNA Archive Kit system (Applied Biosystems, Foster City, CA, USA). All qRT-PCR amplifications were performed on ABI Prism Sequence Detector 7900 HT (Applied Biosystems, Foster City, USA) as described previously.

Gene	*Reference Sequence*	*TaqMan assay ID*	*Amplicon length (bp)*
ITGA11	NM_001004439.1	Hs00201927_m1	64
ACTA2	NM_001141945.1 NM_001613.2	Hs00426835_g1	105
PDGFR2	NM_002609.3	Hs01019589_m1	62
FAP	NM_004460.2	Hs00990806_m1	67
TGFβ1	NM_000660.4	Hs00998130_m1	81
MMP9	NM_004994.2	Hs00957562_m1	67
S100A4	NM_002961.2	Hs00243201_m1	57
THY1	NM_006288.3	Hs00264235_s1	99
DDR2	NM_001014796.1 NM_006182.2	Hs01025953_m1	102
COL1A2	NM_000089.3	Hs00164099_m1	68
Il1b	NM_008361.3	Mm00434228_m1	90
Itga3		Mm00442910_m1	72
Egf	NM_010113.3	Mm00438696_m1	96
Tagln	NM_011526.1	Mm00441661_g1	64
Fgf2	NM_008006.2	Mm00433287_m1	61
Actb		Mm00607939_s1	115

Table 13: List of TaqMan® Gene Expression Assay used for the study

TaqMan assay for ITGA11 (Table 13) was used to verify knock-down of ITGA11 mRNA in shRNA-CAF1 cells. PCR array data from mice tumours were independently validated by performing qRT-PCR using TaqMan assays for *Il1b*, *Itga3, Egfr*, *Tagln* and *Fgf2*. *Actb* (Applied Biosystems) were used as an endogenous control (details listed in Table 13). Comparative $2^{-\Delta\Delta Ct}$ method was used to quantify the relative mRNA expression.

4 Statistics

Statistical analysis was performed using IBM SPSS Statistics 21.0 (SPSS Inc., Chicago, USA) and Microsoft Excel 2010. The data are expressed as mean ± Standard deviation or ± Standard error of the mean (SEM). Paired t-test or the independent Mann Whitney U tests were used to compare differences between the means of tumour volumes. Spearman's correlation was used to examine the correlation of the manual tumour measurements with corresponding bioluminescence signals. Differences were considered statistically significant when $p < 0.05$.

Threshold cycle (Ct) was used to calculate $2^{-\Delta\Delta Ct}$ value for each gene using PCR Array Data Analysis Web Portal (SABiosciences). $2^{-\Delta\Delta Ct}$ values were then exported to microarray data analysis software (J-Express, 2009).

The graphs were generated using graph pad prism software.

5 Results

5.1 Expression of integrin α11 in the patient cohort

At protein level, except some endothelial cells, no immunostaining was observed for integrin α11 on FF tissue samples of HNOM and LP. Integrin α11 expression was found to be significantly higher in the stromal compartment of HNSCC when compared to LP ($p<0.001$) and NHOM ($p=<0.001$). A rich or poor pattern of integrin α11 expression was observed in 64.7% and 35.3% of the HNSCC cases respectively. The quantitative PCR performed on the same samples showed that the mRNA level for integrin α11 (ITGA11) was at significantly higher levels in HNSCC than in LP ($p=0.021$) and NHOM ($p=0.004$).

FF samples	Status	LP	NHOM	Rich (OSCC)	Poor (OSCC)	α-SMA (OSCC)
IHC	Integrin α11 (OSCC)	p<0.001	p=<0.001	64.7%	35.3%	p<0.001 r=0.735
	α-SAM (OSCC)			52.9 %	47.1%	
qPCR	*ITGA11* (OSCC)	p=0.021	p=0.004			
	ACTA2 (OSCC)	p=0.007	p=<0.001			
	ACTA2 (LP)		p=0.012			

Table 14: IHC and qPCR results from FF tissue samples for integrin α11 and α-SMA

FFPE samples	Tumour centre		Tumour Front	
	Rich	Poor	Rich	Poor
α-SMA	39.2%	60.8%	30%	70%
Poor survival prediction	p=0.06		p=0.021	

Table 15: IHC results from α-SMA staining on FFPE tissue samples

Quantitative RT-PCR for α-SMA (*ACTA2*) was also performed on the same samples which showed a significant overexpression in HNSCC when compared with NHOM (p=<0.001) and LP (p=0.007). Furthermore, an upregulated expression of *ACTA2* was found in LP when compared with NHOM (p=0.012).

We also investigated whether the expression of integrin α11 and α-SMA (a well-known prognostic biomarker in tongue SCC) in cancer stroma was associated with clinical stage, differentiation, local invasiveness, metastasis and survival, by performing linear regression and Kaplan Meier survival analysis (SPSS statistical program, version 19). No correlation was found between survival and expression of α-SMA or α11 as detected on FF samples. A positive relation was found between clinical TNM staging and the presence of the inflammatory infiltrate positive for integrin α11. α-SMA expression correlated with differentiation, distant metastasis and recurrence. A strong positive correlation between the staining scores of integrin α11 and α-SMA was found. Double staining for α11 and α-SMA showed their co-localization. However, there were few cases which were predominantly positive either for α11 or for α-SMA.

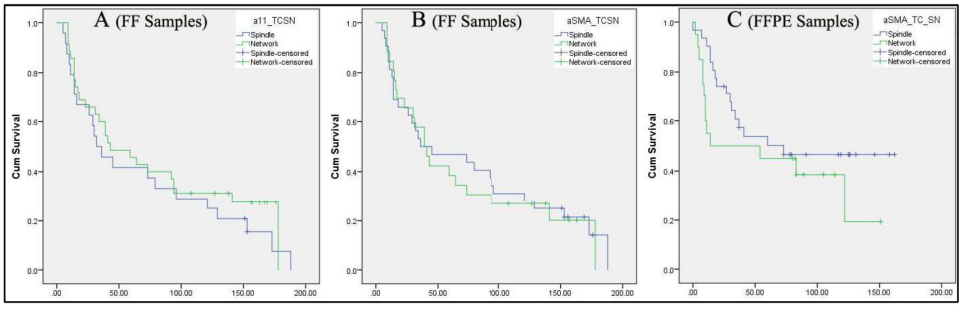

Figure 17: Survival (months) plots for tumour centre of both FF and FFPE samples.

The staining for α11 could not be optimized on FFPE. Parallel FFPE tissue samples from the archive, when stained with α-SMA, revealed negative staining for normal and dysplastic lesions but positive for stroma of HNSCC with various intensity of staining. This was true for all the locations of the oral cavity.

Presence of rich pattern α-SMA positive fibroblasts at the invasive tumour front (ITF) was predictive of the poor survival (p=0.021) for all the locations of the oral cavity and also for other locations except the tongue, when evaluated separately.

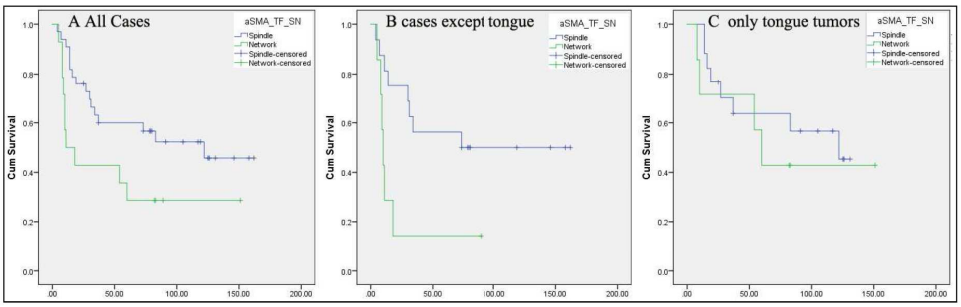

Figure 18: Survival (months) plots for α-SMA staining on tumour front of FFPE samples

5.2 Successful knock-down of integrin α11 in CAFs using retroviral shRNA constructs

Two of the three shRNA constructs targeting integrin α11 significantly suppressed the expression of integrin α11at both mRNA and protein level ($CAF1^{\alpha 11KD}$ as compared to the $CAF1^{\alpha 11CTRL}$). The construct with the most effective integrin α11 knock-down was chosen and used for further studies.

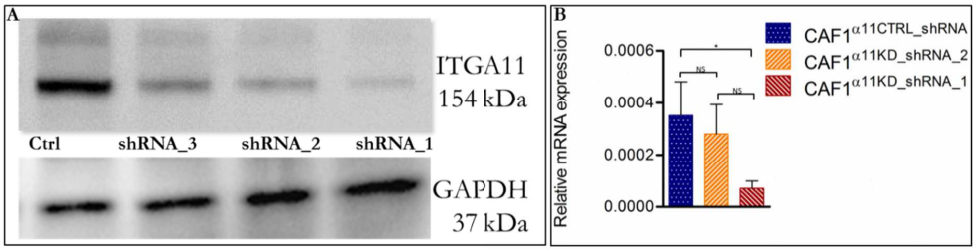

Figure 19: Verification of down regulation of integrin α11 in CAF1. (NS=Not significant)

After knock down, both CAF1$^{\alpha 11CTRL}$ and CAF1$^{\alpha 11KD}$ retained the characteristic fibroblast. There was no significant difference between CAF1$^{\alpha 11CTRL}$ and CAF1$^{\alpha 11KD}$ concerning the cell proliferation (WST-1 assay) and (p=0.96) population doubling time (p=0.76).

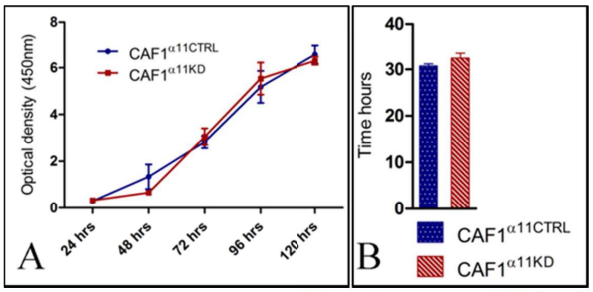

Figure 20: No significant difference in proliferation assay (WST1) (A) as well as in population doubling time (B)

5.3 CAF$^{\alpha 11KD}$ show reduced ability to rearrange the collagen matrix and reduced motility than CAF$^{\alpha 11WT}$

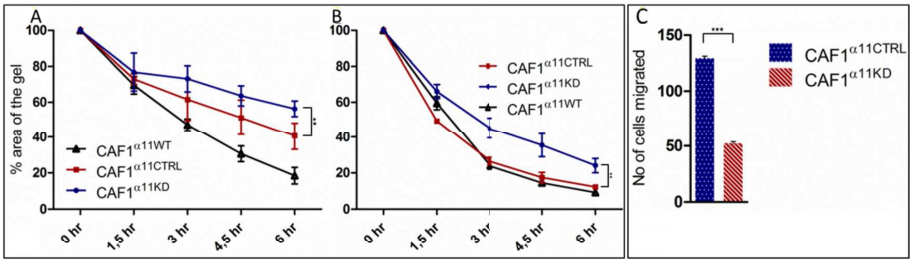

Figure 21: Ability of the CAF1 cells to: reorganize the collagen matrix (A,B), migrate through matrigel (C).

CAF1$^{\alpha 11KD}$ cells had reduced ability to remodel floating collagen lattices when compared with CAF$^{\alpha 11CTRL}$ cells in all experimental conditions DMEM (p=0.007), DMEM with 5% FBS (p=0.001) and DMEM with 10% FBS (24.09% ± 3.98% versus 12.21% ± 1.41 p=0.002). CAF1$^{\alpha 11KD}$ cells migrated less through a layer of matrigel in a transwell migration assay when compared to CAF1$^{\alpha 11CTRL}$ cells (17.4±2.57 cells versus 54.6 ± 4.5 cells, p=5.43x10^{-7}).

5.4 OSCC cells invaded less in 3D organotypic models constructed with CAF$^{\alpha 11KD}$

LuC4 cells showed significant deeper invasion in the collagen matrix when co-cultured with CAF1$^{\alpha 11CTRL}$ as compared to CAF1$^{\alpha 11KD}$ both in terms of 'invasion distance' (428µm ± 44 µm versus 199 µm ± 70 µm, p=0.0001) and 'percentage of matrix thickness invasion' (51% ± 5% versus 34% ± 12%, p=0.0003).

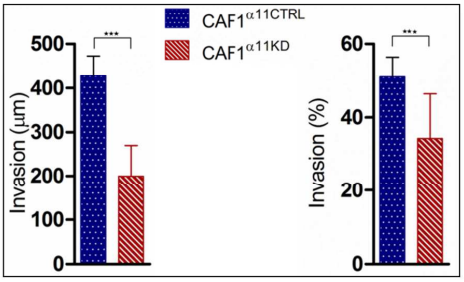

Figure 22: OT invasion

5.5 Expression of several molecules previously associated with the CAF phenotype was reduced by knock-down of ITGA11

Taqman RT-PCR was used to examine differentially expressed CAF-related genes associated with integrin α11 down-regulation (TaqMan assay details listed in Table 13). The analysis revealed several CAF-related genes significant down regulated in CAF$^{\alpha 11KD}$ when compared to CAF$^{\alpha 11CTRL}$ cells as follows: *ITGA11* (P=0.004), *ACTA2* (P=0.0004), *PDGFR2* (p=0.004), *FAP* (p=0.007), *TGFβ1* (p=0.0005), *MMP9* (p=0.002), *S100A4* (p=0.003), *THY1* (p=0.006), *DDR2* (p=0.007), *COL1A2* (p=0.0001).

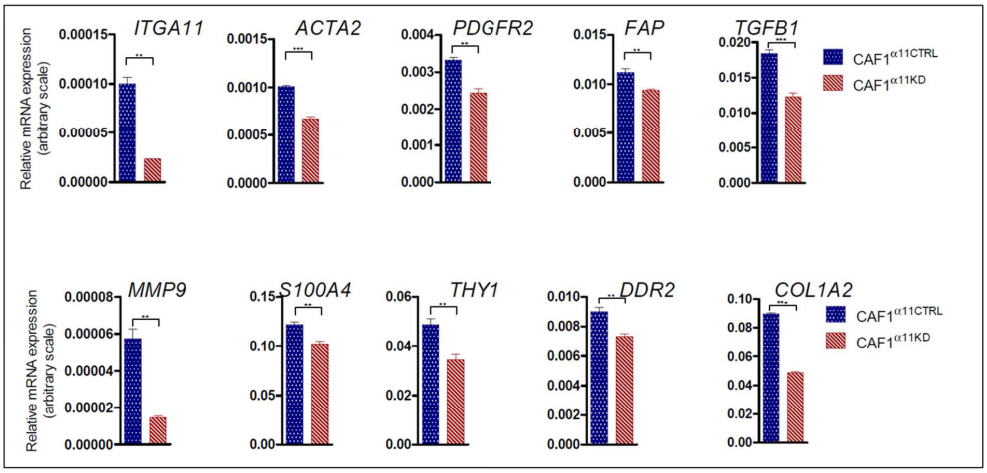

Figure 23: expressed stromal modelling related genes associated with integrin α11 down-regulation

PCR array was also used to examine differentially expressed stromal modelling related genes associated with integrin α11 down-regulation in human oral CAFs. CAF1$^{\alpha 11KD}$ replicates clustered separately from the replicates of CAF1$^{\alpha 11CTRL}$ when using unsupervised hierarchical clustering and expression of several molecules involved in stromal remodelling was significantly altered by down regulation of ITGA11 (Paper III). Of interest, several molecules related to angiogenesis and matrix remodelling such as IGF1, MMP7 and MMP9 were found downregulated in the CAF$^{\alpha 11KD}$ fibroblasts.

5.6 Vessel formation assay

Tube formation assay was conducted in three independent experiments. Results presented here are in an aggregate. Additionally, the tube formation experiment was repeated in conditioned medium supplemented with BSA 0.1% (instead of serum) in 96 well plates coated with Matrigel. Similar result was obtained with higher tube induction in conditioned medium from CAF1$^{\alpha 11CTRL}$.

Conditioned medium from CAF1$^{\alpha 11KD}$ cells induced less pseudo capillary formation by endothelial cells on Matrigel layer, compared to conditioned medium from CAF1$^{\alpha 11CTRL}$. Several parameters for vessel formation were measured using Image J angiogenesis analyser plugin.

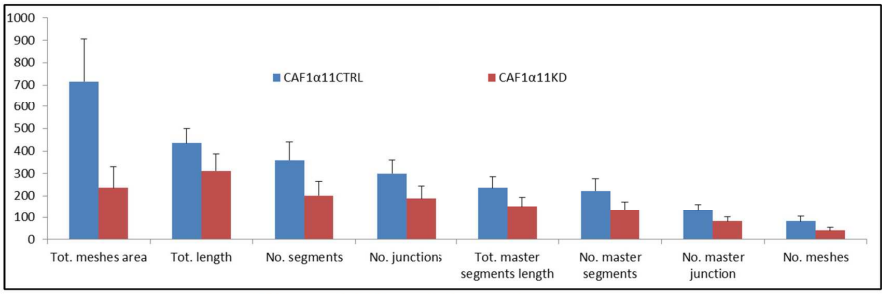

Figure 24: Vessel formation

All the measured parameters: total mesh area, total length (total segment length + total branch length + total isolated branch length), number of segments, number of junctions, total master segment length, number of master segments, number of master junction and number of meshes (loops) were higher for endothelial cells cultured with conditioned medium from CAF1$^{\alpha 11CTRL}$ (Figure 24). The definition of the parameters and the metrics criteria were well defined as previously published [170].

5.7 Establishing a microenvironmentally-induced animal model by using BLI

When DOK^{WT} were co-injected with CAFs in the tongue of the mice the incidence of tumour formation was increased from 16.66% to 57.14%. There was no significant difference between the tumours formed by DOK^{WT} or DOK^{LUC} where we had a constant increase in intensity of the signal that was in line with the increase observed by the manual measurement.

Further experiments showed that when different CAFs types, e.g. CAF15_13 and CAF15_23 were co injected with the DOK^{LUC}, the bioluminescence measurements were more sensitive and more prone to detect discrete differences in tumour formation than the manual measurements, although it was not statistically significant. Nevertheless, the histological measurements were significantly different between these groups (CAF15_13 and CAF15_23) ($p=0.028$) and supported the bioluminescence measurements.

5.8 CAF$^{\alpha 11KD}$ supported formation of smaller tongue tumours than CAF$^{\alpha 11WT}$ when co-injected with DOK^{Luc} in NSG mice

None of DOK^{WT}, DOK^{Luc}, CAF1^{WT}, CAF1$^{\alpha 11KD}$ or CAF1$^{\alpha 11CTRL}$ formed tumours when xenotransplanted alone in the tongue of. CAFs increased the tumorigenic potential of DOKs when co-injected, as previously reported (Paper II).

Assessment of the manual measurement of the tumours formed in the tongues of NSG mice when DOK^{Luc} were co-injected either with CAF1$^{\alpha 11KD}$ or CAF1$^{\alpha 11CTRL}$, showed significantly smaller tumour formation with CAF1$^{\alpha 11KD}$ (9.56 ± 3.31 mm^3) when compared with tumour formed by co-injection with CAF1$^{\alpha 11CTRL}$ (28.46 ± 6.46 mm^3, p=0.03). The tumour incidence was 7/7 and 6/7 respectively.

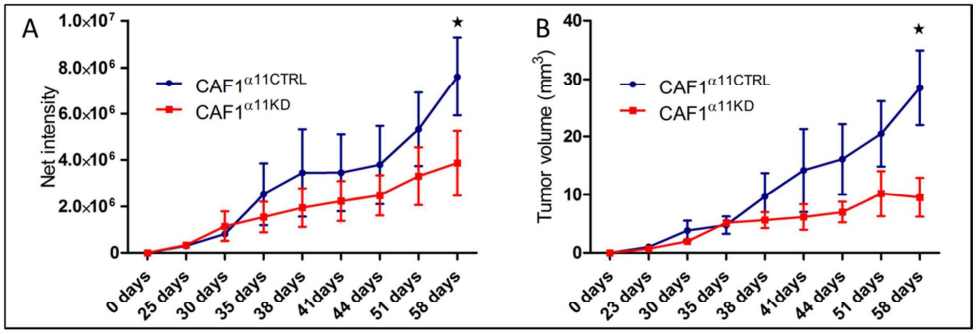

Figure 25: Tumour assessment by BLI (A) versus manual measurement (B)

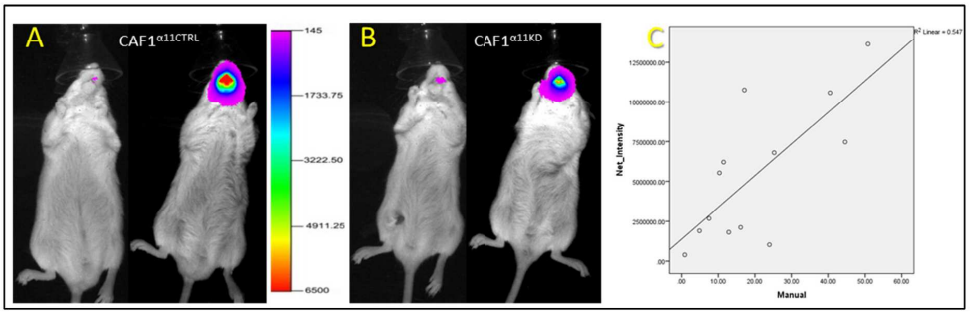

Figure 26: Initial and final set of pictures from Bioluminescence imaging for both (A) CAF1$^{\alpha 11CTRL}$ and (B) CAF1$^{\alpha 11KD}$ group. (C) Scatterplot showing the correlation of the manual measurements with Net intensity of BLI imaging

The net intensity (BLI) reading was significantly different between two groups p=0.02 as well the BLI measurement had a significant correlation with manual measurements (r=0.687 p=0.01).

5.9 Immunohistological characterization of xenograft mice tongue tumours

DOK^{Luc}/ $CAF1^{\alpha 11CTRL}$ xenografts showed an intense staining of α-SMA in the stroma, surrounding the cancer islands compared to a weak or no staining for α-SMA observed in DOK^{Luc} + $CAF1^{\alpha 11KD}$ xenografts.

Significantly higher population of Ki67-stained proliferating cancer cells was observed in control group (p=0.025) when compared to DOK^{Luc} + $CAF1^{\alpha 11KD}$ xenografts. However, there was no significant difference in EGFR staining between the two experimental groups.

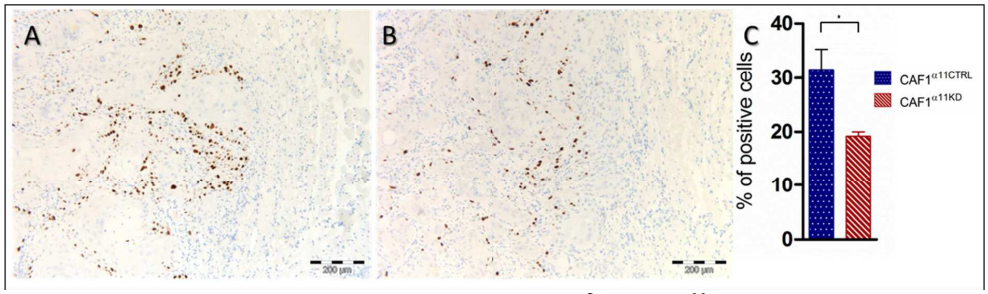

Figure 27: Ki-67 staining on tumours formed by DOK^{Luc} $CAF1^{\alpha 11}$ xenograft. Positive cells identified as proliferating human DOK^{Luc} cells.

Factor VIII staining of tumour tissues showed significant difference between these DOK^{Luc}/ $CAF1^{\alpha 11CTRL}$ and DOK^{Luc} + $CAF1^{\alpha 11KD}$ xenografts for the developing vessels in the tumour mass (p=0.0004), with the control group having the greater number of vessels.

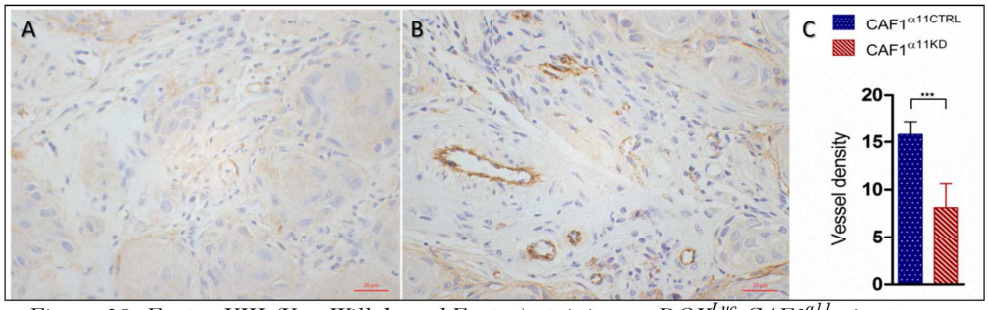

Figure 28: Factor VIII (Von Willebrand Factor) staining on DOK^{Luc} CAF1$^{\alpha 11}$ mice tongue xenograft.

5.10 4NQO exposed through drinking water, induced smaller tumours in α11$^{-/-}$ SCID mice

All SCID mice exposed to 4NQO in drinking water developed tumours, while the control (water only) group was tumour free. Morphological changes in oral mucosa of 4NQO exposed mice started to appear at average of 15 weeks. Progression of these morphological changes took approximately four week until the lesions were measurable in α11$^{+/+}$ SCID mice, whereas it took seven weeks for development from papillomas to tumours in α11$^{-/-}$ SCID mice. Significantly bigger tumours were formed in α11$^{+/+}$ SCID mice as compared to α11$^{-/-}$ mice (p=0.06).

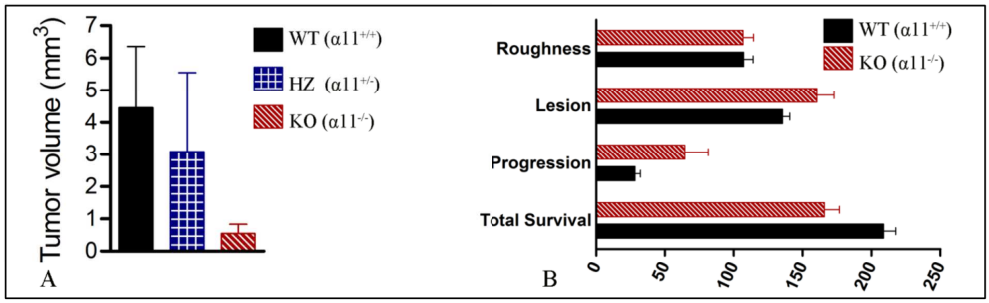

Figure 29: 4NQO induced tumour volume, timeline of the tumour development and progression in days.

5.11qRT-PCR analysis for the altered gene on 4NQO developed tumours in $\alpha11^{+/+}$ and $\alpha11^{-/-}$ mice

PCR array assay was used for tongue tumours of the mice (4NQO in drinking water) in order to determine the altered wound healing related genes in $\alpha11^{-/-}$ SCID mice when compared to $\alpha11^{+/+}$ SCID mice. Independent validation of the differentially expressed genes from PCR array was done by performing qRT-PCR using TaqMan assays for *Tagln, Fgf2, Egf, Itga3 and Il1b*. Consistent with the PCR array results, *Tagln* (P =0.02) *Fgf2* (P =0.05) and *Egf* (P =0.009) were found significantly up-regulated in $\alpha11^{-/-}$ SCID mice when compared to $\alpha11^{+/+}$ SCID mice.

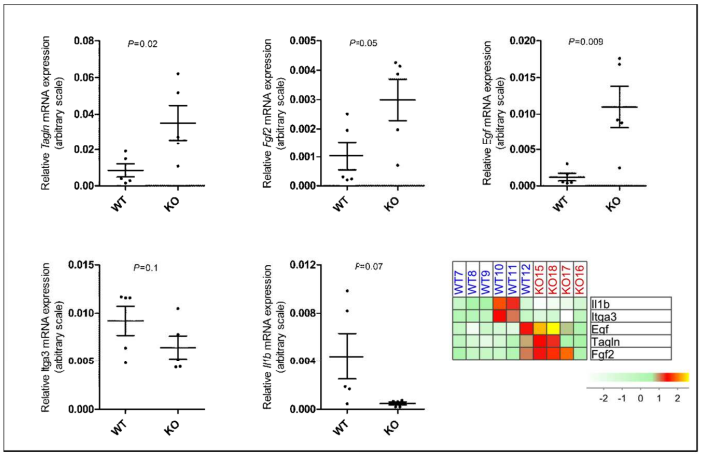

Figure 30: Taq man assay validation of altered genes reported in mouse wound healing assay.

6 Discussion

6.1 Integrin α11 as a diagnostic biomarker in HNSCC

Integrin α11 has been shown to be involved in the carcinogenesis of lung tumours [119, 120]. In this study we have found that integrin α11 was upregulated at both protein and mRNA levels in HNSCC compared to both NHOM and LP, indicating its potential as a diagnostic marker. We also wanted to investigate if the level of expression of integrin α11 has the potential to be a prognostic marker for survival of HNSCC patients, and for this purpose we also analysed in parallel the prognostic value of the level of expression of α-SMA, a previously establish marker of poor prognosis in oral and tongue carcinoma.

We observed similar results as reported by previous studies for α-SMA expression [109, 110, 171, 172], showing a correlation of 'rich' expression of α-SMA with poor patient survival in HNSCC. This observation was found only when α-SMA was evaluated at ITF for FFPE samples, but not at the TC in either FF or FFPE samples. This is in line with previous studies showing the importance of analysing the ITF and the problems due to expression heterogeneity in assessing the prognostic value of other potential biomarkers such as p53 [173], E-cadherin [174], Ki67[173], syndecan-1 [175].

In 1992, ITF was defined as the most progressed, three to six tumour cell layers or detached tumour cell groups at the progressing edge of an OSCC [176]. Its significance for the progression and prognostic determination in OSCC/HNSCC was then determined. Realizing the limitation of imprecise definition of ITF of the previous studies, we have defined the ITF as the 100μm broad tissue area around the outermost invasive tumour islands. We found more than one third of the samples not expressing either α11 or α-SMA, while the rest of the cases showed variable degree of protein expression. This difference in the degree of staining emphasized the inter tumour as well as intra tumour heterogeneity. We have scored three different, randomly selected

areas in order to compensate for the intra-tumour heterogeneity [70]. We found a correlation between a shorter survival time and the α-SMA expression at ITF in a rich pattern when we considered all the other locations in the oral cavity (3/4 of the cases in the study), excluding the tongue.

In contrast to the previous studies using either FF or FFPE samples, we have used both the FF and FFPE samples and we found a strong correlation between expression of α-SMA in FF and FFPE samples, nevertheless, only the evaluation of α-SMA at the ITF in FFPE correlated with survival of patients. When analysing more carefully, we observed that there was a difference in the expression of α-SMA over the cases, with 94.23% of samples expressed it on FFPE tissues samples and only 61.8% of the samples expressing it in FF tissue samples. This difference was due to a more expression of stromal α-SMA at the ITF than at tumour centre.

Though a significant correlation between the status of cancer and the staining pattern for both integrin α11 and α-SMA was found, we were not able to show any correlation to the patient survival in the FF samples. The small tissue bits that we had as FF samples were devoid of ITF and integrin α11 antibody could be only used in the FF samples, limiting us to analysing it only at the TC of the samples. The survival correlated with the α-SMA scoring only for the ITF of the FFPE samples, and there was a strong positive correlation between integrin α11 and α-SMA staining in HNSCC, indicating that the expression of these two proteins follows the same pattern in the tumour stroma. Moreover, double staining for integrin α11 and α-SMA showed stromal cells with co-localization of their staining, indicating that our study might have underestimated the value of integrin α11 as a prognostic factor due to inadequate tissue available for analysis.

Considering the facts of (1) co-localization of integrin α11 and α-SMA staining, and (2) correlation of expression of α-SMA at the ITF but not at the TC of FFPE samples to the survival, one might theorize that if integrin 11 could have been investigated at

the ITF a correlation with the survival would have been found. This highlights the importance of the ITF for the evaluation of a prognostic biomarker for cancer studies.

6.2 Establishing a new model for microenvironmentally-induced carcinogenesis

Instead of using normal cells, we used already transformed, but not fully malignant DOK cells in order to limit the time of the study (by eliminating the long process of initial mutations necessary for tumour development from normal cells). This model was established in collaboration with the Centre for Clinical Dental Research, Department of Clinical Dentistry UiB and with Haematology Section, Department of Clinical Science. The efficiency of the BLI measurement was higher than the one of the manual measurements, and this was confirmed by the histological examination. For example, we found out after histological analysis that one of the swellings interpreted as a tumour by the manual measurement (but without signal in the BLI assessment) was actually just retention of the matrix in which the cells were injected. The BLI measurement was also more efficient in detecting about 50% of the developed tongue tumours before we could measure them manually, and this was finally confirmed by histology, though the manual as well as BLI measurement were consistent over the study (BLI-1) duration. This is in line with other studies that have also suggested increased sensitivity of the BLI measurement when compared to florescence [177] and magnetic resonance imaging [178]. Though not significant, BLI was more sensitive for early detection of tumours then manual measurement in another subsequent study (BLI-3), where DOK^{Luc} were injected with different strains of CAFs.

6.3 Biological role of integrin α11 in oral carcinogenesis

After assessing the expression pattern of integrin α11 in the human tissue samples we further studied the role of integrin α11 in oral carcinogenesis.

Syngeneic animal experiments were performed using the recently developed $\alpha11^{-/-}$ SCID mice model [120]. In line with the results on lung cancer, our results presented

here revealed a longer lag phase and smaller tumours of 4NQO-induced tumours in $\alpha11^{-/-}$ SCID mice when compared to $\alpha11^{+/+}$ SCID mice, indicating a role for integrin α11 in initiation of oral tumours in mice.

Transgelin (SM22) was one of the molecules expressed significantly higher in the mice tongue tumours of this syngeneic model. SM22 was found to be expressed by quiet smooth muscle cells and to be a promotor of induced cellular senescence by activating $p16^{INK4a}$ /pRB. Both p16 and Rb have been shown to be upregulated in 4NQO induced mice tumours with increased exposure time and associated with later stages of carcinogenesis [61]. Similarly, hypermethylation of the promotor region of $p16^{INK4a}$ genes in 4NQO induced tumours have been shown, in line with other previous studies on OSCC. Hypermethylation of $p16^{INK4a}$ is rare in mild and moderate dysplasia but is seen in high frequency in cases with severe dysplasia and OSCC [179]. Transgelin has been found to be significantly up regulated in lung[180], gastric[181] and oesophageal cancers[182] whereas down regulated in breast[183], colorectal[184] and prostate [185] cancers. Furthermore, the restoration of transgelin suppressed the colon tumorigenicity both *in vivo* and *in vitro* studies, proving its action as a tumour suppressor gene [186]. This is in line with our results of smaller tumour formation and increased transgelin expression in the tumours of $\alpha11^{-/-}$ mice.

We have found less vessel density in the tongue tumours developed from xenografts of $CAF1^{\alpha11KD}$ fibroblasts, as well as less aggressive tumour behaviour. $CAF1^{\alpha11KD}$ expressed less MMP9 as it has been previously shown in laryngeal squamous cell carcinoma [187]. Overexpression of transgelin in HT1080 cells decreased MMP-9 mRNA/protein levels leading to reduce *in-vitro* invasion [188]. Together with the finding that $CAF1^{\alpha11KD}$ expressed less MMP9, this might suggest that the cell type responsible for the increased transgelin expression in the tumours of $\alpha11^{-/-}$ SCID mice could be the fibroblasts. Nevertheless, this is just speculative at this point and needs further confirmatory experiments. Yet, this was further suggested by the micro tube formation assay where the condition medium from the $CAF1^{\alpha11CTRL}$ formed more tubes then compared to $CAF1^{\alpha11KD}$, though the wound healing path focused PCR array

could not identify, apart of IGF1, another classical vascular growth stimulating factor in CAF population with altered α11 expression.

The overexpression of Fgf2 in mice tumour tissues from $\alpha11^{-/-}$ mice is thus surprising and contrasts with the finding of decreased intra tumour vessel density in the $CAF1^{\alpha11KD}$ group of xenotransplantation model BLI-α11 [189].

Nevertheless, the up regulation of Fgf2 might be due to a difference in the timing of the tumours induced in $\alpha11^{-/-}$ and $\alpha11^{+/+}$ mice [190], a study using a similar animal model showing that Fgf2 is upregulated at an earlier, dysplastic stage and then it was downregulated when the invasion occurred [191].

Regardless of the specific mechanism of action, the *in vivo* xenograft experiments with modulated integrin α11 expression on human CAFs showed a clear role for integrin α11 expression on tumour formation and progression. Interestingly, the smaller tumours formed by DOK^{Luc} + $CAF^{\alpha11KD}$ showed a stroma less abundant in collagen and devoid of α-SMA myofibroblasts, when compared to DOK^{Luc} + $CAF^{\alpha11CTRL}$ xenografts . This is in line with the previous studies showing that collagen-binding integrins, such as α1β1, α2β1, and α11β1 regulate myofibroblast differentiation. α11β1 expression in fibroblasts was shown to be regulated by cell/matrix stress involving activin A and Smad3, indicating α11β1 as an important effector of collagen reorganization [104, 116].

Pathway focused wound healing RT^2 Profiler™ PCR arrays for $CAF^{\alpha11CTRL}$ and $CAF^{\alpha11KD}$ and 4NQO-induced tongue tumours from $\alpha11^{+/+}$ and $\alpha11^{-/-}$ SCID mice identified distinct changes in molecules involved in stromal remodelling whose expression was altered by ITGA11 expression. These two set of experiments identified different molecules and this can be explained by the different material used for analysis, one experiment involving mRNA extracted from a pure CAF population ($CAF^{\alpha11CTRL}$ and $CAF^{\alpha11KD}$) while the mRNA extracted from the 4NQO tumours were from both the epithelial and stromal compartments.

Nevertheless, taken together, the results from this study show that the presence of integrin α11 in tumour stroma is associated with formation of bigger and more vascularized tumours indicating a role of integrin α11 in a stroma-endothelial cross-talk that promotes tumorigenesis. A role for integrin α11 in stromal remodelling that would affect invasion of cancer cells has been previously suggested by the studies on lung cancer, but a coupling between expression of integrin α11 in the CAFs and angiogenesis has not been suggested before. This is a novel finding for the role of integrin α11 in carcinogenesis that needs to be further explored for the understanding of the underlying mechanism of integrin α11 in oral carcinogenesis and carcinogenesis in general.

7 Concluding remarks

Expression of integrin α11 in tumour stroma of oral cancer

Sections from the frozen tissues of head and neck cancer, containing only tumour centres, showed very clear expression of integrin α11 in stromal fibroblasts in contrast to the normal oral mucosa and lichen planus. Similar results were obtained for expression of α-SMA, and expression of α11 correlated well with expression of α-SMA. In addition, the pattern of expression of α-SMA in parallel FFPE samples could stratify patients with good prognosis from those with bad prognosis, but only when evaluated at the invasive tumour front. Unfortunately integrin α11 could not be detected in FFPE samples and thus its presence at ITF could not be quantified.

Establishment of a bioluminescence imaging model to evaluate oral carcinogenesis

A non-invasive, yet sensitive and robust *in vivo* model for monitoring and measurement of microenvironmentally-induced oral cancer was successfully established using DOK^{WT}, DOK^{Luc} and CAFs.

Integrin α11 expression and function in cancer-associated fibroblasts of OSCC.

Our results indicate a significant role of integrin α11 in oral carcinogenesis. The data presented here demonstrate that the presence of integrin α11 in the CAFs promotes a more invasive phenotype of OSCC cells and a provides pro-angiogenetic microenvironment through soluble factors. Further characterization of the stromal-endothelial cross-talk guided by the expression of integrin α11 in CAFs is required and might contribute to a better understanding of oral carcinogenesis.

8 Future Perspectives

1. This study demonstrated that integrin α11 can be used as a diagnostic biomarker for HNSCC, but failed to show a predictive power for its presence in the tumour microenvironment. We believe that this is due to the fact that we could not analyse the expression of integrin α11 at the ITF of FFPE tissue samples. Thus, we work for further development of an integrin α11 antibody that is effective on FFPE tissues.
2. Knock-down of the endogenous level of integrin α11 in CAFs, was found to consistently alter the behaviour of adjacent OSCC cells, further confirmation studies are required using more strains of CAFs.
3. An interesting, novel role for integrin α11 in the stromal-endothelial cross talk has been revealed by our studies. This deserves further investigations for revealing the underlying mechanisms of the integrin α11 control over the angiogenesis in oral cancer and carcinogenesis in general.
4. Since integrin α11 seems to be specifically expressed in CAFs, its targeting for neutralizing a pro-angiogenetic stroma is an attractive approach for a personalized treatment that would abrogate an abnormal stroma.

9 References

1. Garant, P.R., *Oral cells and tissues*. 2003, Chicago: Quintessence Pub. Co. ix, 430 p.
2. Nanci, A., *Ten Cate's Oral Histology: Development, Structure, and Function*. 2014: Elsevier Health Sciences.
3. Roed-Petersen, B. and G. Renstrup, *A topographical classification of the oral mucosa suitable for electronic data processing. Its application to 560 leukoplakias.* Acta Odontol Scand, 1969. 27(6): p. 681-95.
4. *Normal oral mucosa*. 2015 [cited: 29 Dec 2015]; Available from: http://www.proteinatlas.org/learn/dictionary/normal/oral+mucosa+1/detail+1.
5. Kumar, V., A.K. Abbas, and J.C. Aster, *Robbins Basic Pathology*. 2012: Elsevier Health Sciences.
6. Alberts, B., *Molecular biology of the cell*. 5th ed. 2008, New York: Garland Science.
7. Berkovitz, B.K.B., G.R. Holland, and B.J. Moxham, *Oral Anatomy, Histology and Embryology*. Fourth ed. 2009: Mosby. 398.
8. Contard, P., et al., *Culturing keratinocytes and fibroblasts in a three-dimensional mesh results in epidermal differentiation and formation of a basal lamina-anchoring zone.* J Invest Dermatol, 1993. 100(1): p. 35-9.
9. Chang, H.Y., et al., *Diversity, topographic differentiation, and positional memory in human fibroblasts.* Proc Natl Acad Sci U S A, 2002. 99(20): p. 12877-82.
10. Rinn, J.L., et al., *Anatomic demarcation by positional variation in fibroblast gene expression programs.* PLoS Genet, 2006. 2(7): p. e119.
11. Rinn, J.L., et al., *A systems biology approach to anatomic diversity of skin.* J Invest Dermatol, 2008. 128(4): p. 776-82.
12. Sorrell, J.M. and A.I. Caplan, *Fibroblast heterogeneity: more than skin deep.* J Cell Sci, 2004. 117(Pt 5): p. 667-75.
13. Rodemann, H.P., et al., *Fibroblasts of rabbit kidney in culture. I. Characterization and identification of cell-specific markers.* Am J Physiol, 1991. 261(2 Pt 2): p. F283-91.
14. Lepekhin, E., et al., *Differences in motility pattern between human buccal fibroblasts and periodontal and skin fibroblasts.* Eur J Oral Sci, 2002. 110(1): p. 13-20.
15. Yamaguchi, Y., et al., *Mesenchymal-epithelial interactions in the skin: aiming for site-specific tissue regeneration.* J Dermatol Sci, 2005. 40(1): p. 1-9.
16. Rodemann, H.P., *Differential degradation of intracellular proteins in human skin fibroblasts of mitotic and mitomycin-C (MMC)-induced postmitotic differentiation states in vitro.* Differentiation, 1989. 42(1): p. 37-43.
17. Gron, B., et al., *Oral fibroblasts produce more HGF and KGF than skin fibroblasts in response to co-culture with keratinocytes.* APMIS, 2002. 110(12): p. 892-8.

18. Stephens, P., et al., *Skin and oral fibroblasts exhibit phenotypic differences in extracellular matrix reorganization and matrix metalloproteinase activity.* Br J Dermatol, 2001. 144(2): p. 229-37.

19. Enoch, S., et al., *'Young' oral fibroblasts are geno/phenotypically distinct.* J Dent Res, 2010. 89(12): p. 1407-13.

20. Meran, S., et al., *Involvement of hyaluronan in regulation of fibroblast phenotype.* J Biol Chem, 2007. 282(35): p. 25687-97.

21. Costea, D.E., et al., *Identification of two distinct carcinoma-associated fibroblast subtypes with differential tumor-promoting abilities in oral squamous cell carcinoma.* Cancer Res, 2013. 73(13): p. 3888-901.

22. Rodemann, H.P., et al., *Selective enrichment and biochemical characterization of seven human skin fibroblasts cell types in vitro.* Exp Cell Res, 1989. 180(1): p. 84-93.

23. Hakenjos, L., M. Bamberg, and H.P. Rodemann, *TGF-beta1-mediated alterations of rat lung fibroblast differentiation resulting in the radiation-induced fibrotic phenotype.* Int J Radiat Biol, 2000. 76(4): p. 503-9.

24. Rodemann, H.P. and H.-O. Rennekampff, *Functional Diversity of Fibroblasts*, in *Tumor-Associated Fibroblasts and their Matrix*, M.M. Mueller and N.E. Fusenig, Editors. 2011, Springer Netherlands. p. 23-36.

25. Grinnell, F., et al., *Nested collagen matrices: a new model to study migration of human fibroblast populations in three dimensions.* Exp Cell Res, 2006. 312(1): p. 86-94.

26. Kim, J.B., *Three-dimensional tissue culture models in cancer biology.* Seminars in Cancer Biology, 2005. 15(5): p. 365-377.

27. Rhee, S., *Fibroblasts in three dimensional matrices: cell migration and matrix remodeling.* Exp Mol Med, 2009. 41: p. 858-865.

28. Ferlay, J., et al., *Cancer incidence and mortality worldwide: Sources, methods and major patterns in GLOBOCAN 2012.* Int. Journal of Cancer, 2015. 136(5): p. E359-E386.

29. Stewart B. W, W.C.P., *World Cancer Report*. 2014: IARC Nonserial Publication.

30. Torre, L.A., et al., *Global cancer statistics, 2012.* CA Cancer J Clin, 2015. 65(2): p. 87-108.

31. Ferlay, J., et al., *Cancer incidence and mortality patterns in Europe: estimates for 40 countries in 2012.* Eur J Cancer, 2013. 49(6): p. 1374-403.

32. Lubin, J.H., et al., *Total Exposure and Exposure Rate Effects for Alcohol and Smoking and Risk of Head and Neck Cancer: A Pooled Analysis of Case-Control Studies.* Am J Epidemiol, 2009. 170(8): p. 937-947.

33. Isayeva, T., et al., *Human papillomavirus in non-oropharyngeal head and neck cancers: a systematic literature review.* Head Neck Pathol, 2012. 6 Suppl 1: p. S104-20.

34. Warnakulasuriya, S., *Global epidemiology of oral and oropharyngeal cancer.* Oral Oncol, 2009. 45(4-5): p. 309-16.

35. Mehrotra, R. and D.K. Gupta, *Exciting new advances in oral cancer diagnosis: avenues to early detection.* Head Neck Oncol, 2011. 3: p. 33.

36. Nair, D.R., et al., *Oral cancer: Premalignant conditions and screening--an update.* J Cancer Res Ther, 2012. 8 Suppl 1: p. S57-66.

37. Wikner, J., et al., *Squamous cell carcinoma of the oral cavity and circulating tumour cells.* World J Clin Oncol, 2014. 5(2): p. 114-124.

38. Mithani, S.K., et al., *Molecular genetics of premalignant oral lesions.* Oral Dis, 2007. 13(2): p. 126-33.

39. Saintigny, P., et al., *Gene expression profiling predicts the development of oral cancer.* Cancer Prev Res (Phila), 2011. 4(2): p. 218-29.

40. Persson, M., et al., *Recurrent fusion of MYB and NFIB transcription factor genes in carcinomas of the breast and head and neck.* Proceedings of the National Academy of Sciences, 2009. 106(44): p. 18740-18744.

41. Mitani, Y., et al., *Comprehensive analysis of the MYB-NFIB gene fusion in salivary adenoid cystic carcinoma: Incidence, variability, and clinicopathologic significance.* Clin Cancer Res, 2010. 16(19): p. 4722-31.

42. The Cancer Genome Atlas, N., *Comprehensive genomic characterization of head and neck squamous cell carcinomas.* Nature, 2015. 517(7536): p. 576-582.

43. *Mutational landscape of gingivo-buccal oral squamous cell carcinoma reveals new recurrently-mutated genes and molecular subgroups.* Nat Commun, 2013. 4: p. 2873.

44. Vogelstein, B. and K.W. Kinzler, *Cancer genes and the pathways they control.* Nat Med, 2004. 10(8): p. 789-99.

45. Leemans, C.R., B.J.M. Braakhuis, and R.H. Brakenhoff, *The molecular biology of head and neck cancer.* Nat Rev Cancer, 2011. 11(1): p. 9-22.

46. Futreal, P.A., et al., *A CENSUS OF HUMAN CANCER GENES.* Nat Rev Cancer., 2004. 4(3): p. 177-183.

47. Stratton, M.R., P.J. Campbell, and P.A. Futreal, *The cancer genome.* Nature, 2009. 458(7239): p. 719-724.

48. Braakhuis, B.J.M., et al., *A Genetic Explanation of Slaughter's Concept of Field Cancerization: Evidence and Clinical Implications.* Cancer Res, 2003. 63(8): p. 1727-1730.

49. Califano, J., et al., *Genetic progression model for head and neck cancer: implications for field cancerization.* Cancer Res, 1996. 56(11): p. 2488-92.

50. Choi, S. and J.N. Myers, *Molecular pathogenesis of oral squamous cell carcinoma: implications for therapy.* J Dent Res, 2008. 87(1): p. 14-32.

51. Hecht, S.S. and D. Hoffmann, *Tobacco-specific nitrosamines, an important group of carcinogens in tobacco and tobacco smoke.* Carcinogenesis, 1988. 9(6): p. 875-884.

52. Hsia, C.-C., et al., *Enhancement of formation of the esophageal carcinogen benzylmethylnitrosamine from its precursors by Candida albicans.* Proceedings of the National Academy of Sciences of the United States of America, 1981. 78(3): p. 1878-1881.

53. Fracalossi, A.C., et al., *Ras gene mutation is not related to tumour invasion during rat tongue carcinogenesis induced by 4-niiroquinoline 1-oxide.* J Oral Pathol Med, 2011. 40(4): p. 325-33.

54. Minicucci, E.M., et al., *The role of the TP53 gene during rat tongue carcinogenesis induced by 4-nitroquinoline 1-oxide.* Exp Toxicol Pathol, 2011. 63(5): p. 483-9.

55. MacDonald, D.G., *Comparison of epithelial dysplasia in hamster cheek pouch carcinogenesis and human oral mucosa.* J Oral Pathol Med, 1981. 10(3): p. 186-191.

56. Nakahara, W., F. Fukuoka, and T. Sugimura, *Carcinogenic action of 4-nitroquinoline-N-oxide.* Gan, 1957. 48(2): p. 129-37.

57. Kanojia, D. and M.M. Vaidya, *4-nitroquinoline-1-oxide induced experimental oral carcinogenesis.* Oral Oncol, 2006. 42(7): p. 655-67.

58. Wallenius, K. and U. Lekholm, *Oral cancer in rats induced by the water-soluble carcinogen 4-nitrochinoline N-oxide.* Odontol Revy, 1973. 24(1): p. 39-48.

59. Ohne, M., et al., *Experimental tongue carcinoma of rats induced by oral administration of 4-nitroquinoline 1-oxide (4NQO) in drinking water.* Oral Surg Oral Med Oral Pathol, 1985. 59(6): p. 600-7.

60. Steidler, N.E. and P.C. Reade, *Initiation and promotion of experimental oral mucosal carcinogenesis in mice.* J Oral Pathol, 1986. 15(1): p. 43-7.

61. Ribeiro, D.A., et al., *Imbalance of tumor suppression genes expression following rat tongue carcinogenesis induced by 4-nitroquinoline 1-oxide.* In Vivo, 2009. 23(6): p. 937-42.

62. Dayan, D., et al., *Experimental tongue cancer in desalivated rats.* Oral Oncol, 1997. 33(2): p. 105-9.

63. Rivera Martínez, C.A., *4NQO Carcinogenesis: A Model of Oral Squamous Cell Carcinoma.* Int. J. Morphol, 2012. 30: p. 309-314.

64. Schoop, R.A.L., M.H.M. Noteborn, and R.J. Baatenburg de Jong, *A mouse model for oral squamous cell carcinoma.* J Mol Histol., 2009. 40(3): p. 177-181.

65. Vered, M., et al., *4NQO-Induced Rat Tongue Carcinoma: An Ultrastructural Study.* Ultrastruct Pathol., 2008. 32(5): p. 199-205.

66. *Screening for Oral Cancer: U.S. Preventive Services Task Force Recommendation Statement*, U.P.S.T. Force, Editor. 2013: US.

67. Almangush, A., et al., *Depth of invasion, tumor budding, and worst pattern of invasion: prognostic indicators in early-stage oral tongue cancer.* Head Neck, 2014. 36(6): p. 811-8.

68. Brandwein-Gensler, M., et al., *Oral squamous cell carcinoma: histologic risk assessment, but not margin status, is strongly predictive of local disease-free and overall survival.* Am J Surg Pathol, 2005. 29(2): p. 167-78.

69. Pentenero, M., S. Gandolfo, and M. Carrozzo, *Importance of tumor thickness and depth of invasion in nodal involvement and prognosis of oral squamous cell carcinoma: a review of the literature.* Head Neck, 2005. 27(12): p. 1080-91.

70. Teh, M.T., et al., *Exploiting FOXM1-orchestrated molecular network for early squamous cell carcinoma diagnosis and prognosis.* Int J Cancer, 2013. 132(9): p. 2095-106.

71. Costea, D.E., et al., *Identification of two distinct carcinoma-associated fibroblast subtypes with differential tumor-promoting abilities in oral squamous cell carcinoma.* Cancer Res, 2013.

72. Vaidya, M.M., et al., *Cytokeratin expression in precancerous lesions of the human oral cavity.* Oral Oncol, 1998. 34(4): p. 261-4.

73. Ranganathan, K., et al., *Cytokeratin expression in oral submucous fibrosis--an immunohistochemical study.* J Oral Pathol Med, 2006. 35(1): p. 25-32.

74. Alam, H., et al., *Loss of keratins 8 and 18 leads to alterations in alpha6beta4-integrin-mediated signalling and decreased neoplastic progression in an oral-tumour-derived cell line.* J Cell Sci, 2011. 124(Pt 12): p. 2096-106.

75. Alam, H., et al., *Fascin overexpression promotes neoplastic progression in oral squamous cell carcinoma.* BMC Cancer, 2012. 12: p. 32.

76. Dhanda, J., et al., *SERPINE1 and SMA expression at the invasive front predict extracapsular spread and survival in oral squamous cell carcinoma.* Br J Cancer, 2014. 111(11): p. 2114-21.

77. Ljokjel, B., et al., *The impact of HPV infection on survival in a geographically defined cohort of oropharynx squamous cell carcinoma (OPSCC) patients in whom surgical treatment has been one main treatment.* Acta Otolaryngol, 2014. 134(6): p. 636-45.

78. Ljokjel, B., et al., *The impact of HPV infection, smoking history, age and operability of the patient on disease-specific survival in a geographically defined cohort of patients with oropharyngeal squamous cell carcinoma.* Acta Otolaryngol, 2014. 134(9): p. 964-73.

79. Soland, T.M. and I.J. Brusevold, *Prognostic molecular markers in cancer - quo vadis?* Histopathology, 2013. 63(3): p. 297-308.

80. Califano, J., et al., *Unknown primary head and neck squamous cell carcinoma: molecular identification of the site of origin.* J Natl Cancer Inst, 1999. 91(7): p. 599-604.

81. Califano, J., et al., *Genetic progression and clonal relationship of recurrent premalignant head and neck lesions.* Clin Cancer Res, 2000. 6(2): p. 347-52.

82. Correa, P., *A human model of gastric carcinogenesis.* Cancer Res, 1988. 48(13): p. 3554-60.

83. Andea, A., F. Sarkar, and V.N. Adsay, *Clinicopathological correlates of pancreatic intraepithelial neoplasia: a comparative analysis of 82 cases with and 152 cases without pancreatic ductal adenocarcinoma.* Mod Pathol, 2003. 16(10): p. 996-1006.

84. Fearon, E.R. and B. Vogelstein, *A genetic model for colorectal tumorigenesis.* Cell, 1990. 61(5): p. 759-67.

85. Hanahan, D. and R.A. Weinberg, *The hallmarks of cancer.* Cell, 2000. 100(1): p. 57-70.

86. Hanahan, D. and R.A. Weinberg, *Hallmarks of cancer: the next generation.* Cell, 2011. 144(5): p. 646-74.

87. Kalluri, R. and M. Zeisberg, *Fibroblasts in cancer.* Nat Rev Cancer, 2006. 6(5): p. 392-401.

88. Svennevig, J.-L. and H. Svaar, *Content and distribution of macrophages and lymphocytes in solid malignant human tumours.* Int. J. Cancer, 1979. 24(6): p. 754-758.

89. Mantovani, A., et al., *The origin and function of tumor-associated macrophages.* Immunol Today, 1992. 13(7): p. 265-70.

90. Paget, S., *The distribution of secondary growths in cancer of the breast. 1889.* Cancer Metastasis Rev, 1989. 8(2): p. 98-101.

91. De Wever, O. and M. Mareel, *Role of tissue stroma in cancer cell invasion.* J Pathol, 2003. 200(4): p. 429-47.

92. Radisky, D.C., *Fibroblasts act as co-conspirators for chemotherapy resistance.* Cancer Biol Ther, 2008. 7(9): p. 1348-9.

93. Costea, D.E., et al., *Species-Specific Fibroblasts Required for Triggering Invasiveness of Partially Transformed Oral Keratinocytes.* Am J Pathol, 2006. 168(6): p. 1889-1897.

94. Gaggioli, C., et al., *Fibroblast-led collective invasion of carcinoma cells with differing roles for RhoGTPases in leading and following cells.* Nat Cell Biol, 2007. 9(12): p. 1392-400.

95. Lewis, M.P., et al., *Tumour-derived TGF-beta1 modulates myofibroblast differentiation and promotes HGF/SF-dependent invasion of squamous carcinoma cells.* Br J Cancer, 2004. 90(4): p. 822-32.

96. Baum, B., J. Settleman, and M.P. Quinlan, *Transitions between epithelial and mesenchymal states in development and disease.* Sem Cell Dev Biol, 2008. 19(3): p. 294-308.

97. Gabbiani, G., *Some historical and philosophical reflections on the myofibroblast concept.* Curr Top Pathol, 1999. 93: p. 1-5.

98. Gabbiani, G., G.B. Ryan, and G. Majno, *Presence of modified fibroblasts in granulation tissue and their possible role in wound contraction.* Experientia, 1971. 27(5): p. 549-550.

99. Hinz, B., et al., *Mechanical Tension Controls Granulation Tissue Contractile Activity and Myofibroblast Differentiation.* Am J Pathol, 2001. 159(3): p. 1009-1020.

100. Davis, J. and J.D. Molkentin, *Myofibroblasts: trust your heart and let fate decide.* J Mol Cell Cardiol, 2014. 70: p. 9-18.

101. Hinz, B., et al., *The Myofibroblast: One Function, Multiple Origins.* Am J Pathol, 2007. 170(6): p. 1807-1816.

102. Hinz, B., et al., *Alpha-Smooth Muscle Actin Expression Upregulates Fibroblast Contractile Activity.* Mol. Cell. Biol, 2001. 12(9): p. 2730-2741.

103. Kovacs, E.J. and L.A. DiPietro, *Fibrogenic cytokines and connective tissue production.* The FASEB Journal, 1994. 8(11): p. 854-61.

104. Sergio Carracedo, N.L., Svetlana N. Popova, Roland Jonsson, Beate Eckes, Donald Gullberg, *The Fibroblast Integrin α11β1 is induced in a mechanosensotive manner involving activin A and regulates myofibroblast differentiation.* J Biol Chem. 285(14): 10434–10445 2010.

105. Masur, S.K., et al., *Myofibroblasts differentiate from fibroblasts when plated at low density.* Proc Natl Acad Sci U S A, 1996. 93(9): p. 4219-4223.

106. Hautmann, M.B., C.S. Madsen, and G.K. Owens, *A Transforming Growth Factor β (TGFβ) Control Element Drives TGFβ-induced Stimulation of Smooth Muscle α-Actin Gene Expression in Concert with Two CArG Elements.* J. Biol. Chem, 1997. 272(16): p. 10948-10956.

107. Tsujino, T., et al., *Stromal myofibroblasts predict disease recurrence for colorectal cancer.* Clin Cancer Res, 2007. 13(7): p. 2082-90.

108. Yazhou, C., et al., *Clinicopathological significance of stromal myofibroblasts in invasive ductal carcinoma of the breast.* Tumour Biol, 2004. 25(5-6): p. 290-5.

109. Kellermann, M.G., et al., *Myofibroblasts in the stroma of oral squamous cell carcinoma are associated with poor prognosis.* Histopathology, 2007. 51(6): p. 849-53.

110. Bello, I.O., et al., *Cancer-associated fibroblasts, a parameter of the tumor microenvironment, overcomes carcinoma-associated parameters in the prognosis of patients with mobile tongue cancer.* Oral Oncology, 2011. 47(1): p. 33-38.

111. Özdemir, B.C., et al., *Depletion of Carcinoma-Associated Fibroblasts and Fibrosis Induces Immunosuppression and Accelerates Pancreas Cancer with Diminished Survival.* Cancer cell, 2014. 25(6): p. 719-734.

112. [cited: 2016 Jan 31]; Available from: http://www.consultant360.com/story/depleting-carcinoma-associated-myofibroblasts-may-worsen-pancreatic-cancer-outcomes.

113. Wipff, P.-J., et al., *Myofibroblast contraction activates latent TGF-β1 from the extracellular matrix.* J. Cell Biol., 2007. 179(6): p. 1311-1323.

114. Wipff, P.-J. and B. Hinz, *Integrins and the activation of latent transforming growth factor β1 – An intimate relationship.* Eur. J. Cell Biol. 2008. 87(8–9): p. 601-615.

115. Munger, J.S., et al., *A Mechanism for Regulating Pulmonary Inflammation and Fibrosis: The Integrin αvβ6 Binds and Activates Latent TGF β1.* Cell, 1999. 96(3): p. 319-328.

116. Talior-Volodarsky, I., et al., *α11 integrin stimulates myofibroblast differentiation in diabetic cardiomyopathy.* Cardiovasc. Res. 2012. 96(2): p. 265-275.

117. Carracedo, S., et al., *The fibroblast integrin alpha11beta1 is induced in a mechanosensitive manner involving activin A and regulates myofibroblast differentiation.* J Biol Chem, 2010. 285(14): p. 10434-45.

118. Bystrom, B., et al., *Alpha11 integrin in the human cornea: importance in development and disease.* Invest Ophthalmol Vis Sci, 2009. 50(11): p. 5044-53.

119. Zhu, C.Q., et al., *Integrin alpha 11 regulates IGF2 expression in fibroblasts to enhance tumorigenicity of human non-small-cell lung cancer cells.* Proc Natl Acad Sci U S A, 2007. 104(28): p. 11754-9.

120. Navab, R., et al., *Integrin alpha11beta1 regulates cancer stromal stiffness and promotes tumorigenicity and metastasis in non-small cell lung cancer.* Oncogene, 2015.

121. Balkwill, F. and A. Mantovani, *Inflammation and cancer: back to Virchow?* Lancet, 2001. 357(9255): p. 539-45.

122. Plummer, M., S. Franceschi, and N. Munoz, *Epidemiology of gastric cancer.* IARC Sci Publ, 2004(157): p. 311-26.

123. Walboomers, J.M., et al., *Human papillomavirus is a necessary cause of invasive cervical cancer worldwide.* J Pathol, 1999. 189(1): p. 12-9.

124. Lu, C.F., et al., *Infiltrating macrophage count: a significant predictor for the progression and prognosis of oral squamous cell carcinomas in Taiwan.* Head Neck, 2010. 32(1): p. 18-25.

125. Leek, R.D., et al., *Association of macrophage infiltration with angiogenesis and prognosis in invasive breast carcinoma.* Cancer Res, 1996. 56(20): p. 4625-9.

126. Campbell, M.J., et al., *Proliferating macrophages associated with high grade, hormone receptor negative breast cancer and poor clinical outcome.* Breast Cancer Res Treat, 2011. 128(3): p. 703-11.

127. Forssell, J., et al., *High macrophage infiltration along the tumor front correlates with improved survival in colon cancer.* Clin Cancer Res, 2007. 13(5): p. 1472-9.

128. Shimura, S., et al., *Reduced infiltration of tumor-associated macrophages in human prostate cancer: association with cancer progression.* Cancer Res, 2000. 60(20): p. 5857-61.

129. Kerr, K.M., et al., *Partial regression in primary carcinoma of the lung: does it occur?* Histopathology, 1998. 33(1): p. 55-63.

130. Mills, C.D., et al., *M-1/M-2 Macrophages and the Th1/Th2 Paradigm.* J. Immunol, 2000. 164(12): p. 6166-6173.

131. Zhu, J. and W.E. Paul, *CD4 T cells: fates, functions, and faults.* Blood, 2008. 112(5): p. 1557-69.

132. Fridman, W.H., et al., *The immune contexture in human tumours: impact on clinical outcome.* Nat Rev Cancer, 2012. 12(4): p. 298-306.

133. Lv, L., et al., *The accumulation and prognosis value of tumor infiltrating IL-17 producing cells in esophageal squamous cell carcinoma.* PLoS One, 2011. 6(3): p. e18219.

134. Hanahan, D. and J. Folkman, *Patterns and emerging mechanisms of the angiogenic switch during tumorigenesis.* Cell, 1996. 86(3): p. 353-64.

135. Ferrara, N., *Vascular endothelial growth factor.* Arterioscler Thromb Vasc Biol, 2009. 29(6): p. 789-91.

136. Carmeliet, P., *VEGF as a key mediator of angiogenesis in cancer.* Oncology, 2005. 69 Suppl 3: p. 4-10.

137. Bergers, G. and S. Song, *The role of pericytes in blood-vessel formation and maintenance.* Neuro Oncol, 2005. 7(4): p. 452-64.

138. Strauss, L., et al., *Dual role of VEGF family members in the pathogenesis of head and neck cancer (HNSCC): possible link between angiogenesis and immune tolerance.* Med Sci Monit, 2005. 11(8): p. BR280-92.

139. Horak, E.R., et al., *Angiogenesis, assessed by platelet/endothelial cell adhesion molecule antibodies, as indicator of node metastases and survival in breast cancer.* Lancet, 1992. 340(8828): p. 1120-4.

140. Weidner, N., et al., *Tumor angiogenesis: a new significant and independent prognostic indicator in early-stage breast carcinoma.* J Natl Cancer Inst, 1992. 84(24): p. 1875-87.

141. Weidner, N., et al., *Tumor angiogenesis correlates with metastasis in invasive prostate carcinoma.* Am J Pathol, 1993. 143(2): p. 401-9.

142. Sasahira, T., et al., *MIA-dependent angiogenesis and lymphangiogenesis are closely associated with progression, nodal metastasis and poor prognosis in tongue squamous cell carcinoma.* Eur J Cancer, 2010. 46(12): p. 2285-94.

143. Bach, L.A., *Endothelial cells and the IGF system.* J Mol Endocrinol, 2015. 54(1): p. R1-13.

144. Brooks, A.N., E. Kilgour, and P.D. Smith, *Molecular pathways: fibroblast growth factor signaling: a new therapeutic opportunity in cancer.* Clin Cancer Res, 2012. 18(7): p. 1855-62.

145. Takada, Y., X. Ye, and S. Simon, *The integrins.* Genome Biol, 2007. 8(5): p. 215.

146. Humphries, J.D., A. Byron, and M.J. Humphries, *Integrin ligands at a glance.* J Cell Sci, 2006. 119(Pt 19): p. 3901-3.

147. Hynes, R.O., *Integrins: Bidirectional, Allosteric Signaling Machines.* Cell, 2002. 110(6): p. 673-687.

148. Barczyk, M., S. Carracedo, and D. Gullberg, *Integrins.* Cell Tissue Res, 2010. 339(1): p. 269-80.

149. Lee, J.-O., et al., *Crystal structure of the A domain from the a subunit of integrin CR3 (CD11 b/CD18).* Cell, 1995. 80(4): p. 631-638.

150. Legate, K.R. and R. Fässler, *Mechanisms that regulate adaptor binding to β-integrin cytoplasmic tails.* J. Cell Sci, 2009. 122(2): p. 187-198.

151. Tiger, C.-F., et al., *α11β1 Integrin Is a Receptor for Interstitial Collagens Involved in Cell Migration and Collagen Reorganization on Mesenchymal Nonmuscle Cells.* Dev. Biol, 2001. 237(1): p. 116-129.

152. Zhang, W.-M., et al., *α11β1 Integrin Recognizes the GFOGER Sequence in Interstitial Collagens.* J. Biol. Chem, 2003. 278(9): p. 7270-7277.

153. Gullberg, D., et al., *Up-regulation of a novel integrin α-chain (αmt) on human fetal myotubes.* Dev. Dynam, 1995. 204(1): p. 57-65.

154. Velling, T., et al., *cDNA cloning and chromosomal localization of human alpha(11) integrin. A collagen-binding, I domain-containing, beta(1)-associated integrin alpha-chain present in muscle tissues.* J Biol Chem, 1999. 274(36): p. 25735-42.

155. Popova, S.N., et al., *α11β1 Integrin-Dependent Regulation of Periodontal Ligament Function in the Erupting Mouse Incisor.* Mol. Cell. Biol, 2007. 27(12): p. 4306-4316.

156. Henderson, N.C., et al., *Targeting of alphav integrin identifies a core molecular pathway that regulates fibrosis in several organs.* Nat Med, 2013. 19(12): p. 1617-24.

157. Reed, N.I., et al., *The alphavbeta1 integrin plays a critical in vivo role in tissue fibrosis.* Sci Transl Med, 2015. 7(288): p. 288ra79.

158. Schulz, J.N., et al., *Reduced granulation tissue and wound strength in the absence of alpha11beta1 integrin.* J Invest Dermatol, 2015. 135(5): p. 1435-44.

159. Westcott, J.M., et al., *An epigenetically distinct breast cancer cell subpopulation promotes collective invasion.* J. Clin. Invest, 2015. 125(5): p. 1927-1943.

160. Chang, S.E., et al., *DOK, a cell line established from human dysplastic oral mucosa, shows a partially transformed non-malignant phenotype.* Int J Cancer, 1992. 52(6): p. 896-902.

161. Gammon, L., et al., *Sub-Sets of Cancer Stem Cells Differ Intrinsically in Their Patterns of Oxygen Metabolism.* PLoS ONE, 2013. 8(4): p. e62493.

162. Harper, L.J., et al., *Stem cell patterns in cell lines derived from head and neck squamous cell carcinoma.* J Oral Pathol Med, 2007. 36(10): p. 594-603.

163. Schmidt, D. and A.R. von Hochstetter, *The Use of CD31 and Collagen IV as Vascular Markers A Study of 56 Vascular Lesions.* Pathol Res Pract., 1995. 191(5): p. 410-414.

164. Suzuki, M., et al., *CD45RO expression on peripheral lymphocytes as a prognostic marker for adult T-cell leukemia.* Leuk Lymphoma, 1998. 28(5-6): p. 583-90.

165. Covas, D.T., et al., *Multipotent mesenchymal stromal cells obtained from diverse human tissues share functional properties and gene-expression profile with CD146+ perivascular cells and fibroblasts.* Exp Hematol, 2008. 36(5): p. 642-54.

166. Jat, P.S., et al., *Recombinant retroviruses encoding simian virus 40 large T antigen and polyomavirus large and middle T antigens.* Mol. Cell. Biol, 1986. 6(4): p. 1204-1217.

167. Suliman, S., et al., *Establishment of a bioluminescence model for microenvironmentally induced oral carcinogenesis with implications for screening bioengineered scaffolds.* Head Neck, 2015.

168. *Lab_Mouse_vector.* [cited: 2015 December 27]; Available from: https://commons.wikimedia.org/wiki/File:Vector_diagram_of_laboratory_mouse_%28black_and_white%29.svg.

169. *Servier Vector Images.* [cited: 2015 December 27]; Available from: http://www.servier.com/Powerpoint-image-bank.

170. Carpentier, G., et al. *Angiogenesis Analyzer for ImageJ.* in *4th ImageJ User and Developer Conference proceedings*. 2012. Mondorf-les-Bains, Luxembourg.

171. Barth, P.J., et al., *CD34+ fibrocytes, alpha-smooth muscle antigen-positive myofibroblasts, and CD117 expression in the stroma of invasive squamous cell carcinomas of the oral cavity, pharynx, and larynx.* Virchows Arch, 2004. 444(3): p. 231-4.

172. Marsh, D., et al., *Stromal features are predictive of disease mortality in oral cancer patients.* J Pathol, 2010.

173. Kurokawa, H., et al., *The relationship of the histologic grade at the deep invasive front and the expression of Ki-67 antigen and p53 protein in oral squamous cell carcinoma.* J Oral Pathol Med, 2005. 34(10): p. 602-7.

174. Wang, X., et al., *The expression of E-cadherin at the invasive tumor front of oral squamous cell carcinoma: immunohistochemical and RT-PCR analysis with clinicopathological correlation.* Oral Surg Oral Med Oral Pathol Oral Radiol Endod, 2009. 107(4): p. 547-54.

175. Kurokawa, H., et al., *Reduced syndecan-1 expression is correlated with the histological grade of malignancy at the deep invasive front in oral squamous cell carcinoma.* J Oral Pathol Med, 2006. 35(5): p. 301-6.

176. Bryne, M., et al., *Malignancy grading of the deep invasive margins of oral squamous cell carcinomas has high prognostic value.* J Pathol, 1992. 166(4): p. 375-81.

177. Troy, T., et al., *Quantitative comparison of the sensitivity of detection of fluorescent and bioluminescent reporters in animal models.* Mol Imaging, 2004. 3(1): p. 9-23.

178. Jarzabek, M.A., et al., *In vivo bioluminescence imaging validation of a human biopsy-derived orthotopic mouse model of glioblastoma multiforme.* Mol Imaging, 2013. 12(3): p. 161-72.

179. Nakahara, Y., et al., *High frequency methylation of p16INK4A gene during 4-nitroquinoline 1-oxide-induced rat tongue carcinogenesis.* Oncol Rep, 2004. 12(1): p. 101-6.

180. Wu, X., et al., *Transgelin overexpression in lung adenocarcinoma is associated with tumor progression.* Int J Mol Med, 2014. 34(2): p. 585-91.

181. Yu, B., et al., *Stromal fibroblasts in the microenvironment of gastric carcinomas promote tumor metastasis via upregulating TAGLN expression.* BMC Cell Biol, 2013. 14: p. 17.

182. Zhang, Y., et al., *Expression of Cofilin-1 and Transgelin in Esophageal Squamous Cell Carcinoma.* Med Sci Monit, 2015. 21: p. 2659-65.

183. Sayar, N., et al., *Transgelin gene is frequently downregulated by promoter DNA hypermethylation in breast cancer.* Clin Epigenetics, 2015. 7: p. 104.

184. Yokota, M., et al., *Gene expression profile in the activation of subperitoneal fibroblasts reflects prognosis of patients with colon cancer.* Int. J. of Cancer, 2016. 138(6): p. 1422-1431.

185. Prasad, P.D., J.A. Stanton, and S.J. Assinder, *Expression of the actin-associated protein transgelin (SM22) is decreased in prostate cancer.* Cell Tissue Res, 2010. 339(2): p. 337-47.

186. Li, Q., et al., *TAGLN suppresses proliferation and invasion, and induces apoptosis of colorectal carcinoma cells.* Tumour Biol, 2012. 34(1): p. 505-513.

187. Akdeniz, O., et al., *Relationships between clinical behavior of laryngeal squamous cell carcinomas and expression of VEGF, MMP-9 and E-cadherin.* Asian Pac J Cancer Prev, 2013. 14(9): p. 5301-10.

188. Nair, R.R., J. Solway, and D.D. Boyd, *Expression cloning identifies transgelin (SM22) as a novel repressor of 92-kDa type IV collagenase (MMP-9) expression.* J Biol Chem, 2006. 281(36): p. 26424-36.

189. Presta, M., et al., *Fibroblast growth factor/fibroblast growth factor receptor system in angiogenesis.* Cytokine & Growth Factor Reviews, 2005. 16(2): p. 159-178.

190. Grella, A., et al., *FGF2 Overrides TGFbeta1-Driven Integrin ITGA11 Expression in Human Dermal Fibroblasts.* J Cell Biochem, 2015.

191. Raimondi, A.R., A.A. Molinolo, and M.E. Itoiz, *Fibroblast growth factor-2 expression during experimental oral carcinogenesis. Its possible role in the induction of pre-malignant fibrosis.* J Oral Pathol Med, 2006. 35(4): p. 212-7.

Establishment of a bioluminescence model for microenvironmentally induced oral carcinogenesis with implications for screening bioengineered scaffolds.

Salwa Suliman, Himalaya Parajuli, Yang Sun, Anne Christine Johannessen, Anna Finne–Wistrand, Emmet McCormack, Kamal Mustafa, Daniela Elena Costea.

Head and Neck. DOI 10.1002/HED

II

Establishment of a bioluminescence model for microenvironmentally induced oral carcinogenesis with implications for screening bioengineered scaffolds

Salwa Suliman, BDS,[1,2,3] Himalaya Parajuli, BDS,[2,3] Yang Sun, PhD,[4] Anne Christine Johannessen, PhD,[2,5,6] Anna Finne–Wistrand, PhD,[4] Emmet McCormack, PhD,[7,8] Kamal Mustafa, PhD,[1] Daniela Elena Costea, PhD[2,5,6]*

[1]Department of Clinical Dentistry, Centre for Clinical Dental Research, University of Bergen, Bergen, Norway, [2]Gade Laboratory for Pathology, Department of Clinical Medicine, University of Bergen, Bergen, Norway, [3]Centre for International Health, Department of Global Public Health and Primary Care, University of Bergen, Bergen, Norway, [4]Department of Fibre and Polymer Technology, KTH Royal Institute of Technology, Stockholm, Sweden, [5]Centre for Cancer Biomarkers, Department of Clinical Medicine, University of Bergen, Bergen, Norway, [6]Department of Pathology, Haukeland University Hospital, Bergen, Norway, [7]Department of Clinical Science, University of Bergen, Bergen, Norway, [8]Department of Medicine, Haematology Section, Haukeland University Hospital, Bergen, Norway.

Accepted 3 July 2015
Published online 00 Month 2015 in Wiley Online Library (wileyonlinelibrary.com). DOI 10.1002/hed.24187

ABSTRACT: *Background.* Microenvironmental cues play a major role in head and neck cancer. Biodegradable scaffolds used for bone regeneration might also act as stimulative cues for head and neck cancer. The purpose of this study was to establish an experimental model for precise and noninvasive evaluation of tumorigenic potential of microenvironmental cues in head and neck cancer.

Methods. Bioluminescence was chosen to image tumor formation. Early neoplastic oral keratinocyte (DOK) cells were luciferase-transduced (DOK^{Luc}), then tested in nonobese diabetic severe combined immunodeficient IL2rγnull mice either orthotopically (tongue) or subcutaneously for their potential as "screening sensors" for diverse microenvironmental cues.

Results. Tumors formed after inoculation of DOK^{Luc} were monitored easier by bioluminescence, and bioluminescence was more sensitive in detecting differences between various microenvironmental cues when compared to manual measurements. Development of tumors from DOK^{Luc} grown on scaffolds was also successfully monitored noninvasively by bioluminescence.

Conclusion. The model presented here is a noninvasive and sensitive model for monitoring the impact of various microenvironmental cues on head and neck cancer in vivo. © 2015 The Authors Head & Neck Published by Wiley Periodicals, Inc. *Head Neck* **00**: 000–000, 2015

KEY WORDS: cancer, microenvironment, bioluminescence, tissue engineering, scaffold

INTRODUCTION

Recent evidence implicates environmental cues as key factors in cancer progression.[1] Among the important determinants is the surrounding stroma, including fibroblasts, endothelial cells, infiltrating immune cells, and extracellular matrix components.[2,3] The scaffolds used in tissue engineering as provisional matrices for cell proliferation and extracellular matrix deposition can also act as microenvironmental cues. The surrounding tissues might react toward these by foreign body reactions or even tumor formation,[4] and long-term subcutaneous implants of nonabsorbable or slowly degrading materials were shown to be tumorigenic.[5,6] Thus, there is a great concern that certain biomaterials may be potential initiators of malignancies, and the size and surface roughness of certain biomaterials were already suggested to influence tumor formation.[7] To date, at the regulatory level, the basic approach for biomaterials' safety is defined in the International Organization for Standardization 10993.[8,9] These tests start with an initial safety evaluation targeting leachable for cytotoxicity. Genotoxicity and evaluation of mRNA levels of proto-oncogenes and tumor suppressor genes[10] from mammalian or bacterial cells exposed to the biomaterials has also been used as methods for safety check.[11] Current carcinogenicity tests determine the tumorigenic potential of materials and/or their extracts from either single or multiple exposures or contacts over a period of the major portion of the life span of the test animal or transgenic mice.[12] Long-term, conventional 2-year rodent bioassays are often not feasible, with questionable relevance also because of limitations associated with species extrapolation.[13,14] Finding a relevant animal model for every kind of human cancer is impractical, but preclinical animal xenograft tumor models, particularly heterotopic (subcutaneous), have proven useful especially in identifying cytotoxic agents.[15–18] On the other hand, although more technically demanding, the orthotopic xenograft models simulate the same local microenvironment and thus offer the advantage of less complicated translation to the clinical setting.[19]

Scaffolds used for bone regeneration in the oral and maxillofacial area might come in contact with the oral

***Corresponding author:** D. E. Costea, Department of Clinical Medicine and Department of Clinical Dentistry, University of Bergen, 5009 Bergen, Norway. E-mail: daniela.costea@k1.uib.no

Contract grant sponsor: This work was funded by VascuBone project, EU FP7; no. 242175 and Bergen Medical Research Foundation (grant no. 20/2009), The Norwegian Cancer Research Association (grant no. 515970/2011), Norwegian Cancer Society (grant no. 732200), and Helse Vest (grant nos. 911902/2013, 911884, and 911789).

epithelium. Because over 90% of head and neck cancers are, as most of the human malignancies, of epithelial origin,[20,21] there is a need to study the potentially carcinogenic effect of degradable bioengineered scaffolds on oral epithelial cells. To study oral and head and neck carcinogenesis, both orthotopic and heterotopic (subcutaneous) models were previously developed by use of malignant cells derived from established oral or head and neck cancer.[22] In this study, we chose to develop a xenotransplantation model by use of an early neoplastic oral keratinocyte (DOK) cell line derived from early neoplastic oral mucosa.[23] These cells were found to be partly transformed but nontumorigenic in nude mice, and were described as having potential as "screening recipients" for carcinogens in vitro.[23]

Different in vivo optical imaging modalities have been tested in various tumor models.[24–26] However, there is a need for a noninvasive head and neck cancer model with the ability to detect possible tumorigenic effects of various microenvironmental cues, including implanted scaffolds. Bioluminescent imaging is a well-established method in preclinical investigation of the complexity of cancers[27–29] including head and neck cancer,[30,31] but for a screening of the potential to fully transform and generate malignant tumors from the early neoplastic cells, the application of bioluminescence would offer a novel noninvasive approach. In carcinogenicity testing of biomaterials, controls of a comparable form and shape should be included. However, in the presented system, the use of appropriate controls is not necessary because the inclusion of a positive environment with the use of carcinoma-associated fibroblasts (CAFs) has been developed. The noninvasive in vivo visualization for several weeks also provides additional unique advantages over the aforementioned established carcinogenicity testing systems.

To achieve real-time bioluminescence in this study, DOK cells were first transduced to contain the firefly luciferase. They were then tested in vivo in NSG mice for their potential as "screening sensors" for diverse microenvironmental cues, such as various types of head and neck CAFs and copolymer scaffolds intended for tissue engineering. The biodegradable poly L-lactide-co-ε-caprolactone (poly[LLA-co-CL]), an aliphatic polyester copolymer of L-lactic acid and ε-caprolactone, has been extensively studied at our laboratory as a scaffold for bone regeneration proving its biocompatibility and osteoconductivity,[8,32] and, hence, was chosen for developing this model.

MATERIALS AND METHODS

Cell choice and maintenance

The DOK cell line was purchased from The European Collection of Cell Cultures (Salisbury, Wiltshire, UK).[23] They were maintained in Dulbecco's modified Eagle's medium (DMEM) supplemented with 10% fetal calf serum (FCS; Invitrogen, Waltham, MA), 20 μg/mL L-glutamine, 5 μg/mL hydrocortisone (all from Sigma, St. Louis, MO).

CAFs ($n = 3$; CAF1, CAF15_13, and CAF15_23) were isolated from histologically confirmed head and neck squamous cell carcinoma, after receiving informed consent. They were maintained in FAD medium: DMEM/Ham's F12 1:3 mixture, 1% L-glutamine, 0.4 μg/mL hydrocortisone, 50 μg/mL ascorbic acid, 10 ng/mL epidermal growth factor, 5 μg/mL insulin, and 20 μg/mL transferrin and linoleic acid (all from Sigma) with 10% FCS.

Luciferase transduction of early neoplastic oral keratinocytes

Virus production. DOK wild type (DOK^{WT}) cells were transduced with a tTA, L192 construct (expressing luciferase).[33] Infectious retroviral vector particles were produced in Phoenix A cells (LGC Standards AB, Boras, Sweden) cultured in DMEM, supplemented with 10% FCS, 1% penicillin-streptomycin, and 1% glutamine. When 70% to 80% was confluent, 8 μL of 50 m*M* chloroquine (Sigma) was added. Four micrograms of DNA construct (tTA, L192) was mixed with 128 μL of 2M calcium chloride ($CaCl_2$) and sterile ddH_2O to a total volume of 1 mL plus 1 mL of 2×HEPES-buffered (Sigma) and transferred onto each plate. After 12-hour incubation, the medium was replaced by a fresh medium and by DOK's medium after 24 hours.

Infection and selection of luciferase-transduced early neoplastic oral keratinocyte. The virus supernatant was collected, filtered, and gene transfer enhanced with protamine sulfate (5 μg/mL). DOK^{WT} were seeded at 3 different seeding densities (25×10^3; 50×10^3; and 100×10^3 cells/well) in a 6-well plate and centrifuged at 1200 g for 90 minutes. The virus supernatant was replaced with the DOK medium 24 hours postinfection. Successfully infected DOK cells were selected by puromycin (1 μg/mL; Sigma). To obtain a cell-clone with a stable, high expression of luciferase, transduced DOK cells were sorted using fluorescence-activated cell sorter (FACS Aria SORP, BD Biosciences, San Jose, CA).

Selection of highly bioluminescent early neoplastic oral keratinocyte luciferase-transduced cells

Approximately 1×10^6 cells of each group in 100 μL DOK medium were transferred to 96-well plate with 1 well containing 100 μL of DOK medium only for background autofluorescence. Luciferin, (1.6 g/L of D-luciferin; Biosynth AG, Staad, Switzerland) was added 10 minutes before imaging in the Time-Domain Small Molecular Imager Optix MX3 (ART; GE Healthcare, Little Chalfont, UK). Using the OptiView acquisition software (ART Advanced Research Technologies, Quebec, Canada), the region of interest was chosen and plates were scanned with the scan step 1.0 mm and integration time 0.1 seconds.

Assessment of cell morphology and proliferation

Both cell types, DOK^{WT} and early neoplastic oral keratinocyte luciferase-transduced (DOK^{Luc}), were cultured at passages (45–48) and their morphology was compared under a light microscope (Nikon TS100; Nikon, Tokyo, Japan). The growth rate was analyzed using a colorimetric assay based on methylthiazol tetrazolium (Sigma) and measured at 570 nm using a microplate reader (BMG LABTECH, GmbH, Ortenberg, Germany).

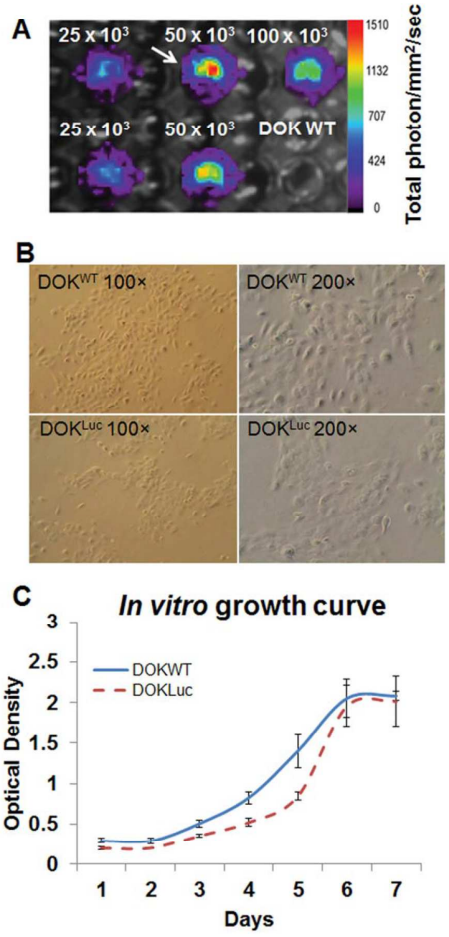

FIGURE 1. (A) Bioluminescence of early neoplastic oral keratinocyte luciferase-transduced (DOK^{Luc}) cells at a density of 50×10^3 early neoplastic oral keratinocyte wild type (DOK^{WT}) transduced 4 times, displaying the highest photons/mm²/sec, white arrow. (B) Light microscopy showing that DOK^{WT} and DOK^{Luc} exhibit the same typical morphology and pattern of growth in the form of coherent islands. (C) Growth curves for both cell types, showing no significant difference ($p = .262$) between the in vitro growth potential of DOK^{WT} and DOK^{Luc}. [Color figure can be viewed in the online issue, which is available at wileyonlinelibrary.com.]

Assessment of tumorigenicity in vivo

Both DOK^{WT} and DOK^{Luc} cells were cultured and allowed to reach their log phase before they were trypsinized and suspended in 50 μL of growth factor-reduced matrigel (BD Biosciences). The cells were inoculated at 2 different densities, low (1×10^3) and high (1×10^5), at 2 different locations, the tongue and subcutaneously in the back of 8 to 10 weeks old male nonobese diabetic severe combined immunodeficient IL2rγ^{null} mice (NSG) (University of Bergen - originally a generous gift from Prof. Leonard D. Shultz, Jackson Laboratories, Bar Harbor, ME; $n = 24$, 6 mice for each group). Weekly for 6 weeks, tumor volumes for both cell types were manually assessed by digital caliper, using the formula [length × (width²)/2]. In the group inoculated with DOK^{Luc}, tumor development was also measured weekly by bioluminescence. We euthanized the mice after 45 days and harvested tissues for histology.

Orthotopic tongue xenograft mouse model for early neoplastic oral keratinocyte + carcinoma-associated fibroblast co-inoculations

To create a positive tumor formation control, 1×10^3 DOK^{WT} were suspended with 1×10^5 CAFs (CAF1) in 50 μL matrigel and inoculated in the tongue of NSG mice ($n = 12$; 6 mice for each group). Tumors were measured manually up to 45 days.

To assess the sensitivity of bioluminescence to differentiate between tumors formed by different strains of CAFs, DOK^{Luc} in a density of 1×10^3 were co-inoculated in combination with 1×10^5 of 2 different strains of CAFs (CAF15_13 and CAF15_23) in the tongue. The total number of animals was 24 with at least 6 for each group. The development of the tumors in this group was followed up manually and evaluated weekly by bioluminescence.

Preparation of cell-seeded poly L-lactide-co-ε-caprolactone scaffolds for ectopic subcutaneous scaffold xenograft

The copolymer poly(LLA-co-CL) was polymerized from ε-caprolactone (Sigma–Aldrich, Germany) and LLA (Boehringer, Ingelheim, Germany) by ring-open-polymerization, as previously described.[32] The average molecular weight of the purified copolymer was 100,000 and polydispersity index 1.3 determined by Size Exclusion Chromatography (Polymer Laboratories, Shropshire, UK). The copolymer was composed of 75 mol % LLA and 25 mol % caprolactone, confirmed by ^{1}H-NMR (Bruker Avance 400, Billerica, MA). The porous scaffolds were prepared by solvent casting particulate leaching[32] and a disc-shaped scaffold (diameter approximately 6 mm, thickness approximately 1.3 mm) was formed with >83% porosities. Porosities were calculated by a Micro-CT (Sky Scan 1172 scanner, Kontich, Belgium) using 40 kV and 2.4 micron voxel and 3D analysis was carried using the software CT-Analyzer version 1.13 (Bruker).

The scaffolds were pre-wet with DOK medium and left for 2 to 3 hours before being then seeded with cells, DOK^{Luc} alone or DOK^{Luc} + CAFs (CAF1). Three different densities of DOK were used (1×10^3, 1×10^5, and 1×10^6); the density of CAFs was fixed to 1×10^5. Plates were vortexed (Eppendorf, Hamburg, Germany) and the cells were allowed to attach overnight before scaffolds were xenotransplanted in 8 to 10-week-old NSG mice.

The mice were anesthetized with Isoflurane (Isoba VetTM; Schering Plough, Kenilworth, NJ) before 2 incisions (1 cm) were made on their back. One incision was

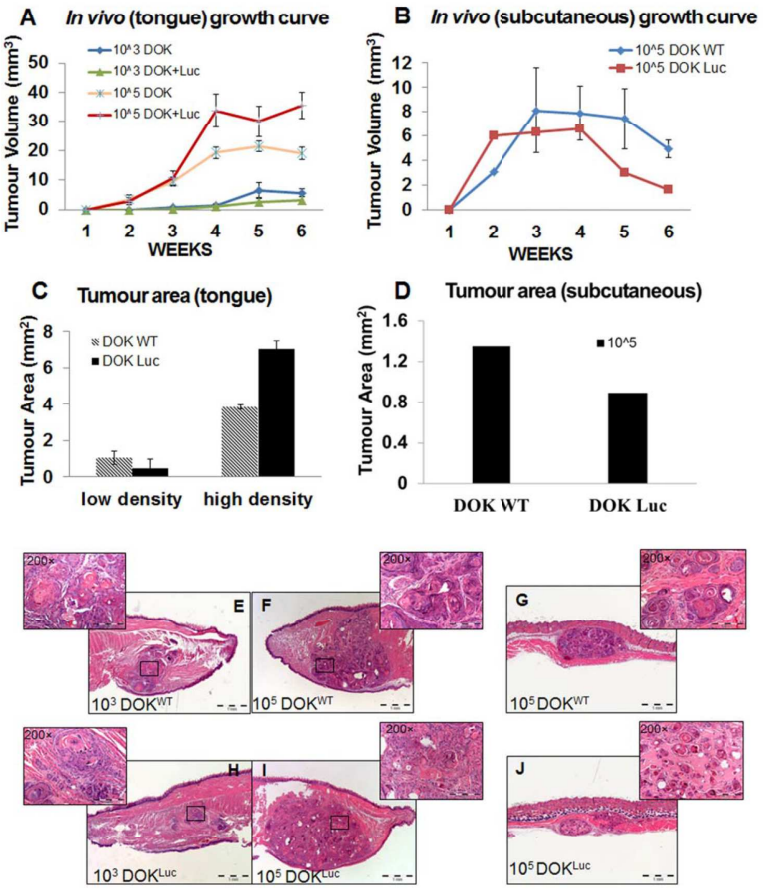

FIGURE 2. Graphs comparing the growth rate (tumor volume) and the total area of tumors formed by either early neoplastic oral keratinocyte wild type (DOK^{WT})or early neoplastic oral keratinocyte luciferase-transduced (DOK^{Luc}) inoculated at cell densities of 10^3 or 10^5 in the tongues (A and C), and subcutaneously (B and D) of NSG mice (*$p < .05$). Histological sections with hematoxylin-eosin stain showing 6 weeks after inoculation of the tongue (E, F, H, and I) and skin (G and J). The tumors retain the characteristics of squamous cell carcinoma (original magnification ×25 and ×200). Scale bar 1 mm = ×25 and 200 μm = ×200. [Color figure can be viewed in the online issue, which is available at wileyonlinelibrary.com.]

made between the upper limbs and another between the lower limbs, providing sufficient space for implantation of scaffolds and to avoid bioluminescence bleeding. Two scaffolds were implanted into each mouse, 1 scaffold with DOK^{Luc} alone and the other with DOK^{Luc} + CAFs. The different densities were distributed among all mice (n = 6). Wounds were closed with Histoacryl tissue adhesive (B. Braun Surgical AS, Melsungen, Germany). At 12 weeks, the animals were euthanized with CO_2 overdose and scaffolds processed for histology.

Optical bioluminescence imaging

Mice were depilated and scanned after intraperitoneal delivery of 150 mg/kg of D-luciferin. Animals were maintained under 1% gas anesthesia during scanning. Images were captured using In Vivo MS FX PRO (Carestream Health, Rochester, NY) and analyzed using Carestream MI SE version 5.0.6.20, 1 exposure of 90-second duration.

Histology and immunohistochemistry

Samples were fixed in 4% paraformaldehyde before embedding in paraffin. Sections of 3 to 4 μm were stained with hematoxylin-eosin (Sigma). For p53 immunostaining, paraffin sections were deparaffinized and rehydrated. Epitope retrieval was performed by heating the sections in citrate buffer pH 6.0 in a microwave. Endogenous enzyme activity and unspecific binding were blocked using peroxidase block (DAKO, Golstrup, Denmark) and 10% normal goat serum (DAKO) for 5 minutes and 30 minutes, respectively, at room temperature. As primary antibody, p53 with a monoclonal specific antibody (DO-7 clone, DAKO) 1:50 was incubated for 1 hour at room temperature. For negative controls, samples were treated with antibody diluents alone. The bound reaction was visualized using 3, 3′-diaminobenzidine tetra hydrochloride (DAB, DAKO). Double staining with vimentin (DAKO) 1:1000 was carried out using a double stain kit (Envision G|2 double stain system; DAKO), in accord with the manufacturer's instructions. Tumor areas were

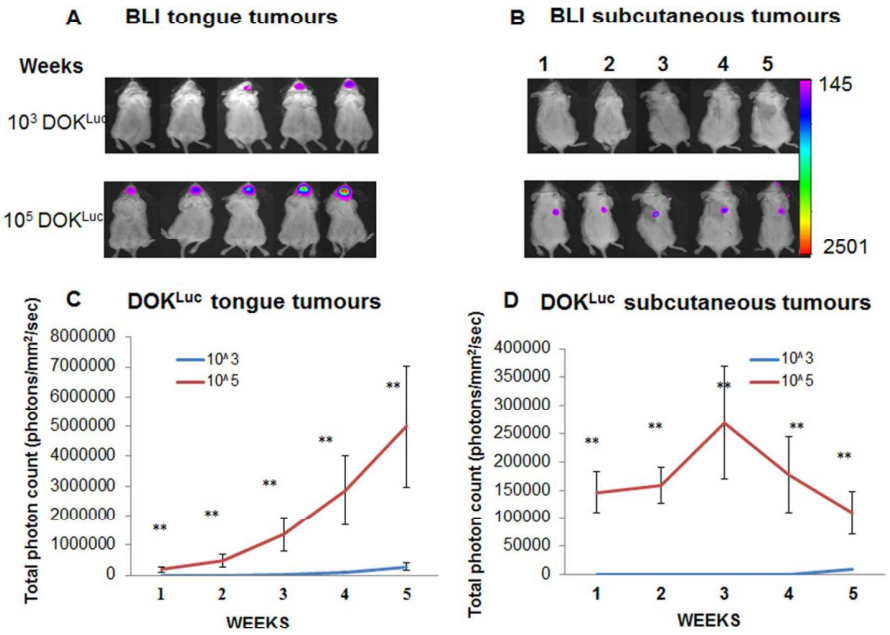

FIGURE 3. Bioluminescence (BLI) of mice for 5 weeks after inoculation with early neoplastic oral keratinocyte luciferase-transduced (DOK^{Luc}) cells (10^5 and 10^3 densities) in the tongue (A) and in the skin (B). Graphs depicting increasing total photon intensities from tongue inoculations (C) with a lower overall photon count produced from 10^3 densities (**$p < .01$). (D) Total photon intensities of cells for 5 weeks after subcutaneous inoculation (**$p < .01$). Data shown as means ± SEM. [Color figure can be viewed in the online issue, which is available at wileyonlinelibrary.com.]

calculated from areas of interest in hematoxylin-eosin sections using Olympus DP Soft 5.0 software (Munster, Germany).

Ethics statement

The ethical approval for patients with head and neck squamous cell carcinoma samples was obtained from the Regional Committees for Medical and Health Research Ethics (REK NO. 2010/48) and lesions were collected following ethical approval and written informed consent of the patients. All animal experiments were approved by the Norwegian Animal Research Authority and conducted in strict accordance with the European Convention for the Protection of Vertebrates used for Scientific Purposes (FOTS no. 20134643/20123961). All procedures were performed under isoflurane gas anesthesia, and all efforts were made to minimize suffering.

Statistical analysis

Average values were analyzed by IBM SPSS Statistics 21.0 (SPSS, Chicago, IL) and the data expressed as mean ± SEM. Paired t test or the independent Mann–Whitney U tests were used to compare differences between the tumors formed. Spearman's correlation was used to correlate the manual tumor measurements and histological measurements with corresponding bioluminescence signals. Differences were considered statistically significant when $p < .05$.

RESULTS

Successful transduction of early neoplastic oral keratinocyte with luciferase containing vector generated a new cell line

The bioluminescence signal recorded for DOK^{Luc} cells cultured in vitro for 2 to 3 weeks posttransduction showed that the seeding density of 50×10^3 displayed the highest photons/mm^2/sec (Figure 1A, white arrow). Cells derived following this protocol were expanded and used for further in vivo experiments. Light microscopy showed that DOK^{WT} and DOK^{Luc} had typical epithelial morphology and similar patterns of growth in the form of coherent islands. No signs of epithelial-to-mesenchymal transition could be observed in either (Figure 1B). The growth curve was comparable for the 2 cell types ($p = .262$), indicating that transduction with luciferase did not alter the in vitro growth potential of these cells (Figure 1C).

The in vivo tumorigenic potential of DOK cells before and after transduction with luciferase expressing gene was evaluated after DOK^{WT} and DOK^{Luc} were inoculated in the tongue and also subcutaneously in NSG mice at low (1×10^3) and high (1×10^5) density. At the high inoculation density, visible tumors were detected with the same incidence after 2 weeks, at both sites, for both DOK^{WT} and DOK^{Luc}. At the low density, tumors formed only in the tongue, and after 4 weeks, with the same incidence for

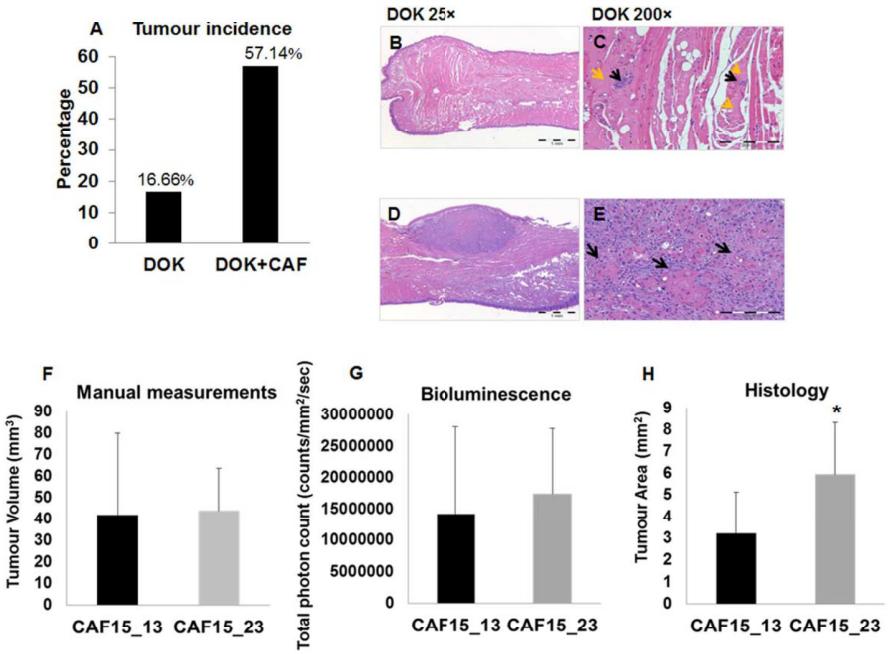

FIGURE 4. (A) Carcinoma-associated fibroblasts (CAFs) increased tumor incidence of early neoplastic oral keratinocytes wild type (DOK)^{WT} when co-inoculated in the tongues of NSG mice. (B and C) Hematoxylin-eosin section of the tumor detected in DOK^{WT} group presenting surviving DOK cells (black arrows) within remnants of matrigel (yellow arrows). (D and E) Hematoxylin-eosin section of tumor formed by DOK^{WT} + CAF; depicting typical squamous cell carcinoma morphology with keratin pearls (black arrows). (F) Graphs comparing the volumes by manual measurements from the last timepoint (week 7) of the tumors formed by 2 different strains of CAFs. (G) Comparison of total photon intensities at week 7 measured by bioluminescence. (H) Comparing tumor area from histology after 7 weeks (*$p = .028$). [Color figure can be viewed in the online issue, which is available at wileyonlinelibrary.com.]

DOK^{WT} and DOK^{Luc}. There was no statistical significance between the volume of the tumors formed in both tongue and subcutaneously by DOK^{WT} and DOK^{Luc} at all timepoints (Figures 2A and 2B). The histological area of the tumors derived from DOK^{WT} and DOK^{Luc} at low density in the tongue (Figure 2C) and at high density subcutaneously (Figure 2D) did not show any statistical significant difference. The only statistical significant difference was found for the tongue tumors formed at higher inoculation density by DOK^{Luc} than tumors formed by DOK^{WT} ($p < .05$; Figure 2C). Tumor xenografts generated from DOK^{WT} (Figures 2E–2G) showed the same histological picture as DOK^{Luc} xenografts (Figures 2H–2J), with epithelial islands of atypical epithelial cells in the host stroma and keratin pearls.

Development of tumors formed after inoculation of early neoplastic oral keratinocyte luciferase transduced cells was easily monitored by bioluminescence

Luciferase activity increased with time after both tongue and subcutaneous inoculations for both inoculation densities (Figures 3A and 3B). The bioluminescence signal was significantly higher for the inoculations of DOK^{Luc} at higher inoculation density at both tongue and subcutaneous locations (Figures 3C and 3D), at all timepoints, correlating well with the tumor growth curve as assessed by the manual measurements.

Both early neoplastic oral keratinocyte wild type and early neoplastic oral keratinocyte luciferase-transduced were responsive to carcinoma-associated fibroblast-derived microenvironmental cues and bioluminescence was more sensitive than manual measurement in detecting differences between various types of microenvironmental cues

Co-inoculating DOK^{WT} with 10^5 CAFs in the tongues of NSG mice increased tumor incidence from 16.66% to 57.14% (Figure 4A). Histological sections of the tumors formed by DOK^{WT} + CAF showed typical squamous cell carcinoma histology with invasive epithelial islands growing in the host stroma and keratin pearl formation (Figures 4D and 4E). The only 1 tumor formed by the DOK^{WT} alone, which was detected manually, was found histologically to be surviving DOK^{WT} cells within remnants of undissolved matrigel (Figures 4B and 4C). When 2 different types of fibroblasts (CAF15_13 and CAF15_23) were tested for their stimulative support for the in vivo growth of DOK^{Luc}, bioluminescence seemed to be more sensitive than the manual

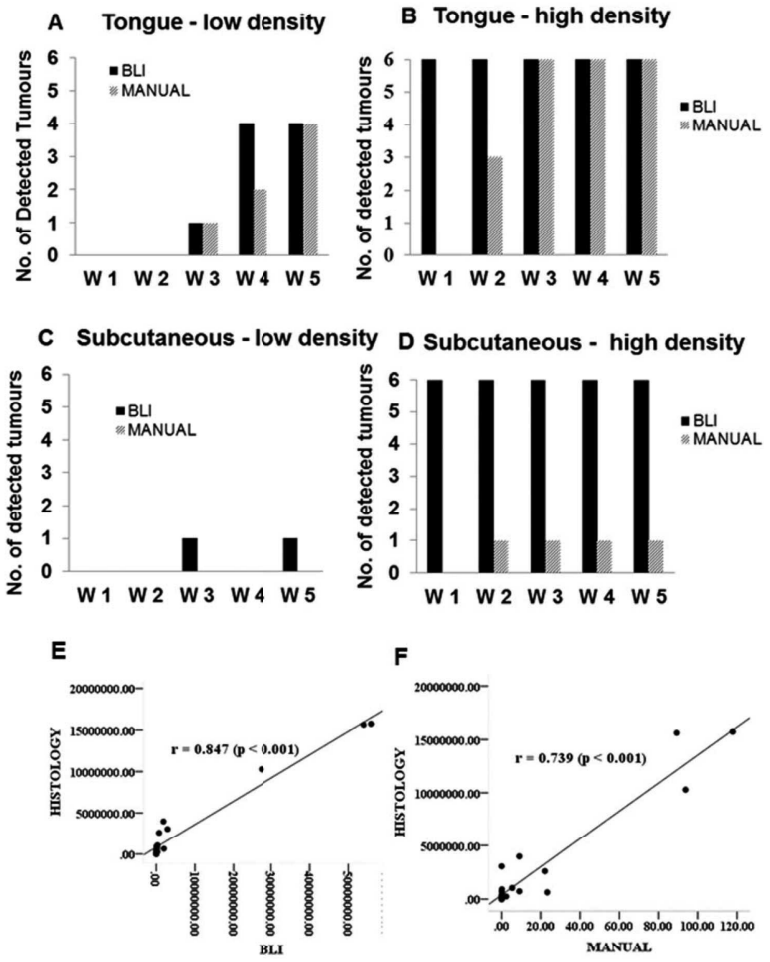

FIGURE 5. (A and B) Comparison of number of tumors detected by bioluminescence (BLI) and manually in the tongue inoculations at both densities. (C and D) Comparison in the skin inoculations ($p = .043$; $n = 24$). (E) Histological areas correlate with bioluminescence signals with a stronger correlation (Spearman's correlation, $r = 0.847$; $p < .001$); than with (F) manual measurements.

measurement in detecting differences in the tumor growth of xenografts (Figures 4F and 4G), although the difference was not statistically significant. This difference was also observed by histological area calculations after 7 weeks, this time with statistical significance ($p = .028$; Figure 4H).

Both bioluminescence and manual measurement showed high correlation with histological area of the tumors, but tumor formation was detected earlier by bioluminescence

Bioluminescence consistently disclosed a higher number of tumors throughout all 5 weeks of monitoring compared to visible tumors measured manually by calipers (Figures 5A–5D). Both the tumor volume as quantified by caliper (manual) measurements and the bioluminescence signal from the corresponding tumor at the last timepoint showed a positive correlation with the tumor area quantified from histological sections (considered to be the "golden standard"). A stronger significant correlation ($r = 0.846$; $p < .001$) was found between the histological tumor area and bioluminescence signals than between the histological tumor area and the manual measurement ($r = 0.739$; $p < .001$; Figures 5E and 5F).

Development of tumors from early neoplastic oral keratinocyte luciferase-transduced grown on poly L-lactide-co-ε-caprolactone scaffolds under different microenvironmental cues was successfully monitored noninvasively by bioluminescence

DOK^{Luc} were cultured on poly(LLA-co-CL) scaffolds at 3 different densities with or without CAFs. Total photon count from bioluminescence showed significantly higher bioluminescence intensity of scaffolds

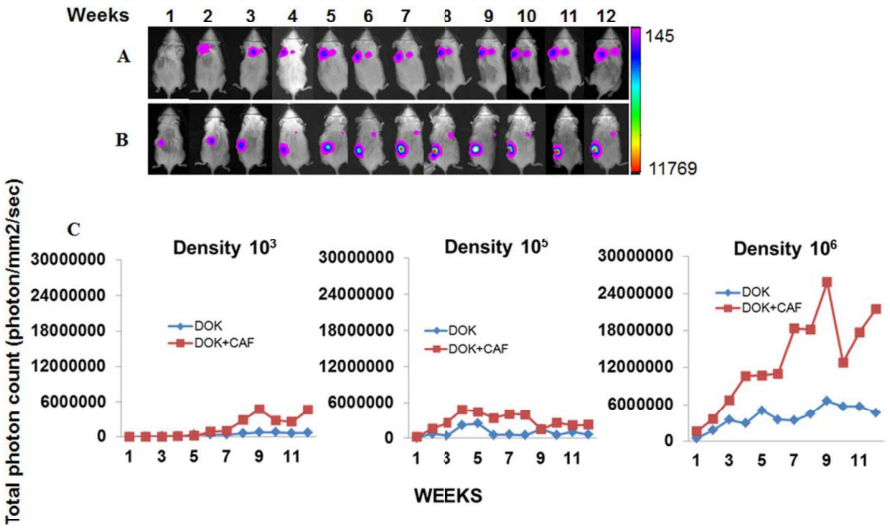

FIGURE 6. (A) Bioluminescence images of a representative mouse carrying a scaffold with a low density (1×10^3) in the upper right back and high density (1×10^6) of early neoplastic oral keratinocyte luciferase-transduced (DOK^{Luc}) alone in the upper left back. (B) Developing tumors with bioluminescence imaging of mice carrying low density (upper right) and high density (lower left) of DOK^{Luc} cocultured with (1×10^5) carcinoma-associated fibroblasts (CAFs). (C) Total photon count from in vivo imaging using DOK^{Luc} at different densities showed significantly higher bioluminescent intensity of scaffolds xenotransplanted with DOK^{Luc} + CAFs than of DOK^{Luc} alone throughout 12 weeks of imaging (10^6: $p < .001$; 10^5: $p < .001$; and 10^3: $p = .017$; $n = 6$). [Color figure can be viewed in the online issue, which is available at wileyonlinelibrary.com.]

xenotransplanted with DOK^{Luc} + CAFs than of DOK^{Luc} alone at all densities, just above the threshold 1 week after xenotransplantation and throughout the 12 weeks of in vivo imaging (10^6: $p < .001$; 10^5: $p < .001$; 10^3: $p = .017$; Figure 6C). In the scaffolds xenotransplanted with DOK^{Luc} alone, no tumors were formed outside the scaffolds and the bioluminescence signal stayed within the same range throughout the 12 weeks of imaging (Figure 6A). In contrast, the bioluminescence intensity of scaffolds cocultured with CAFs increased with time (Figure 6B), indicating an increase in tumor growth over time, and this was confirmed by histology. After 12 weeks, histological analysis of xenotransplants of scaffolds with DOK^{Luc} cells alone showed the presence of few atypical epithelial cells, limited to the scaffold area (Figures 7A, 7B, 7F, and 7G). Around the remnants of the scaffolds, scattered giant cells of mouse origin were observed (Figure 7K, blue arrow). The origin of the epithelial cells was confirmed by immunostaining using an antibody against human p53, recognizing only p53 mutated human cells, DOK. In contrast, the histology of xenografts of DOK^{Luc} + CAFs scaffolds showed squamous epithelial tumor nests (confirmed by p53 positive staining; Figures 7C, 7D, 7I, and 7J), with many of the islands retaining differentiation and containing keratin pearls, growing within and outside the scaffold area, invading the surrounding connective tissue and musculature, thus displaying the characteristic hallmarks of head and neck carcinoma. Few fibroblasts were observed in the xenotransplants even after 12 weeks of growth in vivo in mice (Figure 7K, black arrow). Figure 7E shows the pronounced macroscopic differences observed during harvesting of the scaffolds.

DISCUSSION

This study describes the development of a noninvasive, in vivo model for testing the tumorigenic potential of various microenvironmental cues, including scaffolds intended for use in tissue engineering. Numerous studies[34] support the concept that carcinogenesis, including head and neck cancer, is a multistep process involving a premalignant phase of long-term accumulated chromosomal alterations.[35] The use of normal cells in tumor models is time-consuming, if not irrelevant, because it is well-known that the transformation of human cells is a long process, involving at least 5 to 7 mutagenic events, which are difficult to achieve in an experimental setting.[20,36] For the present model, the DOK cell line, exhibiting early neoplastic epithelial dysplastic features was selected as a "screening sensor."[23] To facilitate the noninvasive visualization of these cells after xenotransplantation, they were transduced with luciferase gene, successfully generating a new cell line, DOK^{Luc}. The in vitro growth and behavioral characteristics of the transfected cells were comparable to those of the parent cells. To evaluate their behavior in vivo, both cell lines (DOK^{WT} and DOK^{Luc}) were xenotransplanted alone at low and high densities, both orthotopically, in the tongue, and ectopically, on the back of NSG mice. With a single exception for the tumor size when injected in the tongue at high density, DOK^{WT} and DOK^{Luc} showed a comparable in vivo behavior as well.

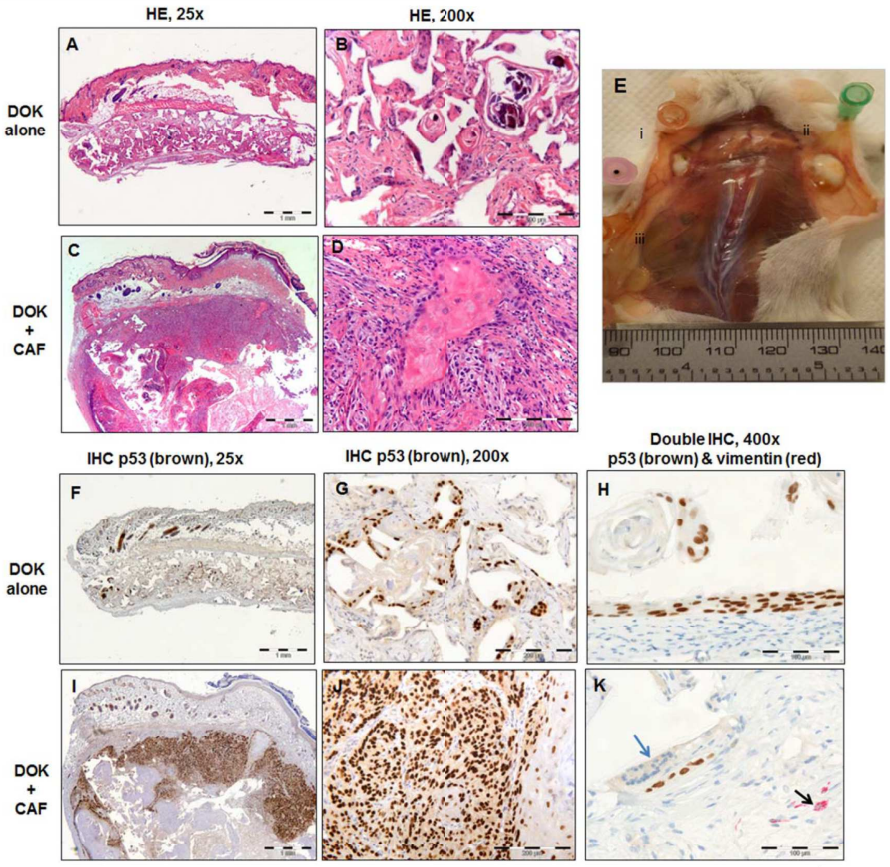

FIGURE 7. (A–D) Hematoxylin-eosin staining showing histology of early neoplastic oral keratinocyte luciferase-transduced (DOK^{Luc}) and DOK^{Luc} + carcinoma-associated fibroblasts (CAFs) xenografts respectively. (E) Dissection of a mouse after 12 weeks showing implanted scaffolds with: (1) 10^5 DOK^{Luc} cells alone; (2) 10^5 DOK^{Luc} cocultured with 10^5 CAF; and (3) empty scaffold. (F and G) Human p53 immunohistochemistry (IHC) showing the presence of few surviving human p53 mutated transformed epithelial cells in a scaffold xenotransplanted with DOK^{Luc} alone. (I and J) Human p53 immunohistochemistry showing islands of atypical epithelial cells within and outside the scaffold in DOK^{Luc} + CAFs xenografts (original magnification ×25 and ×200). Scale bar = 1 mm and 200 μm, respectively. (H and K) Double staining for human vimentin (red cytoplasmic stain) and human p53 (brown nuclear stain). (K) Positive vimentin stained human fibroblasts present after 12 weeks in DOK^{Luc} + CAFs xenografts (black arrow). The giant cells are negative for both human markers (blue arrow). Scale bar 100 μm (original magnification ×400). [Color figure can be viewed in the online issue, which is available at wileyonlinelibrary.com.]

This indicates that the DOK cell line retained a high degree of stability after transfection, although it carried a complex karyotype and multiple mutations, including p53 mutations. In accordance with previous oral carcinogenesis animal studies, the incidence and size of subcutaneous tumors in the present study was lower than those of tongue tumors.[16] This could be related to a greater stimulation of lymphangiogenesis in the tongue area[16] or simply because of the fact that orthotopic models allow cells to grow better in their original environment.

When DOK^{WT} cells were co-inoculated with CAFs in the tongue, the incidence of tumor formation increased by more than 40% compared with tumors formed by DOK^{WT} alone. This further highlights the important role of the microenvironmental cues in tumor initiation and early growth, supporting previous studies.[37,38] The tumor detected by manual measurements formed by DOK^{WT} was proven later on, histologically, to contain mainly remnants of matrigel, which might have given the mass that could be measurable by the caliper, and only few islands of nonproliferative DOK cells. This illustrates one of the drawbacks of the manual measurements that can be avoided by the use of other methods, such as bioluminescence.

In this study, bioluminescence detected more than 50% of the total number of tumors formed in the tongue by DOK^{Luc} from the first week; much earlier than tumor detection with caliper measurements. In the skin tumors,

6 of 7 were visible by bioluminescence from the first week. One of the tumors was from low density inoculations, which were too small for detection by manual measurements, but it was later confirmed histologically. The total number of tumors detected by bioluminescence was significantly greater than manual detection ($p = .043$), and in concordance with the histological findings, indicating higher sensitivity for early detection using the bioluminescence method.

The measurements from the last timepoint of tumor growth assessment period showed higher bioluminescence signals from tumors with CAF15_23 than those with CAF15_13; this difference was not detected by the manual measurements. Histological evaluation confirmed statistically bigger tumors formed by DOK^{Luc} co-injected with the CAF15_23, a difference that was not indicated by the manual measurements. This brings further indications for the greater sensitivity of the bioluminescence method compared to the manual method that might carry subjective evaluations (eg, inflammation, tongue pull, position of the mouse, and lesion margins).

Degradable copolymer scaffolds were used to further optimize and validate the model for use in screening tests for tumorigenesis of various microenvironmental cues from biomaterials. The manual monitoring of tumors at early stages was impossible because the tumors initially developed within the scaffold. However, this was not an impediment for bioluminescence. The correlation between bioluminescence signals and the golden standard method of histological examination was higher, confirming the method is more sensitive than manual measurements. Therefore, bioluminescence was further used solely to monitor the scaffolds when developing the model.

A challenge for using the bioluminescence method would be monitoring of bigger tumors. We monitored a drop in intensity for a tumor developed from very high seeding density of DOK^{Luc} + CAFs xenografts (1×10^6). We interpreted that to be an underestimation of the real bioluminescence signal from the cells because that tumor was later found to be cystic. Cystic content or necrosis that can occur in large or late stage tumors might reduce the production of light because of decreased proliferation or hypoxia.[27,39] Therefore, we recommend inoculating fewer cells per area of scaffold in order to circumvent these limitations and monitor tumor formation for longer period of times, as required in carcinogenesis studies. Although the use of such immunodeficient models greatly aids the development of "humanized" models of cancer using biomaterials,[25] it does come with the caveat of no innate host immunity. Whereas this limitation prevents the current study of role of the immune system in tumor prevention in such models or the use of immunotherapeutic interventions, steps have been made to circumvent such constraints. Recent efforts have demonstrated that introduction of distinct human immune components are possible in mice xenografted with cancer cell lines,[40] suggesting that further evolution of the NSG mice system may yet render models to study human immune reactions in cancer.

Our model provides an abridged alternative to the years spent in rodent models to get tumors from biomaterials implanted solely in animals and foreign body tumorigenesis has several stages, with specific sequences of preneoplastic characteristics.[12,41] The processing time is reduced because of the ability of screening several animals simultaneously, which makes it cheaper compared to other high throughput imaging methods used in the field, such as MRI.

CONCLUSIONS

The model generated and validated in this study is a sensitive and reliable model for monitoring microenvironmentally induced carcinogenesis providing early, consistent surveillance of tumor development associated with implantation of scaffolds for tissue engineering.

Acknowledgments

The authors thank Dr. Joan Bevenius–Carrick, Dr. Andrew Davis, and Prof. Mustafa Nur Elhuda for English revision and constructive criticism of the manuscript. We are grateful to Tereza Osdal (University of Bergen) for assistance with cell transduction, Gunnvor Øijordsbakken (Gade Laboratory for Pathology) for support with histology, and Mihaela Popa (Kin*N* Therapeutics AS, Bergen) for bioluminescence imaging training. The bioluminescence imaging was performed at the Molecular Imaging Centre (MIC), University of Bergen.

REFERENCES

1. De Wever O, Mareel M. Role of tissue stroma in cancer cell invasion. *J Pathol* 2003;200:429–447.
2. Kalluri R, Zeisberg M. Fibroblasts in cancer. *Nat Rev Cancer* 2006;6:392–401.
3. Mantovani A, Allavena P, Sica A, Balkwill F. Cancer-related inflammation. *Nature* 2008;454:436–444.
4. Anderson JM, Rodriguez A, Chang DT. Foreign body reaction to biomaterials. *Semin Immunol* 2008;20:86–100.
5. Nakamura T, Shimizu Y, Okumura N, Matsui T, Hyon SH, Shimamoto T. Tumorigenicity of poly-L-lactide (PLLA) plates compared with medical-grade polyethylene. *J Biomed Mater Res* 1994;28:17–25.
6. Nakamura T, Shimizu Y, Takimoto Y, et al. Biodegradation and tumorigenicity of implanted plates made from a copolymer of epsilon-caprolactone and L-lactide in rat. *J Biomed Mater Res* 1998;42:475–484.
7. Kirkpatrick CJ, Alves A, Köhler H, et al. Biomaterial-induced sarcoma: a novel model to study preneoplastic change. *Am J Pathol* 2000;156:1455–1467.
8. Idris SB, Dånmark S, Finne–Wistrand A, et al. Biocompatibility of polyester scaffolds with fibroblasts and osteoblast-like cells for bone tissue engineering. *J Bioact Compat Polym* 2010;25:567–583.
9. ISO/EN ID. Biological evaluation of medical devices-part 5. Test for cytotoxicity: in vitro methods. Geneva, Switzerland: International Organisation of Standardisation; 1992.
10. Kato S, Akagi T, Sugimura K, Kishida A, Akashi M. Evaluation of biological responses to polymeric biomaterials by RT-PCR analysis IV: study of c-myc, c-fos and p53 mRNA expression. *Biomaterials* 2000;21:521–527.
11. Carraway J, Ghosh C. The challenge to global acceptance of part 3 of ISO 10993. *Med Device Technol* 2006;17:16–18.
12. Takanashi S, Hara K, Aoki K, et al. Carcinogenicity evaluation for the application of carbon nanotubes as biomaterials in rasH2 mice. *Sci Rep* 2012;2:498.
13. Cohen SM. Human carcinogenic risk evaluation: an alternative approach to the two-year rodent bioassay. *Toxicol Sci* 2004;80:225–229.
14. Ward JM. The two-year rodent carcinogenesis bioassay – Will it survive? *J Toxicol Pathol* 2007;20:13–19.
15. Ahmed SU, Zair M, Chen K, et al. Generation of subcutaneous and intrahepatic human hepatocellular carcinoma xenografts in immunodeficient mice. *J Vis Exp* 2013;79:e50544.
16. Hadler–Olsen E, Wetting HL, Rikardsen O, et al. Stromal impact on tumor growth and lymphangiogenesis in human carcinoma xenografts. *Virchows Arch* 2010;457:677–692.
17. Ruggeri BA, Camp F, Miknyoczki S. Animal models of disease: preclinical animal models of cancer and their applications and utility in drug discovery. *Biochem Pharmacol* 2013;87:150–161.
18. Sano D, Myers JN. Xenograft models of head and neck cancers. *Head Neck Oncol* 2009;1:32.

19. Bibby MC. Orthotopic models of cancer for preclinical drug evaluation: advantages and disadvantages. *Eur J Cancer* 2004;40:852–857.
20. Debnath J, Brugge JS. Modelling glandular epithelial cancers in three-dimensional cultures. *Nat Rev Cancer* 2005;5:675–688.
21. Warnakulasuriya S. Global epidemiology of oral and oropharyngeal cancer. *Oral Oncol* 2009;45:309–316.
22. Yang K, Zhao N, Zhao D, Chen D, Li Y. The drug efficacy and adverse reactions in a mouse model of oral squamous cell carcinoma treated with oxaliplatin at different time points during a day. *Drug Des Devel Ther* 2013;7:511–517.
23. Chang SE, Foster S, Betts D, Marnock WE. DOK, a cell line established from human dysplastic oral mucosa, shows a partially transformed non-malignant phenotype. *Int J Cancer* 1992;52:896–902.
24. Khemthongcharoen N, Jolivot R, Rattanavarin S, Piyawattanametha W. Advances in imaging probes and optical microendoscopic imaging techniques for early in vivo cancer assessment. *Adv Drug Deliv Rev* 2013;74:53–74.
25. Lee J, Li M, Milwid J, et al. Implantable microenvironments to attract hematopoietic stem/cancer cells. *Natl Acad Sci U S A* 2012;109:19638–19643.
26. McCormack E, Silden E, West RM, et al. Nitroreductase, a near-infrared reporter platform for in vivo time-domain optical imaging of metastatic cancer. *Cancer Res* 2013;73:1276–1286.
27. Jarzabek MA, Huszthy PC, Skaftnesmo KO, et al. In vivo bioluminescence imaging validation of a human biopsy-derived orthotopic mouse model of glioblastoma multiforme. *Mol Imaging* 2013;12:161–172.
28. Kotopoulis S, Delalande A, Popa M, et al. Sonoporation-enhanced chemotherapy significantly reduces primary tumour burden in an orthotopic pancreatic cancer xenograft. *Mol Imaging Biol* 2014;16:53–62.
29. Zinn KR, Chaudhuri TR, Szafran AA, et al. Noninvasive bioluminescence imaging in small animals. *ILAR J* 2008;49:103–115.
30. Pinsky MS, Song W, Dong Z, et al. Activation of iCaspase-9 in neovessels inhibits oral tumor progression. *J Dent Res* 2006;85:436–441.
31. Warner KA, Miyazawa M, Cordeiro MM, et al. Endothelial cells enhance tumor cell invasion through a crosstalk mediated by CXC chemokine signaling. *Neoplasia* 2008;10:131–139.
32. Dånmark S, Finne–Wistrand A, Wendel M, Arvidson K, Albertsson A-C, Mustafa K. Osteogenic differentiation by rat bone marrow stromal cells on customized biodegradable polymer scaffolds. *Bioact Compat Polym* 2010;25:207–223.
33. McCormack E, Haaland I, Venås G, et al. Synergistic induction of p53 mediated apoptosis by valproic acid and nutlin-3 in acute myeloid leukemia. *Leukemia* 2012;26:910–917.
34. Hanahan D, Weinberg RA. Hallmarks of cancer: the next generation. *Cell* 2011;144:646–674.
35. Vineis P, Schatzkin A, Potter JD. Models of carcinogenesis: an overview. *Carcinogenesis* 2010;31:1703–1709.
36. Leemans CR, Braakhuis BJ, Brakenhoff RH. The molecular biology of head and neck cancer. *Nat Rev Cancer* 2011;11:9–22.
37. Clark AK, Taubenberger AV, Taylor RA, et al. A bioengineered microenvironment to quantitatively measure the tumorigenic properties of cancer-associated fibroblasts in human prostate cancer. *Biomaterials* 2013;34:4777–4785.
38. Costea DE, Hills A, Osman AH, et al. Identification of two distinct carcinoma-associated fibroblast subtypes with differential tumor-promoting abilities in oral squamous cell carcinoma. *Cancer Res* 2013;73:3888–3901.
39. Black PC, Shetty A, Brown GA, et al. Validating bladder cancer xenograft bioluminescence with magnetic resonance imaging: the significance of hypoxia and necrosis. *BJU Int* 2010;106:1799–1804.
40. McCormack E, Adams KJ, Hassan NJ, et al. Bi-specific TCR-anti CD3 redirected T-cell targeting of NY-ESO-1- and LAGE-1-positive tumors. *Cancer Immunol Immunother* 2013;62:773–785.
41. Moizhess TG. Carcinogenesis induced by foreign bodies. *Biochemistry (Mosc)* 2008;73:763–775.